Max-Planck-Institut
für Meteorologie

MAX-PLANCK-GESELLSCHAFT

International Max Planck Research School
on Earth System Modelling

On the discrepancy between observed and simulated dynamical responses of Northern Hemisphere winter climate to large tropical volcanic eruptions

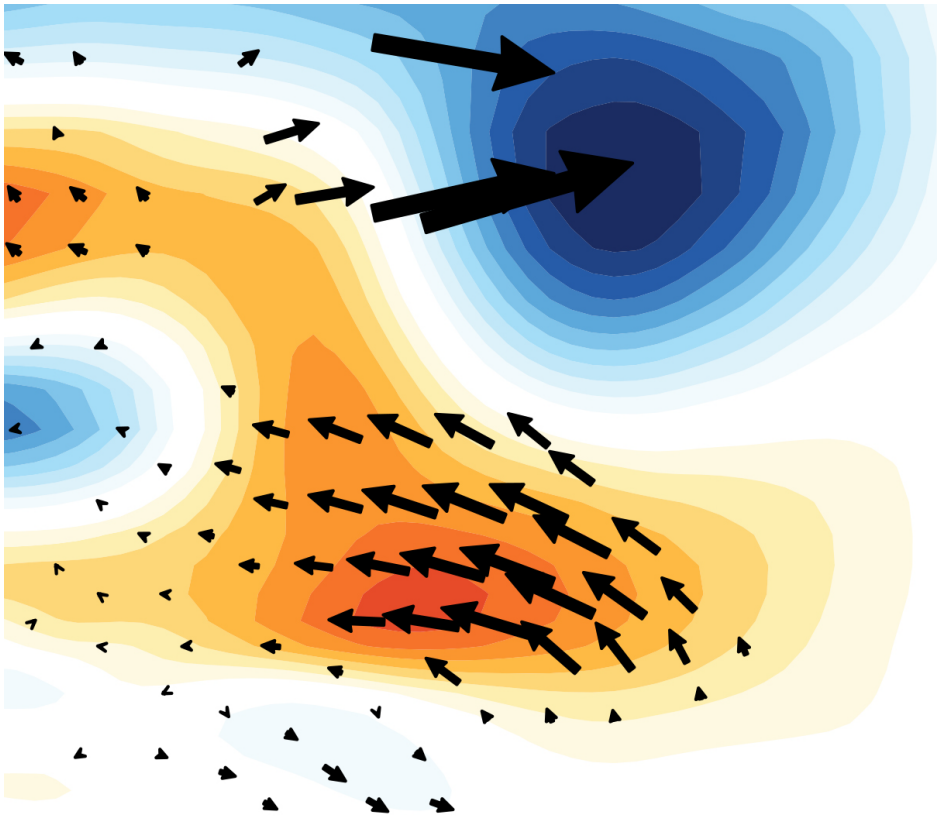

Matthias Bittner

Hamburg 2015

Berichte zur Erdsystemforschung
Reports on Earth System Science

173
2015

Hinweis

Die Berichte zur Erdsystemforschung werden vom Max-Planck-Institut für Meteorologie in Hamburg in unregelmäßiger Abfolge herausgegeben.

Sie enthalten wissenschaftliche und technische Beiträge, inklusive Dissertationen.

Die Beiträge geben nicht notwendigerweise die Auffassung des Instituts wieder.

Die "Berichte zur Erdsystemforschung" führen die vorherigen Reihen "Reports" und "Examensarbeiten" weiter.

Notice

The Reports on Earth System Science are published by the Max Planck Institute for Meteorology in Hamburg. They appear in irregular intervals.

They contain scientific and technical contributions, including Ph. D. theses.

The Reports do not necessarily reflect the opinion of the Institute.

The "Reports on Earth System Science" continue the former "Reports" and "Examensarbeiten" of the Max Planck Institute.

Anschrift / Address

Max-Planck-Institut für Meteorologie
Bundesstrasse 53
20146 Hamburg
Deutschland

Tel./Phone: +49 (0)40 4 11 73 - 0
Fax: +49 (0)40 4 11 73 - 298

name.surname@mpimet.mpg.de
www.mpimet.mpg.de

Layout

Bettina Diallo and Norbert P. Noreiks
Communication

Copyright

On the discrepancy between observed and simulated dynamical responses of Northern Hemisphere winter climate to large tropical volcanic eruptions

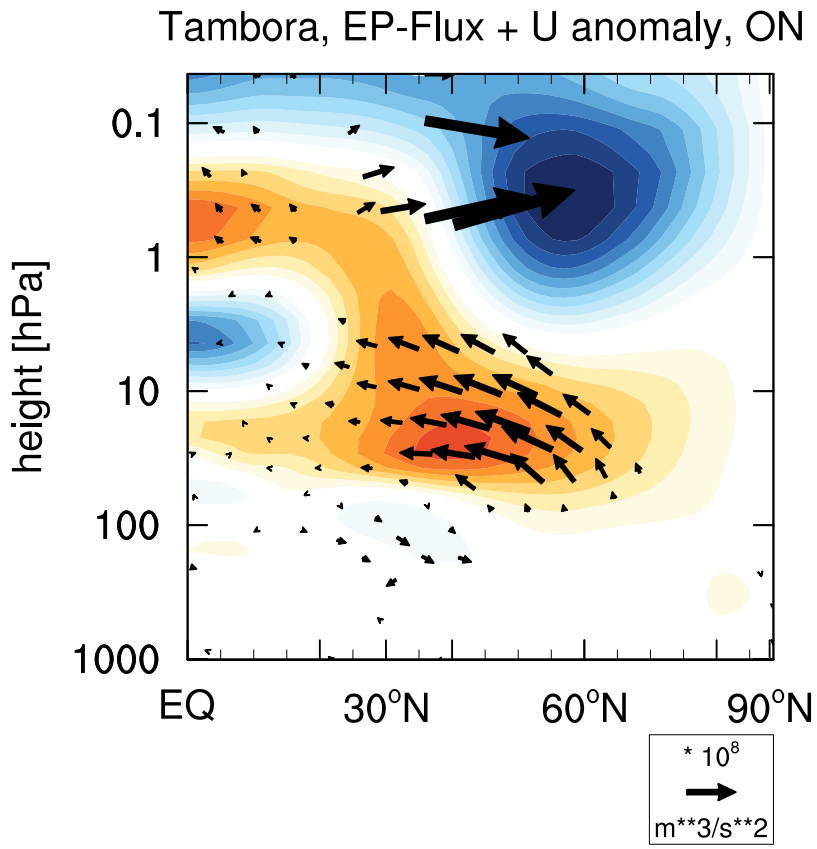

Matthias Bittner

Hamburg 2015

Matthias Bittner

Max-Planck-Institut für Meteorologie
Bundesstrasse 53
20146 Hamburg

Als Dissertation angenommen
vom Fachbereich Geowissenschaften der Universität Hamburg

auf Grund der Gutachten von
Prof. Dr. Martin Claußen
und
Dr. Hauke Schmidt

Hamburg, den 16. 10. 2015
Professor Dr. Christian Betzler
Leiter des Departments Geowissenschaften

Berichte zur Erdsystemforschung / Max-Planck-Institut für Meteorologie 1xx
Reports on Earth System Science / Max Planck Institute for Meteorology 20yy

ISSN 1614-1199

Abstract

Strong tropical volcanic eruptions lead not only to significant cooling of the surface and heating in the tropical stratosphere, but also influence the circulation of the atmosphere. Coupled climate models however have problems in capturing the observed dynamical response to volcanic eruptions, i.e. a stronger polar vortex in the Northern Hemisphere (NH) stratosphere and a subsequent shift of the North Atlantic Oscillation (NAO) to a positive phase in wintertime. This thesis aims at identifying potential causes for the apparent failure of coupled climate models to simulate the dynamical response to volcanic eruptions and thereby improving the current understanding of the volcanic impact on the NH circulation. For this purpose, simulations of the Max Planck Institute Earth System Model (MPI-ESM) in different configurations as well as simulations of 13 additional models that participated in the 5^{th} Phase of the Coupled Model Intercomparison Project (CMIP5) are applied.

The dynamical response to volcanic forcing is assessed in two configurations of the MPI-ESM (MPI-ESM-LR and MPI-ESM-MR). These configurations differ in particular in their representation of the middle and upper atmosphere, where the MPI-ESM-MR has a finer vertical resolution. In terms of their response to tropical volcanic eruptions, differences between the two model configurations occur in the tropical stratosphere. The positive temperature anomaly, due to the absorption of radiation by the volcanic aerosols, is modulated by the quasi-biennial oscillation (QBO), which is only present in the MPI-ESM-MR. However, neither configuration shows a significant impact of tropical volcanic eruptions on NH winter circulation. Averaged over the nine largest eruptions from 1880 until present day, neither a strengthened stratospheric polar vortex nor a shift of the NAO to a positive phase is simulated. The observed volcanic winter warming pattern, i.e. a positive surface temperature anomaly over Northern Europe and Siberia resulting from the shift of the NAO, is not captured by either of the two configurations. The only consistent surface temperature signal is a negative anomaly in low latitudes due to the reflection of incoming short wave radiation by the volcanic aerosols.

Simulations with the MPI-ESM-LR of a very strong Tambora-size eruption show a significantly strengthened polar vortex, which highlights that, given a strong enough forcing, the model can reproduce the observed response of the stratospheric circulation in the NH. But in contrast to the traditional assumption of a direct impact of the increased stratospheric meridional temperature gradient on the NH polar vortex via the thermal wind balance, significant changes in the vertical wave propagation strengthen the polar vortex. The meridional temperature gradient changes most at 30°N, leading to a positive zonal wind anomaly in that region and subsequent deflection of planetary waves to low latitudes, especially in early winter. These waves will deposit less momentum in the polar stratosphere, which will accordingly strengthen the polar vortex.

A multi-model ensemble was used to test the assumption that an overestimation of

the interannual variability of the polar vortex in early winter is responsible for the problem of coupled models to reproduce the dynamical response to volcanic eruptions. However, models which exhibit a comparably higher interannual variability actually capture the strengthening of the polar vortex in post-eruption winters more successfully. For eruptions of the size of Krakatau and Pinatubo, the multi-model ensemble shows a strengthening of the polar vortex in the first post-eruption mid-winter, which challenges the assumption of a general failure of coupled climate models to simulate the dynamical response to volcanic eruptions. The response of the polar vortex in mid-winter significantly depends on the polar vortex anomaly in early winter. A positive polar vortex anomaly in early winter can persist until mid-winter after a volcanic eruption, which is not the case in volcanically unperturbed winters.
Due to the large internal variability of the NH stratosphere, it is difficult to separate the volcanically forced response of the polar vortex from natural variations. A large 100-member ensemble of historical simulations from 1850-2005 with the MPI-ESM-LR is applied to quantify the contribution of internal variability by determining the minimum number of ensemble members needed to identify a significant response after volcanic eruptions. An ensemble of at least 15 members is needed to detect a significant response of the polar vortex to the Pinatubo eruption, which is larger than any single model provided to the CMIP5 archive. Increasing the post-volcanic sample size by adding smaller eruptions than Pinatubo narrows the uncertainty of the mean response, but also weakens the signal by so much that potentially more ensemble members are necessary to detect the response significantly. As observations of the polar vortex after volcanic eruptions are restricted to the winters after El Chichón and Pinatubo, the considerable influence of internal variability at least questions the conclusions drawn about the apparent inability of climate models to reproduce the dynamical impact of volcanic eruptions on the NH stratosphere. Given a strong enough forcing, coupled climate models show a stronger polar vortex, but a large ensemble is needed to detect a significant response.

Zusammenfassung

Starke, tropische Vulkanausbrüche führen nicht nur zu einer signifikanten Abkühlung in Bodennähe und einer Erwärmung in der tropischen Stratospäre, sondern sie beeinflussen auch die Zirkulation der Atmosphäre. Gekoppelte Klimamodelle zeigen jedoch Defizite die beobachteten, post-vulkanischen dynamischen Auswirkungen korrekt wiederzugeben. Die Verstärkung des nordhemisphärischen (NH) Polarwirbels in der Stratosphäre im NH Winter und die daraus resultierende, positive Phase der Nordatlantischen Oszillation (NAO) werden im Allgemeinen nicht verlässlich simuliert. In dieser Arbeit werden potentielle Gründe für das scheinbare Unvermögen der gekoppelten Klimamodelle untersucht. Zudem wird durch die detaillierte Analyse auch das Prozeßverständnis der Auswirkungen von tropischen Vulkanausbrüchen auf die nordhemisphärische Winterzirkulation verbessert. Hierzu werden sowohl Simulationen von verschiedenen Konfigurationen des Max-Planck-Institut Erdsystemmodells (MPI-ESM) benutzt als auch zusätzlich Ergebnisse 13 weiterer Klimamodelle analysiert.

Die dynamischen Auswirkungen von vulkanischen Eruptionen werden zunächst in zwei unterschiedlichen Konfigurationen des MPI-ESM untersucht (MPI-ESM-LR und MPI-ESM-MR). Diese unterscheiden sich unter anderem in ihrer Darstellung der mittleren und hohen Atmosphäre, welche im MPI-ESM-MR wesentlich feiner aufgelöst wird. Bezüglich der Auswirkungen von Vulkaneruptionen zeigen sich Unterschiede zwischen den Konfigurationen in der tropischen Stratosphäre. Eine positive Temperaturanomalie, hervorgerufen durch die Strahlungsabsorption der vulkanischen Aerosole, wird durch die quasi-zweijährigen Oszillation (QBO) moduliert, welche ausschließlich im MPI-ESM-MR simuliert werden kann. Jedoch zeigt keine der beiden Konfigurationen einen signifikanten Einfluss von tropischen Vulkaneruptionen auf die Winterzirkulation in den hohen Breiten der Nordhemisphäre. Gemittelt über die neun stärksten, tropischen Vulkaneruptionen seit 1880 wird weder eine Verstärkung des stratosphärischen Nordpolarwirbels noch eine positive Phase der NAO simuliert. Die beobachteten Bodentemperaturänderungen nach tropischen Vulkaneruptionen — eine Erwärmung in Nordeuropa und Sibirien sowie eine Abkühlung in Südeuropa, welche aus der positiven Phase der NAO resultieren — wird in keiner der beiden untersuchten Konfigurationen des MPI-ESM wiedergegeben. Die einzig konsistente, bodennahe Temperaturänderung ist eine Abkühlung der niederen Breiten durch die erhöhte Reflektion der eingehenden solaren Strahlung an den vulkanischen Aerosolen.

Simulationen einer Vulkaneruption der Stärke des Tamboraausbruchs 1815 zeigen eine signifikante Verstärkung des Nordpolarwirbels. Damit wird deutlich, dass bei einer genügend großen Störung das Modell, in diesem Falle das MPI-ESM-LR, in der Tat die beobachteten Auswirkungen auf die Zirkulation der nordhemisphärischen Stratosphäre wiedergeben kann. Die Verstärkung des Polarwirbels wird nicht wie traditionell angenommen direkt durch den verstärkten, meridionalen Temperaturgradienten und dessen Einfluss auf den zonalen Wind über die thermische Windbeziehung erzeugt.

Die Ergebnisse dieser Arbeit zeigen, dass die größte Änderung des meridionalen Temperaturgradienten in der Stratosphäre bei etwa 30°N und 10 hPa aufritt und zu einer ostwärts gerichteten Windanomalie in dieser Region führt. Hierdurch werden vertikalwandernde, planetare Wellen in niedere Breiten abgelenkt und können folglich den nordhemisphärischen Polarwirbel nicht mehr durch Abgabe ihres Impulses in der polaren Stratosphäre abschwächen.
Basierend auf einer veröffentlichten Arbeit wurde die Arbeitshypothese aufgestellt, dass eine Überschätzung der interannuellen Variabilität des Polarwirbels für die Unterschätzung der dynamischen Auswirkungen von tropischen Vulkaneruptionen in Klimamodellen verantwortlich ist. Diese Hypothese wurde mit einem Ensemble bestehend aus 15 verschiedenen, gekoppelten Klimamodellen getestet. Diese Hypothese musste jedoch verworfen werden, da Modelle welche eine vergleichbar hohe interannuelle Variabilität des Polarwirbels aufweisen, den dynamischen Einfluss der Vulkaneruptionen besser wiedergeben können als Modelle mit einer vergleichbar geringeren Variabilität. Es stellte sich allerdings heraus, dass im Winter nach den Vulkaneruptionen des Krakatau und des Pinatubo das Mittel über alle Modelle eine Verstärkung des nordhemisphärischen Polarwirbels aufweist. Dies stellt die Behauptung des gänzlichen Unvermögens von Klimamodellen bei der Simulation von dynamischen Auswirkungen von Vulkaneruptionen in Frage. Zudem hängt die Stärke der Polarwirbelanomalie in der Mitte des Nordhemisphärenwinters von der Polarwirbelanomalie im Frühwinter ab. Eine positive Anomalie des Polarwirbels im Frühwinter ist persistenter in Wintern nach einer Vulkaneruption als dies in Wintern ohne vorangegangene Vulkaneruption der Fall ist.
Aufgrund der hohen Variabilität der nordhemisphärischen Stratosphäre im Winter in hohen Breiten ist es schwierig die von der Eruption erzeugten Anomalien von den natürlichen Schwankungen des Polarwirbels zu trennen. Ein großes Ensemble mit 100 Mitgliedern des MPI-ESM-LR wurde daher genutzt, um den Einfluss der natürlichen Variabilität zu quantifizieren. Es wurde untersucht, wie viele Ensemblemitglieder notwendig sind, um signifikante Einflüsse von starken, tropischen Vulkaneruptionen zu detektieren. Es zeigt sich zum Beispiel, dass eine Ensemblegröße von mindestens 15 Mitgliedern notwendig ist, um einen signifikanten Einfluss der Pinatuboeruption auf den nordhemisphärischen Polarwirbel festzustellen. Eine Vergrößerung der nachvulkanischen Stichprobe durch Hinzunahme kleiner Vulkaneruptionen schmälert die Unsicherheit der mittleren Anomalie, vermindert gleichzeitig jedoch das Vulkansignal, was dazu führen kann das mehr Mitglieder notwendig sind als dies bei einem einzelnen, großen Ausbruch der Fall ist. Da sich die Beobachtungen des Polarwirbels nach Vulkaneruptionen auf die Ausbrüche des El Chichón und des Pinatubo beschränken, stellt der große Einfluss von natürlichen Schwankungen die Schlussfolgerungen über das generelle Unvermögen von gekoppelten Klimamodellen in Bezug auf ihre Fähigkeit die dynamischen Auswirkungen von Vulkaneruptionen zu simulieren in Frage. Die gekoppelten Klimamodelle zeigen eine Verstärkung des Polarwirbels bei entsprechend großen Eruptionen, jedoch ist ein großes Ensemble notwendig, um ein signifikantes Signal zu detektieren.

Contents

Chapter 1

Introduction

Almost 2,000 years ago, Plutarch suggested that the eruption of Mount Etna in 44 B.C. caused severe famine in Rome and Egypt due to dimming of the sunlight (Forsyth 1988). 1,800 years later, Benjamin Franklin pointed out that the eruption of Laki in Iceland in 1783 might have been responsible for the anomalous cold conditions in 1783-1784 in Europe (Franklin 1784). But despite a long history of interest in the climatic impacts of volcanic eruptions, open questions still remain. While the radiative impacts, i.e. the cooling of the surface due the reflection of incoming solar radiation by the volcanic aerosols, is comparably well understood and reproduced by Earth system models, changes in the circulation after volcanic eruptions are less clear. In particular, impacts on the Northern Hemisphere (NH) winter circulation, which are observed after strong tropical volcanic eruptions, seem to be underestimated or completely missing in the current generation of Earth system models (Driscoll et al. 2012). This thesis aims at identifying possible causes for the apparent failure of Earth system models to reproduce the dynamical response of the NH winter circulation to strong tropical volcanic eruptions.

Explosive volcanic eruptions inject large amounts of sulfur dioxide (SO_2) into the stratosphere, where the SO_2 gas is converted into small aerosols which increase the Earth's albedo and cool the surface. For very small eruptions, the impact on the global mean surface temperature can be undetectable, but for larger eruptions the negative global mean surface temperature anomalies might reach up to several degrees K, depending on the magnitude, the location and the season of the volcanic eruption (Robock 2000). However, exact estimates are difficult to obtain due to sparse sampling of temperature proxies for past eruptions, and regional anomalies are expected to be larger (Robock 2000). To have a significant effect on climate, a sufficient amount of SO_2 emitted by the volcanic eruption must reach the stratosphere, where the volcanic aerosol particles remain for 1-2 years, rather than for weeks as for a tropospheric injection, and influence the earth radiation budget (Zielinski 2000; Timmreck et al. 2012). Once in the stratosphere, the volcanic aerosols do not only influence radiation but also the circulation in the atmosphere. By cooling the tropics more strongly than the high latitudes, due to more incoming solar radiation in low latitudes which can be reflected, the equator-to-pole temperature gradient in the troposphere is decreased. The decreased tropospheric meridional temperature gradient leads to a weakened Hadley circulation as well as weakened subtropical jets (Rind et al. 1992; Zanchettin et al. 2012). Also the Asian summer monsoon is substantially weaker after tropical volcanic eruptions, due to a stronger cooling over land than over ocean (Gillett 2004; Trenberth and Dai

2007; Anchukaitis et al. 2010). Localized heating in the tropical stratosphere, due to absorption of radiation by the volcanic aerosols, leads to changes the high latitude circulation in the northern hemisphere (NH) after volcanic eruptions (Graf et al. 1993). In the winters after volcanic eruptions, a positive phase of the North Atlantic Oscillation (NAO) and associated surface temperature anomalies, consisting of warmer conditions over Northern Europa and Scandinavia and colder conditionals over the Mediterranean and the Middle East, are observed (Robock and Mao 1992). This dynamical response is assumed to originate from stronger climatological westerlies in the polar stratosphere in winter, the so called polar vortex (Kodera 1994).

Modelling the dynamical response of the NH circulation to tropical volcanic eruptions, however, remains challenging. Although the radiative impacts, such as the cooling of the surface at low latitudes and the warming of the tropical stratosphere, are reasonably well captured by the global, coupled climate models, they appear to underestimate the dynamical response of the NH polar vortex and do not simulate a positive NAO phase in the boreal winter following tropical volcanic eruptions (Stenchikov et al. 2006; Driscoll et al. 2012). The global coupled climate models, or Earth system models (ESM), are a necessary and useful tool to make projections into the future to estimate the climate change due to anthropogenic greenhouse gas emissions. But to have confidence in the climate projections, the models need to represent past climate variability reliably. The apparent failure of the climate models to reproduce the dynamical response to volcanic eruption might point to missing features or wrong representation of processes in the models itself, or to a lack of understanding about the mechanism how volcanic eruptions influence the dynamics in the stratosphere and troposphere. In either way, a detailed investigation of the dynamical response to volcanic eruptions in a coupled climate model is necessary and the purpose of this study.

1.1 Aim and outline of the thesis

In this thesis the response of the NH winter climate to strong tropical volcanic eruptions is investigated to identify possible causes for the problems of coupled climate models to reproduce the dynamical impact of tropical volcanic eruptions. While the focus is on the impact on the polar stratosphere and especially on the polar vortex, also the surface climate response will be analyzed. First, the current state of the research will be summarized (section 1.2), followed by the description of the main tool for this analysis, the state-of-the-art Earth system model MPI-ESM (chapter 2). In the framework of the Coupled Model Intercomparison Project phase 5 (CMIP5), the Max Planck Institute for Meteorology (MPI-M) conducted historical simulations from 1850-2005 including all natural (incl. volcanic) and anthropogenic forcings, with two different versions of the MPI-ESM, the MPI-ESM-LR and the MPI-ESM-MR. These two versions differ in the oceanic resolution but also in the vertical resolution in the atmosphere, where the MPI-ESM-MR has a much finer resolution in the stratosphere that allows for a spontaneous development of the QBO in the tropics. Naturally, the question arises **to what extent the higher vertical resolution and the better representation of stratospheric processes improves the volcanic response in the stratosphere and at the**

surface compared to the model version with lower vertical resolution (chapter 3).

While the historical simulations are the basis for most of the analysis in this thesis, additional experiments with a much stronger volcanic forcing compared to the largest eruptions in the historical simulations were carried out as well (chapter 4). The purpose of these simulations is to investigate **whether the MPI-ESM with a stronger volcanic forcing simulates the expected strengthening of the polar vortex**, which is not the case for the comparably smaller eruptions of the historical simulations. Furthermore, the stronger forcing may also yield clearer insights in the exact mechanism how volcanic eruptions influence the NH polar stratosphere.

The apparent failure to reproduce the observed NH winter response to volcanic eruptions is not solely an issue for the MPI-ESM, but a general problem of coupled climate models that participated in the CMIP5. However, a consensus on why models underestimate the volcanic impact has not been reached so far. Based on findings by Kodera and Kuroda (2002), who state that the polar vortex in early winter shows a comparably small interannual variability and is largely radiatively controlled in contrast to mid- and late winter where the interannual variability is large, because the polar vortex in dynamically controlled, I investigate **if the variability of the polar vortex in early winter can influence the response to volcanic eruptions** (chapter 5). Because different climate models exhibit a different variability of the polar vortex, I analyze, in addition to the MPI-ESM, 13 climate models that participated in the CMIP5 with regard to their polar vortex response after volcanic eruptions. The basic idea is that for models with a large early winter variability, the polar vortex is not solely radiatively but also already dynamically controlled. In this case, the response of the polar vortex to volcanic eruptions might be weakened, because the polar vortex will not only respond to the radiative forcing of the volcanic aerosols, but also to wave perturbations. Such behavior would be in contradiction to the findings of Kodera and Kuroda (2002) which is based on reanalysis data and could potentially explain the limited response of the climate models to volcanic eruptions.

Uncertainties in the response to volcanic eruptions arise from three sources: Uncertainty in the volcanic forcing, model uncertainty, and internal variability. A very large 100 member ensemble of MPI-ESM historical simulations provides the opportunity to quantify the uncertainty from internal, interannual variability which is impossible for smaller ensemble sizes and also in the CMIP5 multi-model intercomparison, because different volcanic forcing datasets and different models will contribute to the total uncertainty (chapter 6). The question I address is: **How many ensemble members are needed to identify a significant response to volcanic eruption?** Although I focus on the NH winter stratosphere, I will also examine the mean response and uncertainty of near surface temperature and dynamics. Finally, I will summarize and provide conclusions in chapter 7.

1.2 Current state of the art

1.2.1 The role of the stratosphere in climate

The stratosphere is a layer in the atmosphere situated above the troposphere and below the mesosphere, and extends from about 15 km to 50 km, depending on latitude and season. The lower boundary of the stratosphere is defined by a temperature inversion, the tropopause. Above the tropopause, and in contrast to the troposphere, the temperature increases with height in the stratosphere until a second inversion marks the upper boundary of the stratosphere. The reversal of the vertical temperature gradient in the tropopause is due to the large amount of ozone in the stratosphere. Ozone absorbs a significant amount of the incoming solar short-wave radiation, including harmful ultraviolet radiation. Although the stratosphere is not isolated, but coupled with the troposphere dynamically, radiatively and chemically, the stable stratification of the stratosphere largely prevents exchange of air masses between troposphere and stratosphere and inhibits convection.

With approximately 80% of the total air mass, the troposphere is the dominant layer of the atmosphere. All interactions of the atmosphere with the ocean and the land surface layer as well as our day-to-day weather takes place in this bottom layer. A valid question is therefore why we should care about the stably stratified stratosphere above the troposphere? And indeed, until the 1980s the interaction between troposphere and stratosphere were thought to be primarily one way —the stratosphere passively responding to forcing from the troposphere below (Gerber et al. 2012). But even before that, it was known that the stably stratified stratosphere is not as quiescent as thought in the beginning of the 20^{th} century. Scherhag (1952) discovered violent temperature changes in the polar stratosphere accompanied with wind swings of magnitudes which exceed those observed at the surface. This phenomenon is now known as the Sudden Stratospheric Warming (SSW) event (Labitzke 1972). A meridional circulation from the equator to the pole was revealed by two studies independently (Brewer 1949; Dobson 1956), which is now called Brewer-Dobson-Circulation and is especially important for the ozone transport from the equator, where the ozone is produced, to the high latitudes. The dynamical influence of the troposphere on the stratosphere is primarily due to large scale waves and small scale gravity waves (Charney and Drazin 1961). These waves are generated in the troposphere by instabilities in the atmospheric flow, which are due to e.g. land-sea contrast, orography, convection or fronts. Such waves are also responsible for the SSW events mentioned above. The polar vortex is a powerful westerly wind in the winter hemisphere which is caused by radiative cooling during the polar night. Bursts of planetary waves can destroy the polar vortex, which result in a wind reversal and a heating of the polar stratosphere within days (Matsuno 1971). Waves are also the driver of the quasi-biennial oscillation (QBO), which is an oscillation of easterly and westerly winds in the equatorial stratosphere with a period of 22 to 36 months (Baldwin et al. 2001). Interestingly, one phase of the QBO was first discovered after the eruption of Krakatau in 1883, when the debris of the eruption circled the globe from east to west. When balloon measurements became more frequent in the midst of the 20^{th} century, it was shown that zonally uniform easterly and west-

erly winds originate in the upper stratosphere and propagate down to the tropopause (Veryard and Ebdon 1961). The QBO is driven by vertically propagating waves which deposit easterly and westerly momentum due to radiative attenuation, critical layer absorption and wave breaking (Lindzen and Holton 1968; Holton and Lindzen 1972). An important finding in stratospheric research was the discovery of the ozone hole in southern spring over Antarctica (Farman et al. 1985). Due to anthropogenic release of chlorofluorocarbons (CFC), half of the Antarctic total ozone column is destroyed every austral spring (for an extensive review see Solomon (1999)). A full recovery to 1980 ozone levels is expected to occur around mid to late 21^{th} century, but due to large variability a significant detection ozone recovery is not expected to occur before 2024 (Newman et al. 2006).

Current research, as well as this thesis, focuses on stratosphere-troposphere interactions. In the last two decades, it became clear that the stratosphere is not merely a passive layer responding to forcing from below, but that perturbations in the stratosphere can propagate down to the troposphere and influence surface climate. The signal of an anomalous strong or weak NH polar vortex, defined by the Northern Annular Mode (NAM) which is the dominant mode of intraseasonal variability in the extratropics (Thompson and Wallace 1998), first occurs in the upper stratosphere and often propagates down to the troposphere in approximately one to two weeks and can influence surface climate for up to two months (Baldwin and Dunkerton 1999, 2001). The NAM, sometimes also referred to as the Arctic Oscillation (AO), in the troposphere is characterized by the meridional position of the midlatitude jets, which has a strong impact on surface weather and climate in the NH. A negative NAM index implies an equatorward shift of the midlatitude jet and causes suppressed surface westerlies coinciding with colder weather and more snowfall during wintertime in the northeastern United States and northern Europe (Thompson and Wallace 2001; Tomassini et al. 2012). Vice versa, a positive NAM in the troposphere leads to a poleward shift of the midlatitude jets and advection of warm air to northern Europe. Of course the tropospheric circulation is not solely determined by the stratosphere, but coupling between the strength of the polar vortex in the stratosphere and the midlatitude jet in the troposphere can influence surface conditions (Polvani and Kushner 2002; Gerber and Polvani 2009) and possibly extend the predictability of surface weather (Baldwin et al. 2003), even though extreme polar vortex events are hard to forecast far in advance, as they are initiated in a non-linear process by tropospheric planetary waves (Polvani and Waugh 2004). The enhanced potential for predictability can only be realized in NH winter, when the coupling between stratosphere and troposphere is active (Thompson and Wallace 2000; Charlton and Polvani 2007).

Because tropospheric circulation is influenced by the stratosphere via downward coupling of strong or weak polar vortex events, an important question is what determines the strength of the NH polar vortex in winter. Because the polar vortex responds mainly to the wave forcing from the troposphere (Newman et al. 2001), any change in the amount of wave forcing from the troposphere or in the wave propagation can potentially influence the polar vortex and subsequently the surface (Reichler et al. 2005). Arguably the most prominent natural phenomenon which leads to changes in the tropospheric wave forcing is the El Niño Southern Oscillation (ENSO). van Loon and Labitzke (1987) first showed a statistical relation between ENSO and the extra-

tropical NH stratosphere. They showed that El Niño events are accompanied with a strong Aleutian high and a weak polar vortex in the stratosphere, which has been supported since then by a number of studies (Perlwitz and Graf 1995; Sassi et al. 2004; Manzini et al. 2006; García-Herrera et al. 2006). The weakened polar vortex is associated with a warm temperature anomaly in the polar stratosphere and an increase in the occurrence of stratospheric warmings (Labitzke and Loon 1999). Although a single El Niño event may evolve differently, on average the signal of a weaker and warmer polar vortex propagates downward and influences surface climate (Sassi et al. 2004; Manzini et al. 2006). During La Niña events, the mechanisms work in the opposite sense, but there is some debate whether the effect of La Niña events is statistically distinguishable from neutral conditions (Sassi et al. 2004) and the occurrence of SSW might actually be similar during El Niño and La Niña phases (Garfinkel et al. 2012). Also the QBO, by modulating the propagation of waves in the extratropics, has an impact on the strength and evolution of the NH polar vortex (Holton and Tan 1980; Anstey and Shepherd 2013). The mechanism involves the shift of the zero wind line, which is a critical line for the propagation of planetary waves. The zero wind line separates the westerly winds of the winter hemisphere, where waves can propagate, from the easterly winds in the summer hemisphere, where waves are evanescent (Charney and Drazin 1961). The QBO in its easterly phase shifts the zero wind line poleward and allows more planetary waves to propagate to the high latitudes, where the waves break and ultimately weaken the polar vortex (Holton and Tan 1980). The 11-year solar cycle, by changing the amount of incoming UV radiation, leads to substantial perturbations in stratospheric ozone and subsequent temperature anomalies in the tropics (Haigh 1996; Gray et al. 2010). The temperature anomalies effect the meridional temperature gradient in the stratosphere, which, via the thermal wind balance, has an impact on the polar vortex. The strength of the polar vortex affects the wave propagation in the stratosphere, which in turn can feed back on the vortex itself (Kodera and Kuroda 2002). In recent decades and in the future, the anthropogenic release of greenhouse gases will impact the polar stratosphere and the strength of the polar vortex (Scaife et al. 2012). Most of the recent analyses point towards a weakening of the polar vortex (Karpechko and Manzini 2012). But the robustness of this result has not been established yet and the spread in the magnitude of the weakening of the polar vortex among the models contributes significantly to the spread in Arctic sea level pressure change (Manzini et al. 2014). Finally, observations and theoretical arguments suggest an influence of volcanic eruptions on the polar vortex, which will be discussed in section 1.2.3.

1.2.2 Influence of explosive volcanic eruptions on climate

Strong volcanic eruptions affect the weather and climate on different temporal and spatial scales (Robock 2000; Zielinski 2000; Cole-Dai 2010; Timmreck et al. 2012). The very strong eruption of Tambora 1815 in Indonesia may have caused the so-called "year without summer" where the global averaged temperature decreased by 0.4-0.7 K (Stothers 1984; Auchmann et al. 2012) with exceptionally low temperatures (Rampino and Self 1982) and wet conditions in Europe (Wegmann et al. 2014). The 1883 Krakatau eruption lead to a temperature decrease in the NH of about 0.7 K as

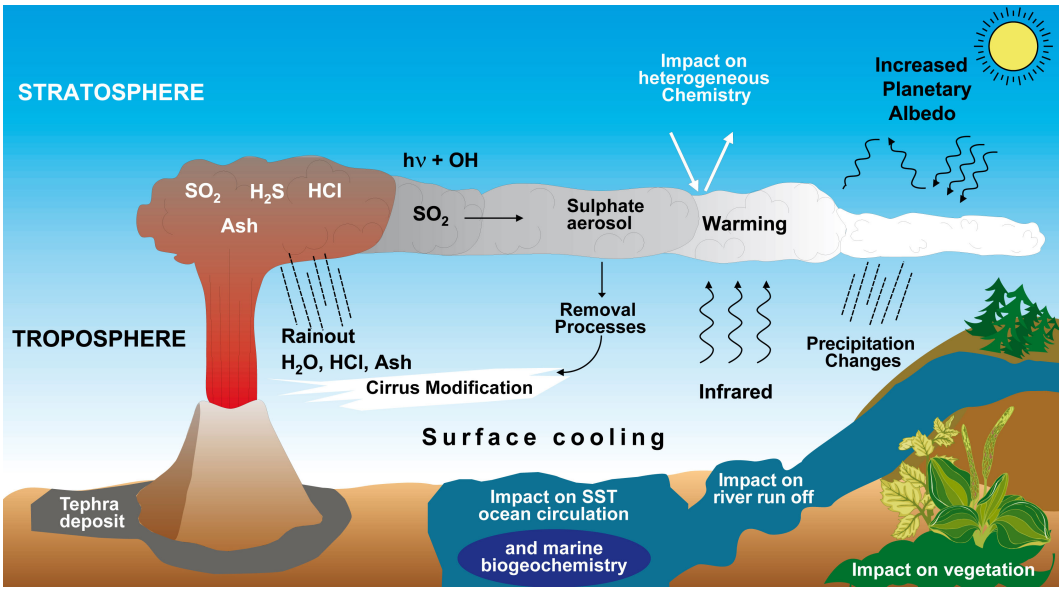

Figure 1.1: Schematic of the volcanic inputs to the atmosphere and their effects on the earth system (from Timmreck (2012)).

seen in proxy records (Robock 2005). In the 2^{nd} half of the 20^{th} Century, the volcanic eruptions of Mount Agung (1963), El Chichón (1982) and Mount Pinatubo (1991) had a significant impact on global weather and climate, which can clearly be seen in observational surface temperature records (Cole-Dai 2010).

A simple schematic (Figure 1.1) explains how volcanic eruptions impact the global climate system. If a volcano erupts, it releases gases such as water vapor (H_2O), carbon dioxide (CO_2), Nitrogen (N_2), sulfur dioxide (SO_2), hydrogen chloride (HCl) and hydrogen fluoride (HF) as well as particulate matter (ash) into the atmosphere (Textor et al. 2004). Ash particles remain largely in the troposphere where they reflect the incoming solar radiation as well as absorb and reemit terrestrial longwave radiation and therefore reduce the diurnal temperature cycle (Robock and Mass 1982; Niemeier et al. 2009). Due to the higher density, the ash is removed relatively quickly out of the atmosphere on a time scale of minutes to a few weeks (Robock 2000). CO_2 and H_2O from eruptions, though being important greenhouse gases, have a negligible effect on the climate due to their high concentration in the atmosphere (Gerlach 2011). The halogen species HCl and HF can have important effects on the atmospheric ozone layer but will be effectively removed from the atmosphere by dissolution in liquid water (Robock 2000; Textor et al. 2004). The most important species with respect to the climate impact of a volcanic eruption is sulfur dioxide. If SO_2 is injected into the stratosphere, it will spread globally within a couple of weeks (Bluth et al. 1992). The SO_2 reacts with hydroxide (OH) and H_2O to form sulfate aerosols (H_2SO_4) which have a typical e-folding lifetime of about 12-14 months (Barnes and Hofmann 1997). Volcanic aerosols of Pinatubo-size eruptions have typical effective radii of about 0.5 μm (Robock 2000) which is approximately the same size as the wavelength of visible light. The aerosols interact with the incoming solar radiation by scattering the light back into space and therefore increasing the planetary albedo. Because the particle size and the wavelength of the visible light are of the same size, some of the light that hits a sulfate aerosol is

scattered forward and increases the diffuse sunlight at earth surface (Mie-Scattering). This forward scattering compensates partly for the reduction in direct sunlight, but the dominant radiative effect is the back scattering into space, leading to a cooling on the surface of the Earth (Robock 2000). This effect is largest at the equator and in the summer hemisphere, because more incoming shortwave radiation reaches the Earth.

Apart from the multi-year climate effect of eruptions such as Pinatubo in 1991, so called "super-eruption" as the Young Toba Tuff eruption approximately 74.000 years BP, have been thought to change the earth climate for even longer timescales (Self 2006). But due to the very large sulfur emissions, the particle size distribution will shift to larger particles and results in a faster fallout, which limits the impact of super-eruptions (Timmreck et al. 2010). Nevertheless, super-eruptions as well as eruptions of the size of Tambora or Pinatubo can have an impact on longer timescales due to ocean and sea-ice interactions. The rapid cooling of the earths surface can lead to substantial changes in the ocean heat content, the sea level height and sea ice concentration (Church et al. 2005; Gleckler et al. 2006; Gregory 2010). Due to reduced solar flux at the surface, the sea ice extent increases in the Arctic after volcanic eruptions and might even have triggered the so called Little Ice Age (Miller et al. 2012), but because of ocean circulation changes, the inter-hemispheric response of the sea ice to large volcanic eruption might not be symmetrical (Zanchettin et al. 2014). However, in certain regions, e.g. the Arctic, large volcanic eruption are a major source of near-decadal (Stenchikov et al. 2009; Segschneider et al. 2013; Zanchettin et al. 2012, 2013b) and even multi-decadal-to-centennial fluctuations (Zhong et al. 2011).

In contrast to the troposphere, which cools due to the increased planetary albedo, the stratosphere shows a positive temperature anomaly after volcanic eruptions (Quiroz 1983; Angell 1997; Stenchikov et al. 1998). Stenchikov et al. (1998) show that the heating is due to absorption of near infra-red (NIR) radiation at the top of the aerosol cloud and absorption of upwelling longwave (LW) radiation from the Earth at the bottom of the aerosol cloud. After the eruption of Pinatubo an increase of the temperature in the tropical stratosphere of 2-3 K was observed (Labitzke and McCormick 1992), but the magnitude of the anomaly is also influenced by other factors such as the phase of the QBO, the concentration of ozone and water vapor, and possible feedback mechanisms (Ramachandran et al. 2000). It has been shown in model simulations that the easterly phase of the QBO after the Pinatubo eruption reduced the positive temperature anomaly at 30 hPa by 1-2 K (Thomas et al. 2009a). The positive temperature anomaly in the tropical stratosphere has implications for the surface climate via dynamical mechanisms, which are discussed in the next section.

1.2.3 Dynamical impact of strong volcanic eruptions

Current understanding of the mechanism how tropical volcanic eruptions influence the Northern Hemisphere circulation

The radiative perturbation of the Earth system due to volcanic aerosols does not only influence the temperature itself, but leads to changes in atmospheric circulation. After tropical volcanic eruptions, the lower latitudes exhibit a stronger cooling compared to

the mid- and high latitudes, because the major part of the sulfate aerosol mass stays in lower latitudes (Trepte et al. 1993; Arfeuille et al. 2014) and because the incoming solar radiation which can be reflected is largest in the tropics. The differential cooling decreases the equator-to-pole temperature gradient in the tropics, which weakens the subtropical jets (Zanchettin et al. 2012) and, together with the increased static stability due to the warming of the lower stratosphere, reduces the intensity of the Hadley Cell (Rind et al. 1992). Also the slowdown of the global water cycle and weakening of the Asian summer monsoon circulation, due to larger cooling over the landmasses of Asia compared to the Indian Ocean, have been found in previous studies (Gillett 2004; Oman et al. 2006; Trenberth and Dai 2007; Anchukaitis et al. 2010; Joseph and Zeng 2011) as well as a weaker monsoon over Africa, which is dynamically linked to increased precipitation over southern Europe in the summer season (Wegmann et al. 2014). The response of the Southern Annular Mode (SAM) to tropical volcanic eruptions is ambiguous. Depending on the eruption magnitude, season and reanalysis dataset used, a negative SAM index or a non-significant response is identified (Crooks and Gray 2005; Robock et al. 2007). But the simultaneous occurrence of El Niño events possibly interfere with the volcanic signal (Crooks and Gray 2005). Model simulations on the other hand simulate a stronger polar vortex in southern hemisphere and a corresponding positive SAM index at the surface (Karpechko et al. 2010).

Changes in the NH circulation in the first two winters after tropical volcanic eruptions lead to the prominent "volcanic winter warming", consisting of anomalous positive temperatures over Northern Europe, Siberia and the United States, and anomalous negative temperatures over the Labrador Sea and the Middle East (Robock and Mao 1992, 1995). The exact mechanism is not clear, but the commonly assumed theory explains the changes in circulation by the increased equator-to-pole temperature gradient in the stratosphere (Figure 1.2). The heating due to NIR and LW absorption is strongest in the tropics (Labitzke and McCormick 1992), which increases the meridional temperature gradient. By the thermal wind relation, this creates a strengthening of the climatological westerlies in the stratosphere, the polar vortex or polar night jet (Graf et al. 1993; Kodera 1994; Perlwitz and Graf 1995). Through stratosphere-troposphere coupling, the signal of the stronger polar vortex can influence the troposphere by shifting dynamical indices such as the AO or the NAO to a positive phase (Baldwin and Dunkerton 2001; Gerber et al. 2012). The NAO (which is essentially the AO over the Atlantic sector (Christiansen 2008)) in its positive phase is associated with positive temperature anomalies over Northern Europe, Siberia and the United States and negative temperature anomalies over Greenland, the Mediterranean and the Middle East (Hurrell 1995; Thompson and Wallace 1998), which is the temperature pattern observed after tropical volcanic eruptions.

However, Stenchikov et al. (2002) state that the stratospheric radiative forcing from volcanic aerosols is largely confined to lower latitudes and may not have a significantly direct effect on the polar vortex strength. They propose two additional mechanisms through which major tropical eruptions influence the polar vortex: First, ozone depletion at high latitudes, primarily due to Clorine activation on aerosol surface, lead to cooling of the polar winter stratosphere, which further increases the meridional temperature gradient resulting in stronger westerlies. However, before large amounts of Clorine were in the atmosphere, the response to volcanic eruptions was apparently as

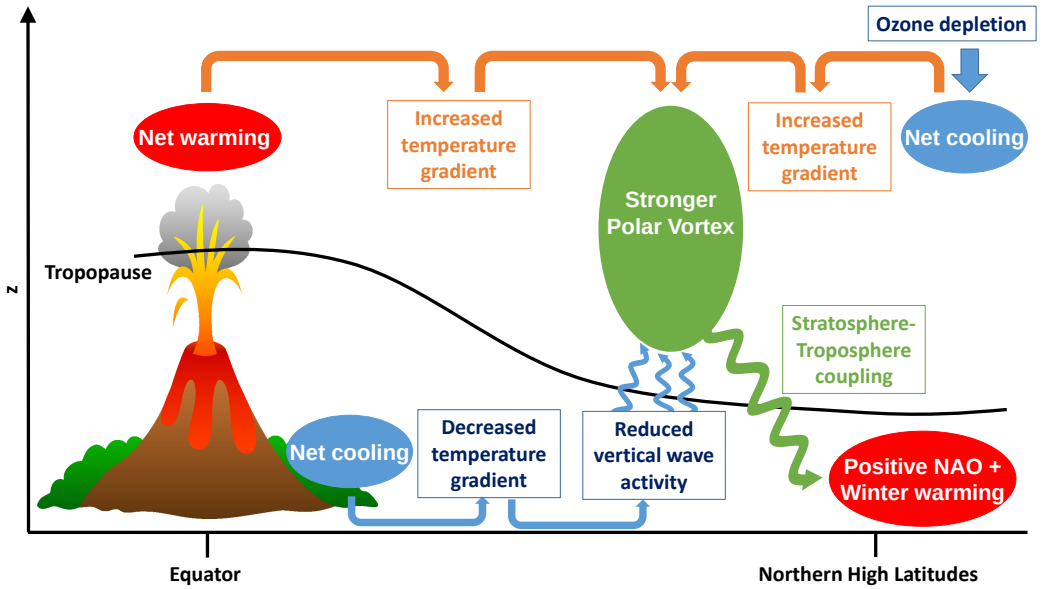

Figure 1.2: Schematic of the dynamical impact of tropical volcanic eruptions on the NH polar vortex.

large as for Pinatubo and El Chichón combined, indicating that ozone loss in high latitudes is unlikely to be a major factor (Marshall et al. 2009). Second, a weaker meridional temperature gradient in the troposphere, due to radiative cooling of the surface in the tropics (Robock and Mao 1995), is proposed to lead to a decreased upward wave flux (Stenchikov et al. 2002). The variability of the polar vortex is mainly determined by the wave flux into the stratosphere (Newman et al. 2001). A decreased wave flux, as proposed after volcanic eruptions, would lead to a stronger and less disturbed polar vortex (Polvani and Waugh 2004). However, reanalysis data show an increased wave flux after the last volcanic eruptions (Graf et al. 2007), which may be due to the eruptions, or alternatively to the strong El Niño events which have coincided with the eruptions.

Observations of the NH dynamical response

Observations of the polar vortex in volcanically-disturbed winters by satellite and/or radiosondes are restricted to the recent past and include only three major tropical eruptions: Agung in 1963, El Chichón in 1982, and Pinatubo in 1991. Based on this small sample size a strengthening of the polar vortex can be observed (Kodera 1995; Graf et al. 2007). However, the winter polar NH stratosphere is a region prone to large interannual variability (e.g., Kodera (1995)). The evolution of the polar vortex is influenced by several phenomena remote from the polar stratosphere, e.g. ENSO, QBO, CO_2, solar influences and volcanic eruptions (see section 1.2.1). Disentangling the effects of all phenomena is difficult, because the combination of forcing factors may not be linear (Camp and Tung 2007; Calvo et al. 2009) and subject to sampling biases (Graf et al. 2014). Because of the relatively short record of stratospheric observations, the effect of volcanic eruptions on the polar vortex is especially hard to distinguish from internal variability.

In contrast to the stratosphere, observational- and paleo records of surface variables cover a much longer timespan and the dynamical response to tropical volcanic eruptions can be identified with larger confidence. Robock and Mao (1992) were the first to find a consistent pattern of positive surface temperature anomalies over Northern Europe and negative surface temperature anomalies in the Middle East averaged over 12 largest eruptions from 1883 to 1992 when they removed the temperature signal of ENSO. They included also high latitude eruptions but concluded in a following study that the observed winter warming signal over the continents is mainly due to the tropical eruptions (Robock and Mao 1995). By using a combination of multi-proxy surface temperature reconstructions and modern instrumental data, Shindell et al. (2004) extended the analysis of the volcanic response back in time to the 17^{th} century and confirm that the temperature anomalies in the winter following a tropical volcanic eruptions resemble a positive phase of the NAO. The mean response of warming over the eastern part of the US, northern Europe and Siberia as well as the cooling over the Middle East is significant at 95% confidence level. They state, however, that the standard deviation of the surface temperature response is larger than the mean signal nearly everywhere, indicating that the anomaly following a single eruption is unlikely to be representative of the mean. Also based on independent multi-proxy reconstructions, Fischer et al. (2007) analyzed the post-volcanic temperature (since 1500), precipitation and geopotential height (since 1769) anomalies over Europe. A positive phase of the NAO connected with significantly warmer and wetter conditions over Northern Europe confirms the assumed dynamical circulation response in the winter following the eruptions. Explicitly focusing on the circulation changes after 13 volcanic eruptions, Christiansen (2008) analyzed monthly mean sea level pressure data for the NH since 1873 and found that the NAO is excited in the first post-eruption winter with statistical significance at the 95% confidence level.

So although there are uncertainties in the proxy reconstructions and their spatial coverage decreases the further one goes back in time, the dynamical response to volcanic eruptions, i.e. the shift of the NAO to a positive phase and the according temperature anomalies over Europe and the United States, seems to be robust in the NH troposphere. There are indications that the positive phase of the NAO originates from a strong polar vortex in the stratosphere. But Graf et al. (2014) found substantial differences between the winter warming pattern under strong polar vortex conditions in volcanically-disturbed winter and volcanically-undisturbed winters in reanalysis data. However, due to the large internal variability of the NH polar stratosphere and the small sample size of volcanic eruptions which are observed, general statements about the state of the polar vortex and stratosphere-troposphere interactions after volcanic eruptions should be taken with care.

Modelling the NH dynamical response

Since the first findings of the volcanic winter warming in observations and the theoretical explanation of this phenomenon, climate models have been used to test and understand the dynamical response to volcanic eruptions. A study by Graf et al. (1993) performed perpetual January simulations with the low resolution (T21) Global Climate Model (GCM) ECHAM2. Using the stratospheric aerosol loading and pattern of the

El Chichón eruption in 1982, they reproduced the circulation response and temperature patterns following tropical volcanic eruptions in the NH. A following study with an improved GCM (ECHAM4) including a full seasonal cycle, a better representation of aerosol parameters by Stenchikov et al. (1998), and interactive calculation of the aerosol radiative effects could successfully reproduce the observed circulation and temperature anomaly following the Pinatubo eruption, but only when using prescribed climatological sea surface temperatures (SST) (Kirchner et al. 1999). If they prescribed the observed SST field, which included an El Niño in the winter of 1991/1992, the simulations did not capture the observed circulation and surface temperature response. Stenchikov et al. (2002, 2004) used the SKYHI GCM in two studies and were able to reproduce the observed AO circulation change following volcanic eruptions. They emphasized that ozone depletion in high latitudes after volcanic eruption can contribute to the strengthening of the polar vortex and that surface cooling of the tropical troposphere alone, i.e. with suppressed heating of the tropical lower stratosphere, can produce a positive AO as well (Stenchikov et al. 2002). In the second study, they investigated the role of the QBO after the Pinatubo eruption (Stenchikov et al. 2004). They showed that the aerosol perturbations to the NH winter circulation are significantly affected by the phase of the QBO, which can enhance the effect on the AO. In both studies however, the atmospheric model was not coupled to an ocean model, but used prescribed climatological SSTs.

Coupled models on the other hand seem to have problems in reproducing the dynamical response to volcanic eruptions. Stenchikov et al. (2006) noted that the response of models that participated in CMIP3 tend to simulate a positive AO in the NH polar stratosphere, but the magnitude of the response in the stratosphere and on the surface, i.e. the winter warming pattern, was much too weak. They hypothesized that the insufficient representation of the stratosphere of most coupled models hampers the adequate treatment of stratospheric processes. However, simulations with the HadGEM1 with two different vertical resolutions did not show any improvement of the NH winter response to volcanic eruptions in the model version with higher vertical resolution over the low resolution version (Marshall et al. 2009). But also the generally too strong climatological polar vortex of the CMIP3 models could potentially degrade the susceptibility to external forcing and weaken the propagation of stratospheric anomalies to the troposphere (Otterå 2008). Simulations with the coupled NCAR Community Climate System Model (CCSM3) of volcanic eruptions in the 13^{th} century showed a stronger polar vortex and positive temperature anomalies over Northern Europe and Siberia (Schneider et al. 2009). However, while the temperature anomalies over Eurasia match observations, the simulations miss the positive temperature anomalies over the US and the sea level pressure anomalies do not resemble a positive phase of the NAO. In contrast, Muthers et al. (2014) used the coupled SOCOL3-MPIOM and found in addition to the stronger polar vortex a shift of the NAO to a positive phase and both, the warming over Eurasia and the North American continent. However, they forced the model with volcanic forcing corresponding to the very large Tambora eruption (approximately 3-4 times larger than Pinatubo) and therefore it is not clear whether the dynamical response still holds for eruptions of smaller magnitudes. Furthermore, they pointed out that the dynamical response is sensitive to the prescribed ozone climatology. Only if the meridional ozone gradient in the lower stratosphere is large, the model

captures the shift of the NAO and the subsequent temperature anomalies significantly.

Apart from these two exceptions, the assessment of the current generation of coupled climate models revealed that on average the models still underestimate or completely miss the dynamical response to tropical volcanic eruptions. Driscoll et al. (2012) analyzed historical simulations from 1850-2005 of 13 models that participated in the CMIP5 and find a general failure of the models to simulate a stronger polar vortex, a positive NAO, or the NH Eurasian winter warming. In contrast to CMIP3 models, a number of models of the current generation have a reasonably well-resolved stratosphere, which has been suggested as a prerequisite in order to successfully simulate the dynamical response to volcanic eruptions (Shindell et al. 2004; Stenchikov et al. 2006). However, a systematic difference in post-eruption geopotential height anomalies in the polar stratosphere between models with or without well-resolved stratosphere could not be found (Charlton-Perez et al. 2013). Moreover, Toohey et al. (2014) question the mechanism by which tropical volcanic eruptions influence the NH polar vortex. Instead of a direct enhancement of the meridional temperature gradient from the equator to the pole, they hypothesize based on model simulations that changes in the stratospheric wave activity indirectly affect the polar vortex.

Chapter 2

Data and methods

2.1 Model description

The main tool for the analysis of the climatic response to tropical volcanic eruptions is the state-of-the-art coupled atmosphere-ocean-land model Max Planck Institute Earth System Model (MPI-ESM). The MPI-ESM consists of different components, which are coupled via the exchange of energy, momentum, water, and trace gases. The different components are the atmospheric model ECHAM6 (Stevens et al. 2013), including the land surface model JSBACH (Reick et al. 2013), and the ocean model MPIOM (Jungclaus et al. 2013), including the ocean biogeochemistry model HAMOCC (Ilyina et al. 2013). The components of the MPI-ESM are coupled through the OASIS3 coupling software (Valcke 2013).

Of the MPI-ESM exist different configurations which differ in their horizontal and vertical resolution in the atmosphere as well as in the ocean component. Two configurations are used in the framework of this thesis, the so called "low resolution" (MPI-ESM-LR) and the "mixed resolution" (MPI-ESM-MR) configurations. The MPI-ESM-LR has a horizontal resolution of the atmospheric component given by a triangular truncation at 63 wave numbers (T63, approximately 1.9° x 1.9° at the equator) and 47 vertical layers extending to 0.01 hPa. The ocean has a GR1.5 grid with two poles, one over Antarctica and one over Greenland. The MPI-ESM-MR has the same horizontal resolution in the atmosphere as the MPI-ESM-LR, but a higher vertical resolution of 95 layers. In the lower and middle troposphere, the vertical grids of the MPI-ESM-LR and MPI-ESM-MR are identical, but in the stratosphere the MPI-ESM-MR grid is much finer (approximately 800 m) compared to the MPI-ESM-LR (approximately 2-3 km). Owing to the much finer resolution, the MPI-ESM-MR allows for the vertical propagation of a wave spectrum that drives momentum deposition in the middle stratosphere. This spectrum of waves drives the quasi-biennial oscillation (QBO) in the tropical stratosphere, which is only present in the MPI-ESM-MR, whereas in the MPI-ESM-LR easterly winds are simulated in the middle stratosphere at low latitudes. Furthermore, the MPI-ESM-MR has a finer horizontal resolution in the ocean (0.4° on a tri-polar grid).

These two configurations of the MPI-ESM were used to perform simulations in the framework of the Coupled Model Intercomparison Project 5 (CMIP5) (Taylor et al. 2011). Two sets of these simulations are used in this thesis. First, a 1000-year control simulation under stationary preindustrial boundary conditions of the MPI-ESM-LR.

Second, historical simulations covering the period 1850 to 2005 of both configurations. The historical simulations are forced with observed changes in natural and anthropogenic parameters (Giorgetta et al. 2013). The anthropogenic forcing include well-mixed greenhouse gases such as Carbon-dioxide (CO_2) and Methane (CH_4), anthropogenic sulfate aerosols as well as man-made land-use change. The natural forcing include variations of the Earth orbit, variations in the solar irradiance, i.e. the 11-year solar cycle, seasonally varying tropospheric aerosols and stratospheric aerosols due to volcanic eruptions, which are described more in detail in chapter 2.1.1. Ozone concentrations in the historic simulations are prescribed according to the data of Cionni et al. (2011). For stratospheric ozone, this dataset provides zonally averaged values and only considers variability caused by ozone depleting substances and by solar variability. Effects related to volcanic aerosol are not represented. Three and ten realization of the historical simulations were performed for the MPI-ESM-MR and MPI-ESM-LR, respectively. The realizations differ in their initial state only, as different starting years were selected for the initialization of the realizations from the respective preindustrial control simulations.

2.1.1 Volcanic forcing

Volcanic aerosol forcing in the MPI-ESM CMIP5 historical simulations is prescribed by an extended version of the Pinatubo aerosol data set by Stenchikov et al. (1998) (Fig. 2.1). This data set is based on measurements of aerosol extinction at 1.02 μm from the satellite instrument SAGE II, with gaps filled with data from ground based LIDAR system, and estimates of effective radii derived from instruments on the Upper Atmosphere Research Satellite. The data set contains monthly mean zonal averages of the aerosol extinction, single scattering albedo and asymmetry factor as a function of pressure and wavelength. The latitudinal resolution is 2° from 89°S to 89°N. The data is given at 40 pressure levels and is interpolated to the actual hybrid model layers during the simulations. This dataset, and its predecessor of Sato et al. (1993), is used in roughly half of the CMIP5 models and it was successfully applied in earlier model studies (Stenchikov et al. 2004; Thomas et al. 2009a,b). Subsequent updates on the SAGE II retrievals have led to significant changes in the aerosol extinction in comparison to the Stenchikov dataset (Arfeuille et al. 2013). However, although the magnitude and altitude of the lower stratospheric heating after the Pinatubo eruption differs between the volcanic forcing dataset by Stenchikov et al. (1998) and a new dataset called SAGE 4λ by Arfeuille et al. (2013), there is no significant difference between these two volcanic forcing datasets with regard to the dynamical response in NH high latitudes (Toohey et al. 2014).

Apart from chapter 3, where the average response of 9 tropical volcanic eruptions will be analyzed, three eruptions will be of special importance in this thesis: Krakatau (1883), El Chichón (1982) and Pinatubo (1991). The eruptions of Krakatau and Pinatubo are of interest as these two are the largest eruptions in the historical period. The eruption of El Chichón is smaller, but one of two eruptions only for which satellite observations exist. The Krakatau eruption took place in August 1883 on an island between Java and Sumatra, Indonesia at 6°S (Rampino and Self 1982) and the

Pinatubo erupted in June 1991 on the Philippine island Luzon at 15°N (Bluth et al. 1992). Satellite based measurements give an estimation of the injected mass of SO_2 into the stratosphere by the Pinatubo eruption of about 17 Tg (Guo et al. 2004). While ice core data generally imply Krakatau produced a slightly smaller stratospheric aerosol loading compared to Pinatubo (Gao et al. 2008; Sigl et al. 2014), based on pyrheliometer data, Sato et al. (1993) estimated the radiative forcing by Krakatau to be slightly larger than that of Pinatubo. The spatial distribution of the AOD for Krakatau is close to the hemispheric mirror-image of the satellite-based Pinatubo forcing (http://data.giss.nasa.gov/modelforce/strataer/), with fairly equal hemispheric partitioning of the AOD. El Chichón erupted in April 1982 in Mexico at 17°N with an estimated lower stratospheric SO_2 mass of 7 Tg (Bluth et al. 1997).

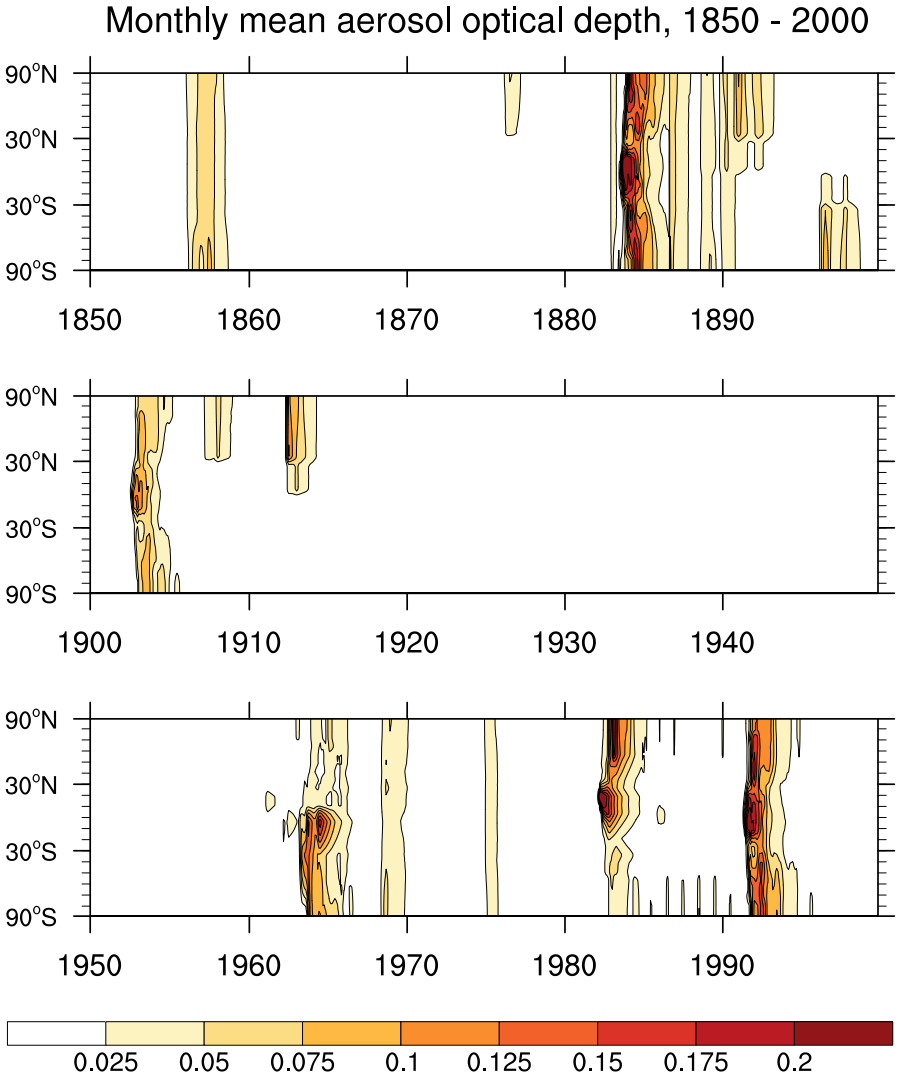

Figure 2.1: Monthly mean zonal averaged aerosol optical depth at 0.55 μm from 1850 to 2000 (Stenchikov et al. 1998) as used in the MPI-ESM historical simulatons.

2.1.2 Model performance

The MPI-ESM, as part of the CMIP5 model ensemble, has been used in numerous studies and is well documented and evaluated (see special issue of the Journal of Advances in Modelling Earth Systems (Stevens 2013)). Generally, the MPI-ESM is in good agreement with observations in terms of simulating the mean climate of the historical period (Giorgetta et al. 2013). However, the global mean surface temperature after volcanic eruption deviates from observation. The MPI-ESM simulates a too strong cooling of the surface which suggests that either the volcanic forcing or the model response to volcanic perturbations is too strong. The overestimation of the volcanic surface cooling is not solely a problem of the MPI-ESM, but is also found in the multi-model mean of 13 different CMIP5 models (Driscoll et al. 2012). Like many coupled ocean-atmosphere models, the MPI-ESM has problems in simulation the sea surface temperature (SST) in the upwelling regions west of the continents and shows too low temperatures in the equatorial Pacific (Jungclaus et al. 2013), which leads to precipitation biases over this areas (Stevens et al. 2013).

Of particular interest for the purpose of this thesis is the performance of the MPI-ESM in the middle atmosphere. A comprehensive assessment of the response of the middle atmosphere to anthropogenic a natural forcings was done by Schmidt et al. (2013). They point out that in general the simulated zonal average patterns of temperature and zonal wind are in good agreement with ERA-40 reanalysis data in the annual as well as NH winter mean of the recent past (1970-2000). The MPI-ESM-LR can reproduce the observed daily and interannual variability of the NH stratosphere (Charlton-Perez et al. 2013) and simulates a similar frequency of Sudden Stratospheric Warming (SSW) events, which are an important manifestation of stratospheric intraseasonal winter variability in the NH. The seasonal distribution of the SSW is however not captured well, as there are too many warming in early winter (Schmidt et al. 2013). The QBO, which is only simulated in the MPI-ESM-MR, shows a realistic period of 28 months but a too strong amplitude (Krismer et al. 2013). The Brewer-Dobson Circulation (BDC), a meridional circulation which transports Ozone from the Equator to high latitudes, is of comparable magnitude to reanalysis data (Bunzel and Schmidt 2012).

Important in the context of this thesis is the response of the NH polar stratosphere to volcanic forcing and the stratosphere-troposphere coupling. Thus, the MPI-ESM needs to capture not only the climatological state and the variability, but also the response of the NH polar vortex to different forcings and the downward propagation of polar vortex anomalies. Schmidt et al. (2013) applied a multiple-linear regression method to isolate the response of the middle atmosphere to the forcings of El Niño, volcanic aerosols, solar irradiance, the QBO (only for the MPI-ESM-MR), and CO_2. The response of the NH polar vortex in boreal winter to the natural forcings is generally in agreement with observations, but the magnitude of the response is too small. This is not only the case for volcanic eruptions (Driscoll et al. 2012), but also for the polar vortex response to the change in total solar irradiance and the El Nino Southern Oscillation (ENSO). However, because the polar vortex anomalies in the high latitudes are supposed to propagate downwards during the course of the winter (Kodera and Kuroda 2002; Cagnazzo and Manzini 2009), analysis of solar and ENSO signals with higher temporal resolution than the annual and winter average of Schmidt et al. (2013) potentially yields more detailed

results. The MPI-ESM is able to capture the downward propagation of strong and weak polar vortex events (Reichler et al. 2012; Bunzel et al. 2013; Manzini et al. 2014) and simulates realistically the dominant mode of variability in the NH winter (Cattiaux and Cassou 2013). Also the leading Empirical Orthonogal Function (EOF) of the DJF mean sea level pressure over the North Atlantic region compares well with observations (Driscoll et al. 2012). Thus, the MPI-ESM is able to simulate all important processes in reasonable agreement with observations. A more detailed investigation of the radiative and dynamical response of the MPI-ESM to tropical volcanic eruptions is provided in chapter 3.

2.2 Reanalysis datasets

In order to evaluate the simulated response to volcanic eruptions, the model must be compared to observational datasets. Unfortunately, observations of the middle atmosphere are usually sparse on the spatial scale and do not cover a long time period. To allow for a comprehensive analysis of global-scale processes, models are used to extend the existing observational time series to global datasets with high temporal resolution. These datasets are referred to as reanalysis datasets. Two of these reanalysis datasets are used in this theses, the ERA-40 and the ERA-Interim, both from the European Centre for Medium-Range Weather Forecasts (ECMWF).

The ERA-Interim is the most state-of-the-art reanalysis dataset of the ECMWF (Dee et al. 2011). It covers the time period from January 1979 until present day, thus it include the major tropical volcanic eruptions of El Chichón in 1982 and Pinatubo in 1991. The temporal resolution of the dataset is 6 hours and the spatial resolution T255 with 60 vertical layers extending from the surface to 1 *hPa*. Due to improved model physics and implementation of the most recent observational time series, the ERA-Interim can be considered as the best estimation of the real atmosphere for comparing with model data.

The disadvantage of the ERA-Interim is the relatively short time coverage and, especially in the case of volcanic eruptions, the absence of data prior to 1979. Therefore, I use a second reanalysis dataset, the predecessor of ERA-Interim called ERA-40 (Uppala et al. 2005). The ERA-40 is a 40-year reanalysis dataset covering the period from September 1957 to August 2002 with 6-hourly temporal resolution. Its spatial resolution is lower compared to ERA-Interim with T159 but has also 60 vertical layers extending from the surface to 1 *hPa*. Satellite data are incorporated since 1972 and cloud motion winds since 1979. Hence, at least before the 1970s, the ERA-40 data in the middle and upper atmosphere can almost entirely considered to be model data. However, owing to its comparably long time period of 40 years, the ERA-40 dataset is valuable to obtain good statistics especially in regions such as the polar vortex, where the interannual variability is large. Furthermore, it includes the volcanic eruptions of Agung in 1964 and Fuego in 1974.

All information provided has been acquired from the ECMWF website (http://www.ecmwf.int), where also additional details can be found.

2.3 Methods

Throughout this thesis, I analyze the response to tropical volcanic eruptions and therefore calculate anomalies in post-eruption winters with respect to a reference period. Because I use the historical simulations, i.e. transient climate simulations, it is not meaningful to apply a common reference period for all volcanic eruptions. In accordance with previous studies (Stenchikov et al. 2006; Driscoll et al. 2012), I define an individual reference period for each eruption to account for different climatic background states. The length of the each individual reference period is limited by the preceding eruption. For example, Pinatubo erupted in June 1991 and the first post-eruptions winter is the winter of 1991-1992. The chosen reference period spans the winters 1984-1985 to 1990-1991. Winter prior to 1984-1985 cannot be taken into account due to the eruption of El Chichón in April 1982. Details for each eruption and the corresponding reference period are provided in chapter 3. However, different background conditions could be a non-negligible factor that can influence the surface temperature and ocean dynamics response to a volcanic eruption on decadal time scales (Zanchettin et al. 2013a). Nevertheless, for the short term stratospheric dynamical response it can be justified to average the response to eruptions in different background conditions as it was done for the assessment of the volcanic response in CMIP3 and CMIP5 simulations (Stenchikov et al. 2006; Driscoll et al. 2012). The post-eruption anomalies are calculated by subtracting the variable of interest in the year after the volcanic eruption from the variable averaged over the years of the reference period. The statistical significance of anomalies is assessed based on a two-tailed t-test.

Chapter 3

The impact of volcanic eruptions in MPI-ESM configurations with different vertical resolution

3.1 Introduction

One suggestion why coupled global climate models fail to reproduce the dynamical response to tropical volcanic eruptions is the possibly insufficient resolution of the stratosphere (Shindell et al. 2004; Stenchikov et al. 2006). But previous studies suggest that there is no evidence that a well resolved stratosphere significantly improves the volcanic signal in the polar stratosphere (Charlton-Perez et al. 2013; Marshall and Scaife 2009). However, both studies only distinguish whether the models have the upper model lid within the stratosphere (low-top) or above the stratopause (high-top). Increasing the vertical resolution of the stratosphere even further as most of the CMIP5 high-top models leads to a better representation of dynamical processes such as wave propagation in the stratosphere (see 2.1) and therefore has the potential to improve the response to volcanic eruptions. In an assessment of the middle atmosphere response to anthropogenic and natural forcing in two configurations of the high-top model MPI-ESM with different vertical resolution, Schmidt et al. (2013) found indications that the configuration with higher vertical resolution captures better the observed volcanic response in the stratosphere, based on a multiple linear regression analysis. In their study however, the focus was on the response of the middle and upper atmosphere only, and a comprehensive study of the volcanic signal on the troposphere was beyond their scope. Following on to this study, I analyze the stratospheric and surface response to tropical volcanic eruption in these two configurations of the high-top model MPI-ESM with different vertical resolution. I will examine the volcanic signal from the initial perturbation in the equatorial stratosphere to its effect on the surface climate in boreal winter.

3.2 Data and Methods

In this section I analyze the volcanic response of the MPI-ESM in two different configurations: the MPI-ESM-LR and MPI-ESM-MR (see chapter 2 for a detailed model

Table 3.1: Major tropical and sub-tropical volanic eruptions from 1860 to 2005. Years refer to the respective end date of the NH winter season. Stratospheric SO_2 injection estimates are from Stothers (1996), Bluth et al. (1997), Andres and Kasgnoc (1998), and Stothers (2001)

	Eruption date	Latitude	Winters analyzed	Referece period	Lower stratosphere SO_2 mass (Tg)
Krakatau	Aug 27, 1883	6.10°S	1884/1885	1860-1883	44
Tarawera	Jun 10, 1886	38.23°S	1887/1888	1860-1883	4-5
Bandai	Jul 15, 1888	36.60°S	1889/1890	1860-1883	4
Santa María	Oct 24, 1902	14.76°N	1904/1905	1890-1902	30
Quizapu	Apr 10, 1932	35.65°S	1932/1933	1915-1932	3
Agung	Mar 17, 1963	9.34°N	1964/1965	1935-1955	20
Fuego	Oct 10, 1974	14.47°N	1976/1977	1966-1974	4
El Chichón	Apr 4, 1982	17.36°N	1983/1984	1977-1982	7
Pinatubo	Jun 15, 1991	15.13°N	1992/1993	1985-1991	20

description). Available for this analysis are ten ensemble members of the MPI-ESM-LR and three ensemble members of the MPI-ESM-MR of the CMIP5 historical simulations from 1850-2005 (Giorgetta et al. 2013). In the same way as in the study of Driscoll et al. (2012), the nine largest tropical and sub-tropical eruptions (between 40°N and 40°S) are selected based on their SO_2 emissions (see Table 3.1) and anomalies for each eruption are calculated as differences of the first and second winter (December-January-February, DJF) after the eruption with respect to an individual reference period before the eruption (see chapter 2.3). In contrast to the study of Driscoll et al. (2012), I focus on a single coupled climate model but use a larger ensemble for the MPI-ESM-LR (only 3 ensemble members were included in the study of Driscoll et al. (2012)) and take into account a second configuration of the same model but with a better resolved stratosphere to investigate the possible improvements of a higher vertical resolution.

The North Atlantic Oscillation (NAO) Index is calculated to investigate the impact of volcanic eruptions on the surface pressure in the north Atlantic region. The first Empirical Orthogonal Function (EOF) is obtained of monthly DJF mean sea level pressure (SLP) anomalies north of 20°N and between 110°W and 70°E. The pressure at each grid point is weighted by the square root of cosine of the respective latitude. The NAO-Index is defined as the principal component of the monthly SLP anomalies projected onto the first EOF.

I compare the model simulations to the ERA-40 reanalysis (Uppala et al. 2005) from September 1957 to August 2002 produced by the European Center for Medium-Weather Forecast (ECMWF). In contrast to the ERA-Interim dataset (Dee et al. 2011), the ERA-40 include the eruptions of Agung in 1964 and Fuego in 1974. Therefore, I choose for this analysis the ERA-40 dataset over the newer ERA-Interim dataset.

3.3 Results

3.3.1 Radiation and temperature response in the middle atmosphere

In the presence of volcanic aerosols, the planetary albedo increases, hence more incoming solar radiation is scattered back into space. Distinct positive anomalies of the globally averaged, de-trended and de-seasonalized 3-months running mean outgoing shortwave radiation anomaly at the top of the atmosphere (TOA) indicate the presence of volcanic aerosols (Fig. 3.1). The TOA short wave anomaly can be seen as proxy of the global radiative forcing of the volcanic eruptions. In this way, it is possible to identify the largest perturbations of the climate system due to stratospheric aerosols. Especially the eruptions of Krakatau (1883), Santa María (1902), Mount Agung (1963), El Chichón (1982) and Mount Pinatubo (1991) show a substantial increase in the globally averaged outgoing short wave radiation at the TOA up to 5 W/m^2. Comparing the two model configurations, no substantial difference can be seen, indicating that the radiative forcing is the same in both, the LR and the MR configuration.

In addition to reflecting solar radiation back to space, the aerosol cloud absorbs parts of the incoming solar and the upwelling near infra-red radiation which leads to an increase

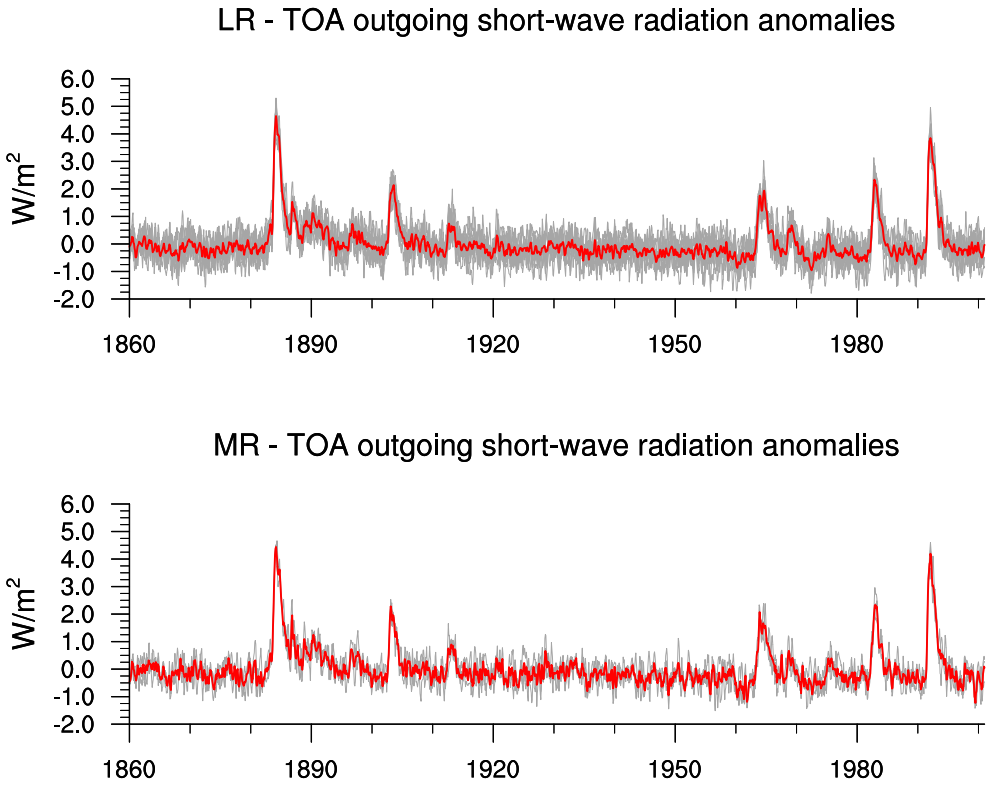

Figure 3.1: 3-months running mean of global averaged de-trended and de-seasonalized top of the atmosphere outgoing shortwave radiation anomalies [W/m^2] for the MPI-ESM-LR (top) and the MPI-ESM-MR (bottom), over the period of 1860-2005. Grey lines show the individual ensemble members, the red line indicates the ensemble average.

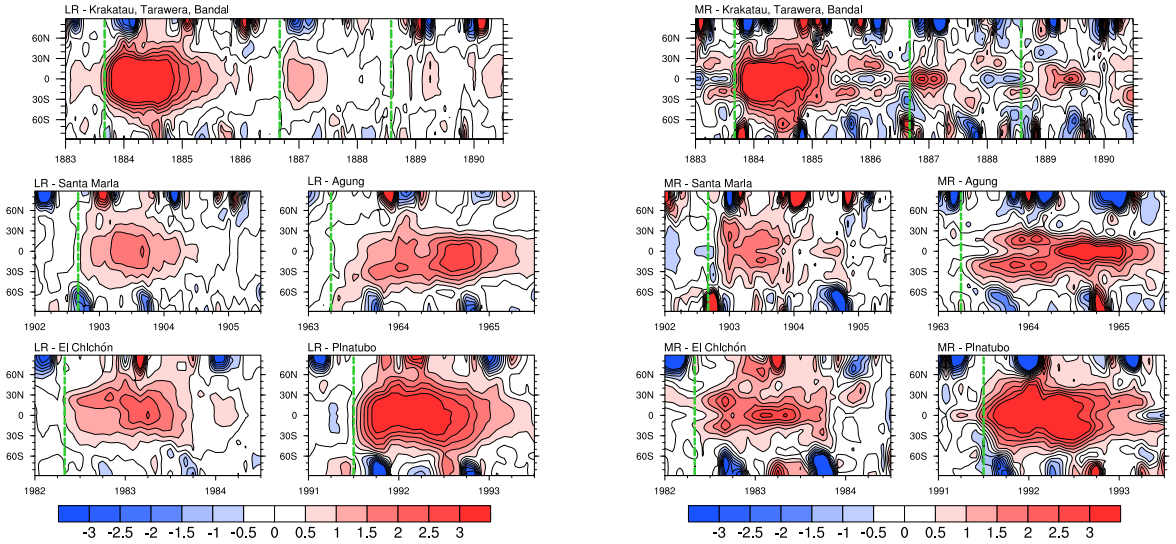

Figure 3.2: De-seasonalized monthly mean temperature anomalies at 50 hPa $[K]$ averaged over 10 and 3 ensemble members for the seven largest eruptions in the CMIP5 historical simulations for LR (left) and MR (right), respectively. Green vertical lines indicate time of the eruption.

of the temperature in the tropical stratosphere. The largest increase in temperature at 50 hPa occurs after the eruptions of Krakatau and Pinatubo (Fig. 3.2), the two strongest eruption in the historical simulations as indiciated by the radiative forcing. The anomalies last for about one to two years after the injection of the aerosols into the stratosphere. In contrast to the TOA outgoing shortwave radiation anomalies, there is a clear difference in the temperature anomalies at 50 hPa between the two model configurations. In the MR configuration, the temperature anomalies show a larger variability, especially in low latitudes, even without volcanic perturbations. Moreover, the maximum anomaly after the volcanic eruptions is not always centered at the equator but symmetrical around the equator at approximately 20°N and 20°S. This is explained by the presence of the QBO in the MR configuration. The secondary circulation of the QBO imposes heating or cooling in a certain level during a specific phase of the QBO. Hence, the temperature signal is a superposition of the volcanically induced heating and the adiabatic heating or cooling due to the phase of the QBO. However, the anomalies shown in Figure 3.2 are an average over three different ensemble members. Because the QBO is not prescribed but interactively calculated, the phase of the QBO differs for the individual ensemble members at the time of the eruption. The superimposed QBO signal itself is therefore blurred by different phases of the QBO. Nevertheless, a clear imprint of the QBO can be seen for example during the eruption of Agung with the maximum heating right after the eruption not centered at the equator but at 20° north and south of the equator and a stronger heating at the equator compared to LR from mid-1964 to 1965.

The simulated temperature response to Pinatubo in 1991 can be compared to satellite observations. For both model configurations the simulated response of 3-4 K is slightly larger than the observed one with 2-3 K (Labitzke and McCormick 1992). But the observed temperature anomaly does not only include the volcanic signal, but is influ-

enced by other sources, in particular the phase of the QBO. The difference between the observed temperature anomaly and the simulated temperature anomaly is to a large extent due to the absence of the QBO in the LR configuration and the incorrect phase correlation in the MR configuration. While the Pinatubo erupted during the easterly phase of the QBO, two of three realizations in the MR configuration are in the westerly phase in the winter of 1991/1992. Thomas et al. (2009a) show that it is crucial to prescribe the correct phase of the QBO to simulate the observed temperature anomalies in the lower stratosphere after the Pinatubo eruption. So given the explained caveats, the model captures the lower stratospheric temperature response reasonably well.

Only during boreal winter, the NH polar stratosphere can couple to the troposphere and influence surface climate (Thompson and Wallace 2000; Charlton and Polvani 2007). Therefore, I will focus on the winter season (DJF) to investigate if a tropical volcanic eruption influences the polar stratosphere and subsequently the NH surface climate. The warming of the equatorial stratosphere, as shown in Figure 3.2 for individual eruptions, can also be seen in the zonal mean temperature anomalies in the first two winters averaged over all nine major eruptions (Fig. 3.3). The maximum heating occurs in the first post-eruption winter in the equatorial stratosphere. In the LR version, the positive anomaly shows a maximum of 2.5 K at about 50 hPa averaged over all nine tropical eruptions. In the troposphere, negative anomalies are simulated, due to the reduction of incoming short wave radiation. Strengthening of the residual meridional circulation leads to negative temperature anomalies in the upper tropical stratosphere by adiabatic cooling (Toohey et al. 2014). A significant positive temperature anomaly occurs in high northern latitudes from the upper stratosphere to approximately 30 hPa for the same reason, but here descending air masses lead to adiabatic heating. In the second winter after the eruption, the equatorial warm anomaly is considerably smaller (1.5 K) but still significant. In the MR configuration, the maximum tropical warming in the first winter after the eruptions is stronger compared to the LR (2.5-3 K) and also at higher altitudes (approximately 30 hPa), whereas in the second winter after the eruptions, the temperature anomaly is of comparable magnitude and altitude in the two configurations. Again, the difference in the zonal mean temperature anomaly pattern between the LR and the MR in the tropical stratosphere is related to the QBO in the MR configuration. While in the reference periods of the MR configuration the east and west phase of the QBO are almost equally distributed, the first post eruption winters are dominated by the west phase of the QBO. Of the 27 first post-eruption winters (3 ensemble members times 9 volcanic eruptions), 18 are in the west phase of the QBO and only 9 in the east phase. Hence, the simulated temperature signal is a superposition of the temperature perturbation by the volcanic aerosols and the secondary circulation of the QBO in its westerly phase. Due to the phase progression of the QBO, in the second post-eruption winter the east phase of the QBO dominates, which explains the downward shift of the maximum temperature anomaly in the MR configuration.

Both configurations slightly underestimate the warming of the tropical stratosphere in comparison with the eruptions of Agung, El Chichón and Pinatubo in the ERA-40 reanalysis dataset (Fig. 3.3, bottom). The underestimation is mainly caused by the smaller eruptions in the volcanic composite of the models. Still, the zonal temperature anomaly pattern is reasonably well captured by the model, especially in the MR config-

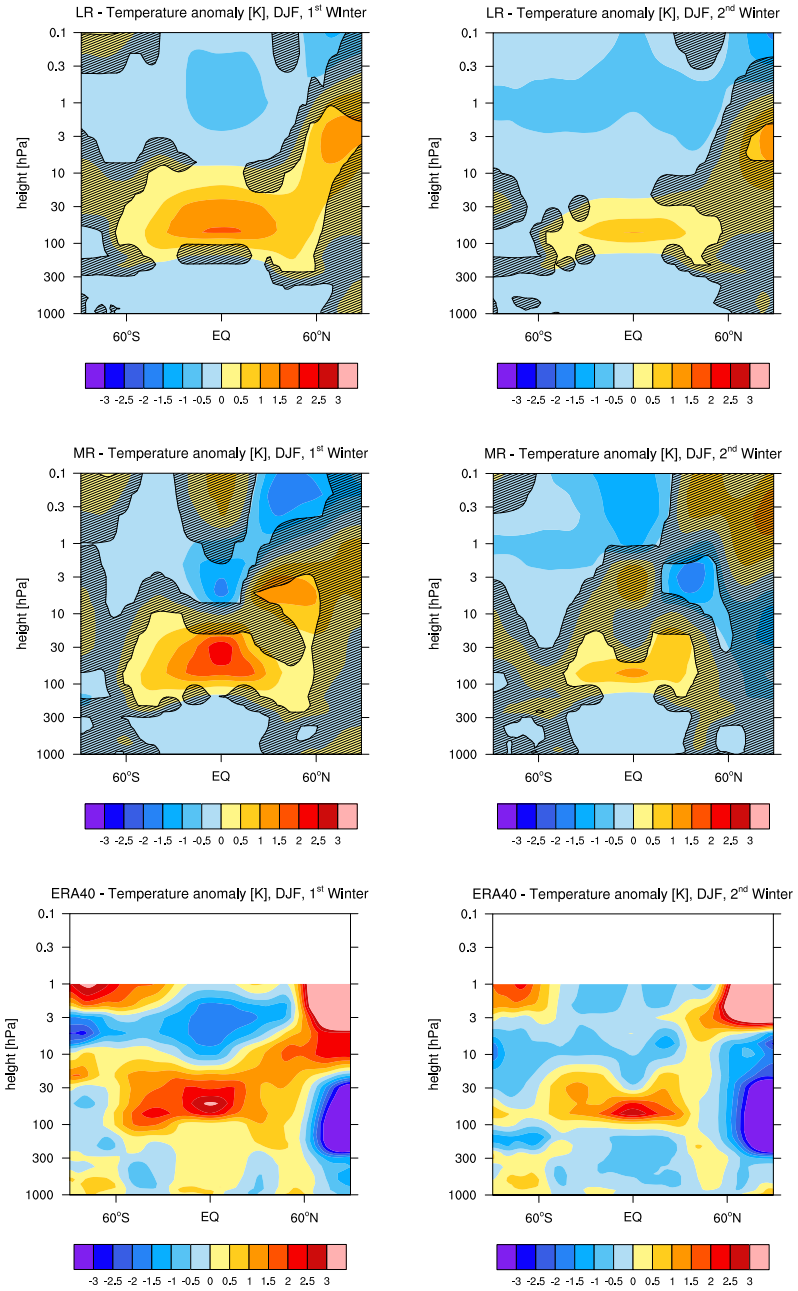

Figure 3.3: Ensemble average of the zonal mean temperature response $[K]$ averaged over the nine largest eruption in the historical simulation of the MPI-ESM-LR (top) and MPI-ESM-MR (middle) ensemble. Shown are DJF anomalies in the first (left) and second (right) winter after the eruptions. Hatched regions are not significant at the 95% confidence level. The zonal mean temperature response averaged over the three largest tropical eruptions since 1957 in the ERA-40 reanalysis are shown in the bottom row.

uration. The altitude of the maximum warming of the tropical stratosphere is in good agreement as well as the cooling in the upper tropical stratosphere and the warming in the upper polar stratosphere. A remarkable difference, however, is the strong negative anomaly in the lower polar stratosphere, which is not simulated in either of the two model configurations. This discrepancy is related to the dynamical response of the po-

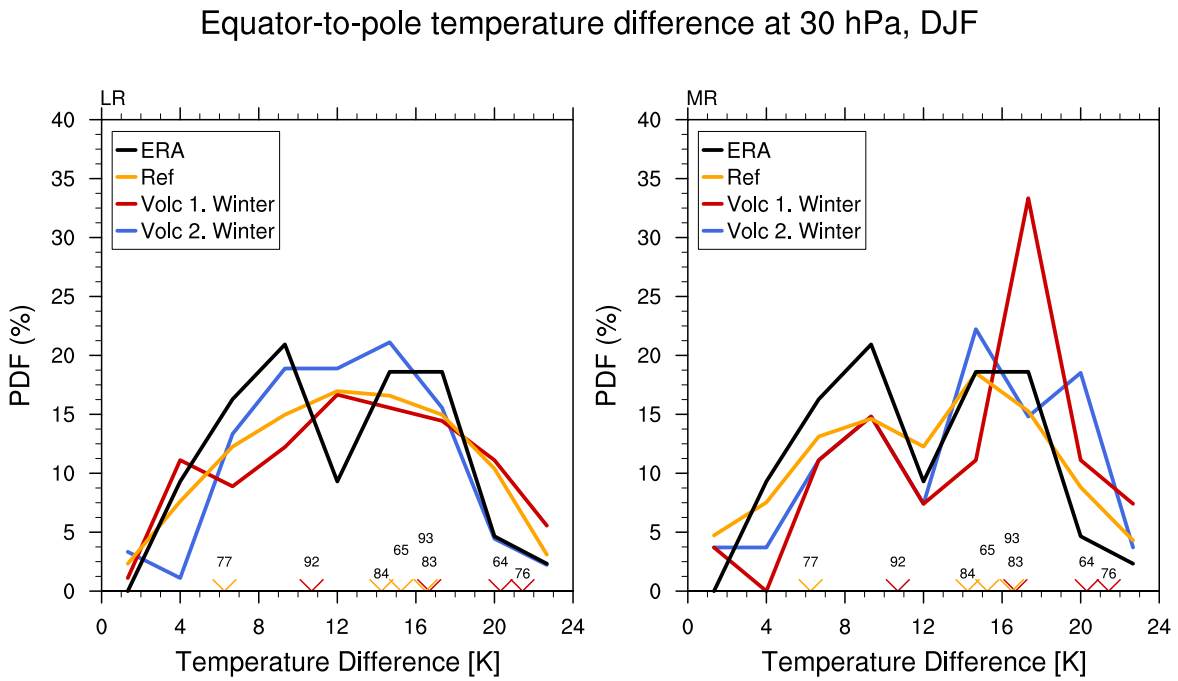

Figure 3.4: Probability Density Function of the equator (20°S-20°N) to Pole (70°N-90°N) temperature difference at 30 *hPa* in DJF for the MPI-ESM-LR (left) and the MPI-ESM-MR (right). The blue line displays the PDF for the pre-eruption reference period, the red line for the first post-eruption DJF and the orange line for the second post-eruption winter. The black line displays the PDF for the volcanically unperturbed ERA-40 period and the markers on the bottom line indicate the temperature difference after the volcanic eruptions in the ERA-40 period, where the numbers give the two last digits of the year of the respective eruption. Red markers indicates the first post-eruption winter, orange markers the second post-eruption winter.

lar vortex to volcanic eruptions, which will be discussed in section 3.3.2. The absence of a negative tropospheric temperature anomaly in the first post-eruption winter in ERA-40 dataset is due to the El Niño events coinciding with all three major tropical volcanic eruptions.

The assumed mechanism how the temperature perturbation in the tropical stratosphere influences the high latitudes is via the increased equator-to-pole temperature gradient. In a previous study Collins (2004) suggested that volcanic eruptions lead to a shift in the likelihood of anomalies, such as a strong polar vortex or a positive phase of the NAO, to occur. To test this assumption in the MPI-ESM simulations, Figure 3.4 shows the probability density function (PDF) of the temperature difference between the equator (20°S-20°N) and the northern polar cap (70°N-90°N) at 30 *hPa*. I choose to focus on the 30 *hPa* level, because at that altitude the maximum temperature anomaly in the tropical stratosphere occurs in the MPI-ESM simulations as well as in the reanalysis dataset. Thus, I expect to see the clearest signal at this height. The black line displays the ERA-40 reanalysis from 1958-2001 and the blue lines the historical period, both excluding years after volcanic eruptions. The temperature gradient after volcanic eruptions in the historical simulations is shown in red for the first year after the eruption and in orange for the second year. Because there are only four eruptions

in the ERA-40 time period, the winters after volcanic eruptions are indicated with markers on the bottom for this dataset.

Without volcanic perturbation, the ERA-40 equator-to-pole temperature gradient yields two modes which are more likely to occur: one with a weaker temperature gradient of about 8 K and one with a stronger temperature gradient of about 16 K. In contrast, the 30 hPa temperature gradient in the historical simulations of the MPI-ESM-LR is Gaussian distributed and does not show a double peak structure. The difference between ERA-40 and LR can be explained by the absence of the QBO in this model configuration. The QBO strongly influences the temperature in the tropical stratosphere by inducing a secondary circulation and adiabatic cooling or heating heating. Thus, depending on the phase of the QBO and the altitude considered, the equator-to-pole temperature gradient is stronger or weaker. Compositing the ERA-40 data according to the QBO phase shows that during QBO west phase the meridional temperature gradient at 30 hPa is stronger (see Appendix A.1). Due to the simulation of the QBO, the double peak structure is also captured by the MR configuration, which agrees reasonably well with the ERA-40 dataset (Fig. 3.4, right).

The post-eruption winters in the reanalysis dataset are clustered in the larger temperature gradient mode, with the remarkable exception of the first winter after the strong eruption of Pinatubo and the less remarkable exception of the second winter after the rather small eruption of Fuego. In these two cases, the QBO was in its easterly phase which counteracts the tropical stratospheric warming of the volcanic aerosols at 30 hPa. In the same way, the very strong temperature gradient in the first year after the Fuego eruption is due to a positive interference of the westerly QBO phase with the heating of the volcanic aerosols. In the LR configuration, neither in the first nor in the second year after the eruptions a higher probability for a stronger temperature gradient is obtained. The post-eruption distributions are not distinguishable from the reference case, given the uncertainty in the exact shape due to the smaller sample size in post-eruption winters. Because the volcanic aerosols significantly increase the temperature in the tropics (see Fig. 3.3), the only possible explanation is a positive temperature over the NH polar cap as well. In contrast to the LR configuration, a higher probability of an increased temperature gradient can be found in the first post-eruption winter of the MR configuration (Fig. 3.4, right), which shows a distinct peak at about 18 K. However, the shift of the probability to a stronger gradient is not entirely due to the heating of the volcanic aerosols, because the phase domination of the QBO west phase in the first winter after volcanic eruption contributes to the positive temperature anomaly in the tropical stratosphere. In the second winter after the eruption, the peak at 18 K diminishes, which is expected due to the smaller influence of the volcanic heating and the predominately easterly phase of the QBO. However, there is still a slightly higher probability for a larger meridional temperature gradient compared to the reference period without volcanic perturbation.

3.3.2 Circulation and surface temperature response

The temperature anomalies in the tropical stratosphere are thought to increase the equator-to-pole temperature gradient and strengthen the NH polar vortex in boreal

winter. In the first winter after the eruptions, the strongest signal in the LR configuration is actually a deceleration of the austral summer easterlies in the southern hemisphere (Fig. 3.5). The polar vortex in the boreal winter of the NH is not significantly strengthened, apart from a small region around 50°N above the tropopause. The negative wind anomaly in the NH upper stratosphere can be related to the weakened temperature gradient at that altitude due to the adiabatic heating in upper polar stratosphere. In the second winter, there is no significant response in the NH stratosphere at all. Only in the region of the polar stratopause the negative zonal wind anomaly remains. In the MR configuration, the most pronounced difference to the LR configuration in the zonal mean zonal wind anomalies is of course the QBO in the tropics. The dominance of the westerly phase in the first post-eruption winter and of the easterly phase in the second post-eruption winter leads to significant anomalies in the zonal mean zonal wind at low latitudes in the stratosphere. Apart from the tropical anomalies, the deceleration of the easterlies in the SH can also be found in the MR configuration. In the NH however, there is no significant response of the polar vortex, apart from the positive anomaly southward of 60°N in the second post-eruption winter. However, in comparison with ERA-40 reanalysis data, the response of the NH polar vortex to tropical volcanic eruptions is in both model configurations too weak (Fig. 3.5, bottom). The strengthening of the polar vortex of more than 10 m/s and 8 m/s in the first and second post eruption winter respectively, is a factor 3-5 larger than the anomaly simulated by the MR configuration. Hence, a considerable advancement of the MR configuration over the LR configuration is not supported by these simulations, especially in the first post-eruption winter.

That there is no significant advancement of the MPI-ESM-MR over the MPI-ESM-LR is in contradiction to the study of Schmidt et al. (2013), where they find that for the same model and the same ensemble members, a strengthened polar vortex after volcanic eruption in the MPI-ESM-MR can be obtained. Schmidt et al. (2013), however, used a multiple linear regression analysis to determine the impact of volcanic forcing. In this way, stronger eruptions (as Pinatubo or Krakatau) have a higher weighting according to their higher AOD value. In my analysis, all nine eruptions, independent of their eruptions magnitude, contribute equally to the mean response. The difference in the results obtained from Schmidt et al. (2013) and the results presented here suggests, that only strong eruptions significantly impact the NH polar vortex, whereas smaller eruptions as Fuego or Bandai are not important for the NH high latitude stratosphere. With this conclusion in mind, the stronger and significant response of the NH polar vortex in the second winter after the eruption, when the radiative forcing is even smaller, is surprising.

However, to what extent the zonal wind response is due to the initial volcanic heating in the tropical lower stratosphere is impossible to quantify with this set of simulations. The polar vortex is not only influenced by the volcanic forcing, but also crucially depends on the boundary conditions such as the phase of the QBO and ENSO as well as internal variability. In contrast to the tropical temperature response in the stratosphere, which is a linear combination with respect to the individual forcings (Thomas et al. 2009a), the response of the polar vortex to a combination of different forcings is likely to be non-linear (Calvo et al. 2009). Due to the large internal variability of the polar vortex (Kodera 1995) and the small ensemble size, it is difficult to unambigu-

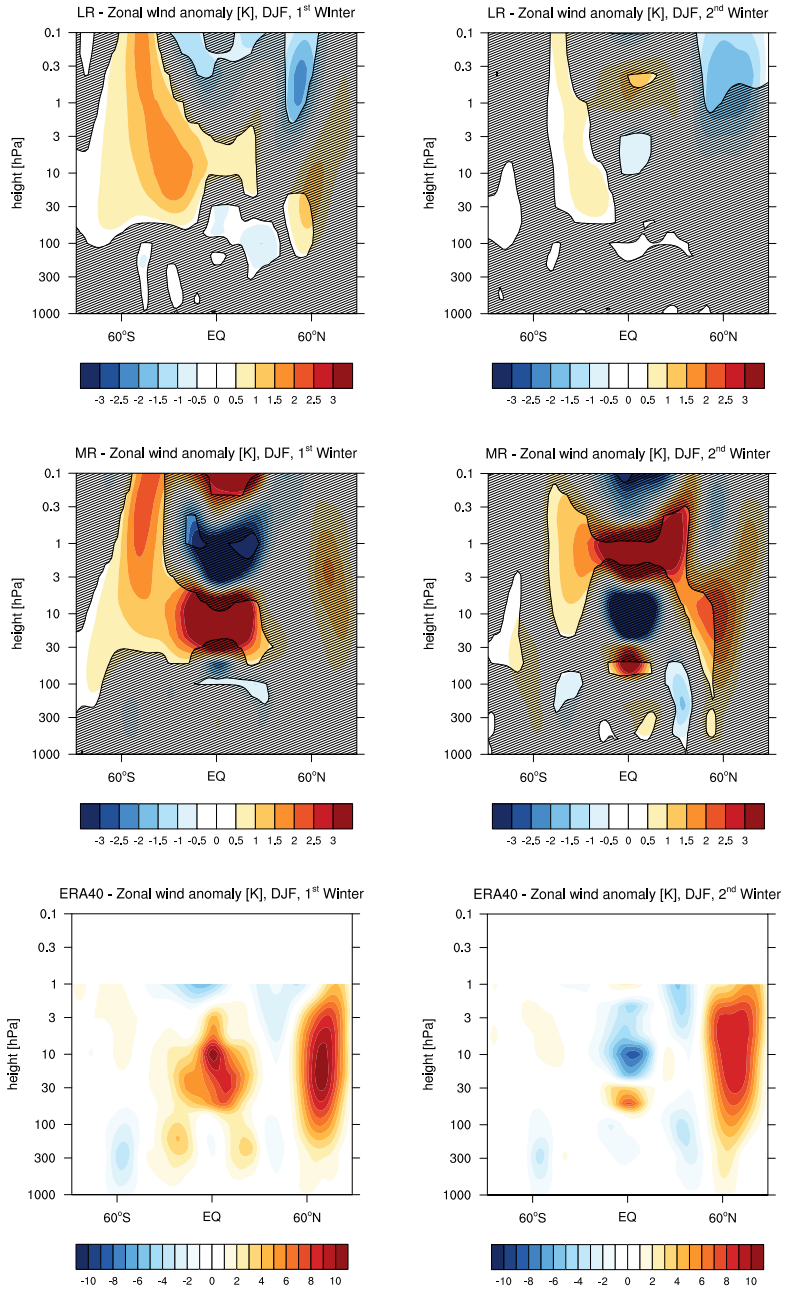

Figure 3.5: Ensemble average of the zonal mean zonal wind response $[K]$ averaged over the nine largest eruption in the historical simulation of the MPI-ESM-LR (top) and MPI-ESM-MR (middle) ensemble. Shown are DJF anomalies in the first (left) and second (right) winter after the eruptions. Hatched regions are not significant at the 95% confidence level. The zonal mean zonal wind response averaged over the three largest tropical eruptions since 1957 in the ERA-40 reanalysis are shown in the bottom row.

ously disentangle the effect of the volcanic eruptions on the polar vortex from other forcing such as the QBO, ENSO and solar irradiance as well as internal variability. Furthermore, the stronger signal in the first post-eruption winter compared to the second post-eruption winter in SH shows that a stronger forcing should yield a stronger response. The variability in the SH is in DJF much smaller than in the NH, so the

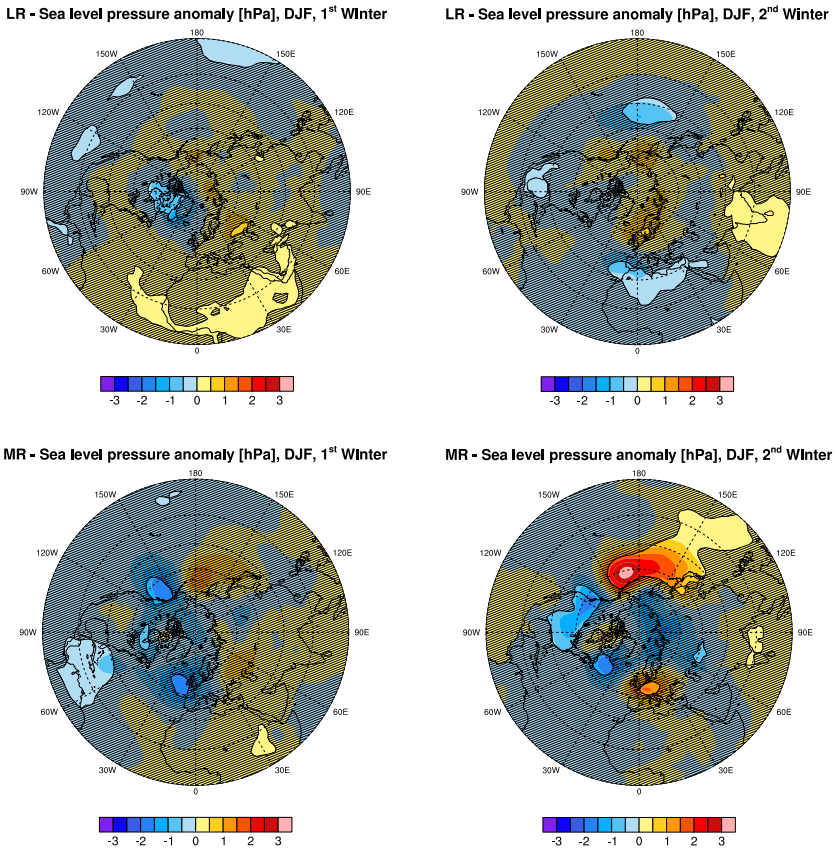

Figure 3.6: Ensemble average of the mean sea level pressure response $[K]$ averaged over the nine largest eruption in the historical simulation of the MPI-ESM-LR (top) and MPI-ESM-MR (bottom) ensemble. Shown are DJF anomalies in the first (left) and second (right) winter after the eruptions. Hatched regions are not significant at the 95% confidence level.

zonal wind signal should reflect the temperature anomaly more accurately. In both, the LR and MR configuration, the zonal mean zonal wind anomaly in the SH is stronger in the first winter.

Ozone depletion after volcanic eruptions might influence the polar vortex more in the second compared to the first winter. After Pinatubo, a stronger ozone loss was observed in the winter 1992/1993 compared to 1991/1992 (Hofmann et al. 1994). As explained in chapter 1.2.3, ozone depletion can contribute to a strengthened polar vortex after volcanic eruptions. But whether ozone depletion has a significant influence during periods where chlorine was not abundant in the atmosphere is taken into question (Marshall and Scaife 2009). There are known feedback mechanisms involving the ocean or sea-ice that can conserve the volcanic signal and influence the NH for longer than two years after the eruption (Church et al. 2005; Ding et al. 2014) and may lead to a delayed winter warming pattern (Zanchettin et al. 2013c). But these mechanisms play a role on decadal timescales and do not amplify the polar vortex in the second compared to the first year after the eruption. Therefore, the clearer signal in the second winter in the MR configuration highlights the potential danger of attributing a polar vortex signal to volcanic forcing in small ensembles, when internal variability plays a major role in determining the state of the polar vortex.

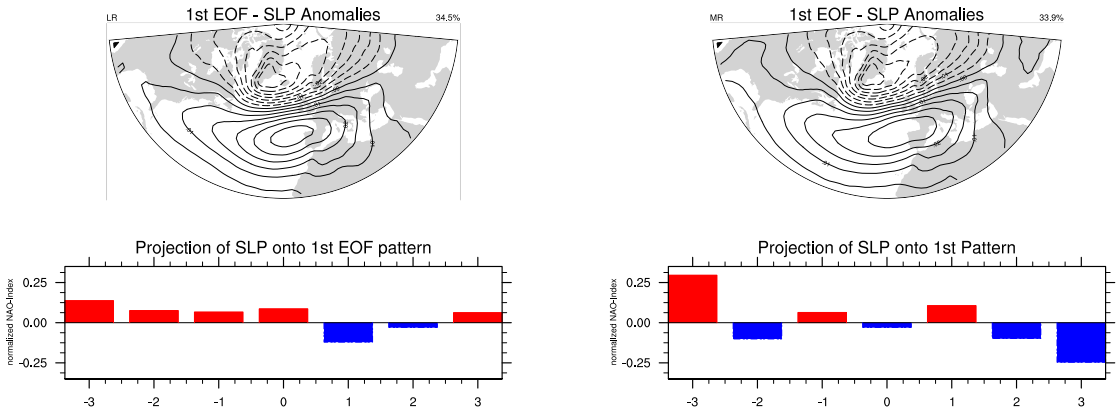

Figure 3.7: Top: Leading Empirical Orthogonal Function (EOF) of the monthly DJF mean the sea level pressure anomalies with respect to the climatological mean in the North Atlantic Sector (110°W-70°E) for the MPI-ESM-LR (left) and the MPI-ESM-MR (right) over the perdiod 1850-2005. The percentage of variance explained by the EOF is given in the top right corner. Bottom: Projection of the sea level pressure onto the leading EOF-Pattern, normalized with respect to the standard deviation (normalized NAO-Index). The NAO-Index is averaged over the largest eruption in the historical period at different lag time. Lag time 0 corresponds to the first winter after the eruption.

So far, the emphasis how volcanic eruptions influence the NH winter lay on the stratosphere. But because observations of the stratosphere after volcanic eruptions are sparse, the proposed mechanism of how volcanic eruptions influence the NH climate relies in addition on surface observations and proxy-data where the volcanic winter warming over Northern Europe and Siberia is robustly documented (Shindell et al. 2004; Christiansen 2008). A strong tropical volcanic eruption is thought to strengthen the polar vortex and subsequently shift the NAO into a positive phase, resulting in higher than average surface temperatures in Northern Europe and Siberia. However, the LR set-up does hardly show any significant response of the sea-level pressure in both, the first and second winter after the eruptions (Fig. 3.6). This comes as no surprise, because if the influence of volcanic eruptions propagates from the stratosphere to the troposphere and there is no significant impact on the polar vortex (Fig. 3.5), one might not expect to see an influence on surface pressure. The only significant response in the North Atlantic sector in the LR configuration is a negative pressure anomaly over the Canadian Archipelago in the first winter and a negative pressure anomaly over North Africa in the second winter after the eruption. The anomaly in the first winter should intensify the climatological Iceland low, hence lead to a more positive phase of the NAO. This is confirmed by the superposed epoch analysis of the NAO-Index, which shows in the first winter after the eruption a positive phase on average (Fig. 3.7, left). The pressure anomaly in the second winter weakens the climatological Azores high, which leads to a more negative phase of the NAO. Note that the anomalies of the NAO-Index in the first two winters after the eruptions are as large as anomalies in the three years before a volcanic eruption, indicating that the anomalies after volcanic eruptions are not distinguishable from internal variability. In the MR configuration, the only significant SLP response in the first winter after an eruption in the Atlantic is a negative anomaly between the Azores and Iceland. In the second post-eruption win-

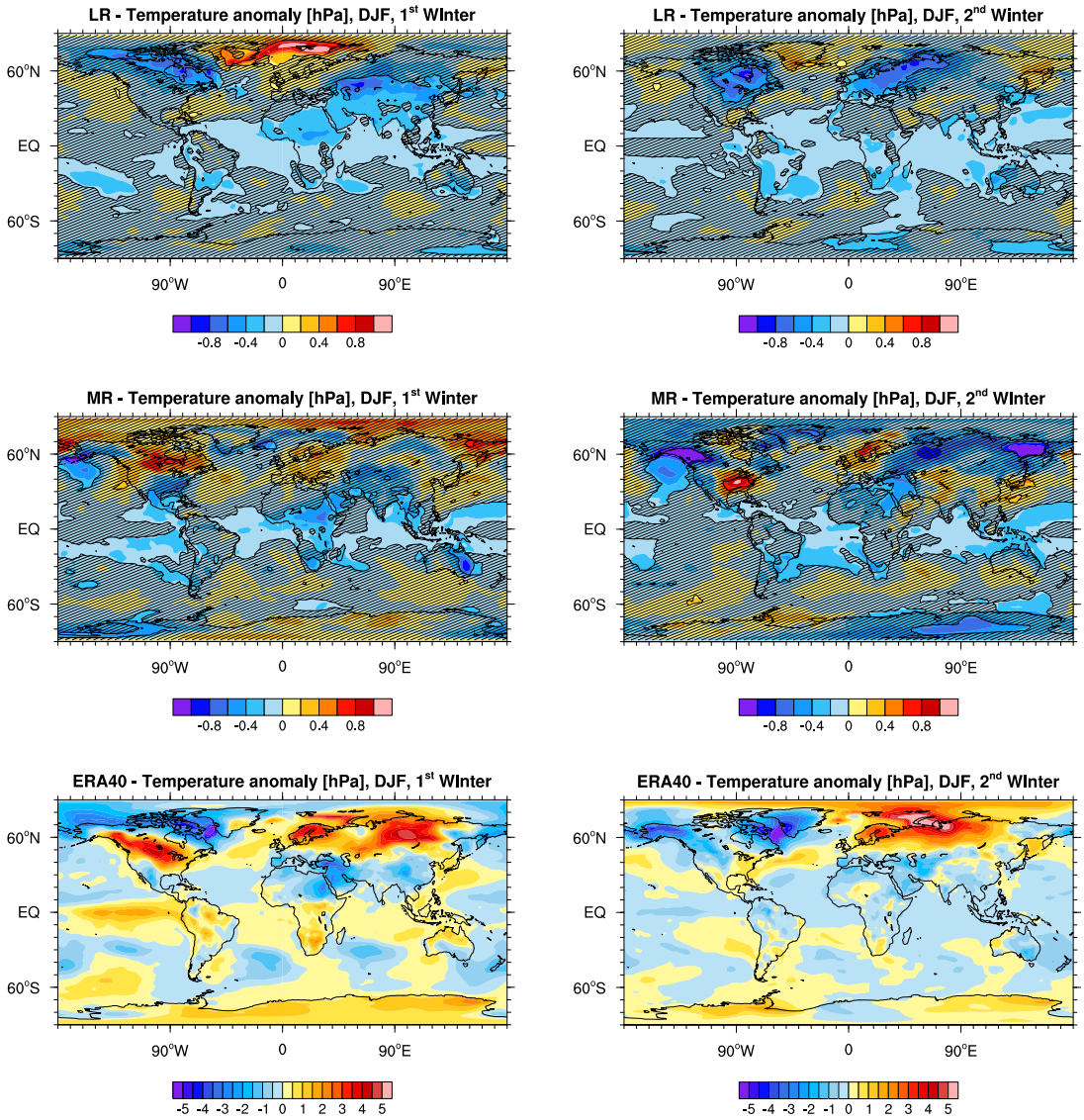

Figure 3.8: Ensemble average of the near surface temperature response $[K]$ averaged over the nine largest eruption in the historical simulation of the MPI-ESM-LR (top) and MPI-ESM-MR (middle) ensemble. Shown are DJF anomalies in the first (left) and second (right) winter after the eruptions. Hatched regions are not significant at the 95% confidence level. The near surface temperature response averaged over the three largest tropical eruptions since 1957 in the ERA-40 reanalysis are shown in the bottom row.

ter, a positive SLP anomaly over Western Europe and a negative SLP anomaly south of Greenland does not fully project onto the NAO pattern, as indicated in Fig. 3.7. Consequently, the impact of volcanic eruptions on the NAO-Index is small in the MR configuration, especially in the first winter after the eruption where basically no change is simulated. Again, anomalies of the NAO index in the MPI-ESM-MR simulations three winters before and four years after the eruptions are substantially larger compared to the first two winter after the eruption, confirming the not detectable impact of volcanic eruptions in this particular metric for the average over nine eruptions.

Because the NAO is the dominant mode of variability in the boreal winter in the

Atlantic sector, it has a large impact on European surface temperature (Hurrell 1995; Thompson and Wallace 1998). The advection of relatively warm, maritime air masses to northern Europe during a positive phase of the NAO, which is observed after volcanic eruptions, leads to warmer and wetter conditions in northern Europe and Siberia, the so called volcanic winter warming. But because volcanic eruptions do not show any considerable influence on the NAO in the MPI-ESM, the typical volcanic winter warming pattern is not simulated (Fig. 3.8). The only consistent and significant feature in both model configurations is the negative temperature anomalies in the tropics, due to the reduction of incoming short wave radiation. In northern high latitudes, the LR configuration simulates a significant warming in the Arctic Ocean, which might be related to advection of warm air into this region. In the second winter after the eruption, the LR configuration shows actually a reversed surface temperature anomaly pattern what one would expect after tropical eruptions, with cooling over Central Europe extending to northern Russia, consistent with the negative phase of the NAO (Fig. 3.7). No significant surface temperature response in Europe can be found in the MR configuration, neither in the first nor in the second winter after the eruptions. Only in the United States and Kamchatka in the second post-eruption winter the surface temperature is significantly changed, which is due to the weakening of the Aleutian low. For comparison, the ERA-40 reanalysis surface air temperature anomalies show the winter warming pattern over Eurasia in the first and second post-eruption winter (Fig. 3.8, bottom). The cooling of the tropics, which is significant in the model simulation, is overcompensated by the El Niño events in the winters of 1963-1964, 1982-1983 and 1991-1992. Because El Niño has a significant impact on surface temperatures not only in the Pacific region but also on the circulation and surface temperature in Europe (Brönnimann 2007), the observed response does not only include the volcanic signal. Still, the observed volcanic winter warming pattern over Northern Europe and Siberia after the same nine volcanic eruptions considered in this chapter (Driscoll et al. 2012) suggests that neither of the two MPI-ESM configurations robustly captures the dynamic response to tropical volcanic eruptions.

3.4 Summary and discussion

I investigated the mean impact of nine strong tropical volcanic eruptions during boreal winter in two configurations of the MPI-ESM, which differ in the vertical resolution in the atmosphere and the horizontal resolution in the ocean (LR and MR). The MR configuration interactively simulates the QBO, which has been shown to influence the temperature anomaly in the tropical stratosphere (Thomas et al. 2009b) as well as the 50 hPa geopotential height anomaly in NH high latitudes (Stenchikov et al. 2004) following tropical volcanic eruptions. The heating of the lower tropical stratosphere due to absorption of near-infrared radiation is captured well in both configurations, although disagreements with observations in the magnitude of the tropical heating arise because of the absence (in the LR configuration) or accidental dominance of the westerly phase of the QBO (in the MR configuration).

Although the MPI-ESM reproduces the stratospheric tropical heating after volcanic eruption reasonably well compared to the available observations, both configurations

lack a consistent and significant response in the NH high latitudes. In particular, the intensification of the polar vortex and the observed winter warming pattern over northern Europe and Siberia is not captured in neither configuration in the first and second winter after the eruptions. Even though the MPI-ESM shows the downward propagation of strong and weak vortex events (Reichler et al. 2012; Bunzel et al. 2013; Manzini et al. 2014) and captures the dominant mode of NH winter variability (Cattiaux and Cassou 2013), the vortex signal after volcanic eruptions may be too small to influence the surface temperature comparably to observations. As already mentioned, the polar vortex exhibits a large interannual variability and quantifying how much the volcanic eruption impacts the vortex in contrast to other factors such as the QBO (in the MR configurations), solar irradiance or ENSO is impossible in this simulation set-up. Especially in the MR configuration with only three ensemble members, one needs to average over different eruptions which makes the signal even less clear, because the magnitude, the season and latitude of the volcanic eruptions play an important role for the distribution of the aerosols and therefore also for the forcing (Toohey et al. 2011, 2013). And even if the stratospheric polar vortex has an influence on the NAO in the winter after the volcanic eruptions in the MPI-ESM, the signal will very likely be too small to be detectable due to the large variability of tropospheric climate in NH winter.

In contradiction to Schmidt et al. (2013), I find no indication of an improved volcanic signal in the polar vortex after volcanic eruptions for the MR configuration with respect the LR configuration. This may be due to the different methods which are applied. In contrast to averaging over nine largest eruptions, Schmidt et al. (2013) detected the signal of various forcings via a multiple linear regression. In this way, stronger volcanic eruptions will have a larger weight in the response due to their larger AOD, which is used as regression coefficient. Hence, the improvement reported by Schmidt et al. (2013) will either be due to the larger eruptions as Pinatubo and Krakatau or be accidental due to the smaller ensemble of the LR configuration used in their study. Indeed, the polar vortex is significantly strengthened in the first post-eruption winter after Krakatau and Pinatubo in MR configuration (not shown), indicating that a stronger forcing might yield a stronger signal. However, with the small ensemble of three members only, the intensification of the polar vortex might just be by chance, due to the large internal variability of the NH polar stratosphere (Kodera 1995). This is exemplified by the larger ensemble of the LR configuration, where even with 10 ensemble members the Pinatubo eruption does not significantly strengthen the polar vortex (not shown). Still, focusing on larger eruptions seems reasonable to identify the response on the polar vortex, but only if enough ensemble members are available. In chapter 4, I will examine the dependence of the strength of the eruption in more detail and in chapter 6, I will investigate with a large ensemble how many members are needed to detect a significant impact of volcanic eruptions.

The phase of the QBO can potentially modify the response of the polar vortex to volcanic eruptions. While Stenchikov et al. (2004) found that the Arctic Oscillation response to a Pinatubo eruption is enhanced when the QBO is in its westerly phase, Thomas et al. (2009b) in contrast find in a disturbed polar vortex after Pinatubo in their model simulations independent of the phase of the QBO. They attribute the response to the prescribed SST field that included the El Niño occurring in the winter of 1991-1992 which might weaken the vortex. Comparing the influence of the QBO phase

in the winters after volcanic eruption on the stratospheric equator-to-pole temperature gradient and the polar vortex strength is only possible to a very limited extent. Because there are only 9 out of 27 eruptions in the historical simulation in the QBO east phase, every conclusion regarding the QBQ east phase lacks robust statistics.

Finally, I do not find evidence that due to its higher vertical resolution the MR configuration robustly captures the observed dynamical response of the NH polar stratosphere better compared the LR configuration. The QBO, which is only present in the MR configuration, changes significantly the heating in the tropical lower stratosphere due to the adiabatic heating of the secondary QBO circulation, but the observed intensification of the polar vortex is not robustly simulated. In consequence, due to computational constraints and no evidence of an improved representation of the volcanic response, I will in the following only use the LR configuration of the MPI-ESM.

Chapter 4

Sensitivity of the Northern Hemisphere winter stratosphere to the strength of volcanic eruptions

4.1 Introduction

The current generation of coupled climate models do not, on average, produce a significantly strengthened polar vortex for the largest tropical eruptions (Driscoll et al. 2012; Charlton-Perez et al. 2013). However, a strengthened polar vortex is the expected dynamical response to a tropical volcanic erption based on observations and theoretical arguments (chapter 1.2.3). An increased vertical resolution and a better representation of stratospheric processes does not necessarily improve the volcanic signal in the stratosphere and at the surface (chapter 3). Because the winter polar NH stratosphere is a region prone to large interannual variability (e.g., Kodera (1995)) and the evolution of the polar vortex depends on several phenomena remote from the polar stratosphere (such as El Niño Southern Oscillation, the Quasi-Biennial Oscillation or the 11-year solar cycle), the impact of volcanic eruptions might be masked if the models are too insensitive to external perturbations. If that is the case, a stronger forcing as used in the historical CMIP5 simulations possibly yields the expected response of a strengthening of the NH polar vortex.

The mechanism by which tropical volcanic eruptions strengthen the polar vortex is still debated. The classical view is that the absorption of radiation by the volcanic aerosols leads to a localized heating in the tropical stratosphere and enhances the meridional temperature gradient (Labitzke and McCormick 1992; Graf et al. 1993; Kodera 1994; Perlwitz and Graf 1995; Kodera and Kuroda 2000). The thermal wind relation implies that the enhanced meridional temperature gradient strengthens the polar vortex due to increased westerlies. But the radiative forcing by the volcanic aerosols is mainly confined to tropical latitudes, so it is questionable whether there is a significant direct impact in the region of the polar vortex (Stenchikov et al. 2002). Ozone depletion, due to Clorine activation on the volcanic aerosols, leads to a negative temperature anomaly in the NH polar stratosphere and can therefore directly strengthen the polar vortex (Stenchikov et al. 2002). But this mechanism can only have a significant impact when Clorine is available in the stratosphere, which is the case for the last two big eruptions of El Chichón 1982 and Pinatubo 1991. But tropical volcanic eruptions prior to El

Chichón show a positive NAO and a winter warming pattern as well, indicating that ozone loss in high latitudes is unlikely to be a major factor (Marshall et al. 2009). Stenchikov et al. (2002) also proposed that the weakened meridional temperature gradient in the troposphere, due to low latitude cooling of the surface (Robock and Mao 1995), leads to a decreased planetary wave flux from the troposphere to the stratosphere. A decreased wave flux is associated with a stronger and more stable polar vortex (Newman et al. 2001). But after the last two tropical eruptions, reanalysis data rather suggest an increased wave flux into the stratosphere (Graf et al. 2007). Furthermore, a modelling study with the MPI-ESM-LR by Toohey et al. (2014) indicate that the high latitude meridional temperature gradient anomaly after Pinatubo-like eruptions is primarily due to dynamical heating by an enhanced stratospheric residual circulation. Depending on the spatial structure of the polar downwelling branch of the residual circulation anomalies, the vortex can be either strengthened or weakened.

Hence, there are indications that the classical assumption of a direct, radiative volcanic impact on the polar vortex via an increased temperature gradient from the equator to the North Pole is too simplistic. The influence of volcanic eruptions seems to be rather indirect, but the exact mechanism is still unclear. A stronger forcing as used in the CMIP5 historical simulations, provided that a strengthened polar vortex is significantly simulated, can help to identify the exact mechanism, because the temperature and zonal mean zonal wind anomalies are expected to be larger and more robust. In this chapter I further investigate the mechanisms connecting stratospheric volcanic forcing and the NH polar vortex and thereby better understand the apparent disagreement between the observed polar vortex response and its representation in CMIP5 models. The main focus is the dynamical link between the low-latitude heating gradient, caused by dominantly tropical aerosol heating, and the polar vortex. I compare the dynamical response to volcanic aerosol forcing in large ensemble simulations for two classes of eruption: Pinatubo-like eruption and the much stronger 1815 Tambora eruption. I chose the Tambora eruption, because it is the largest eruption in the last 500 years where observational records exist. The Tambora eruption caused the „year without summer“ in 1816 (Stothers 1984; Auchmann et al. 2013) with exceptionally low temperatures (Rampino and Self 1982) and wet conditions in Europe (Wegmann et al. 2014). I investigate the role of internal variability on the evolution of the NH polar vortex after major tropical volcanic eruptions, and thus the robustness of the vortex response as a function of the magnitude of volcanic forcing.

4.2 Methods and Data

I performed a 20-member simulation ensemble of a Tambora-type eruption with the MPI-ESM-LR. The eruption of Tambora took place in April 1815 on the Sanggar Peninsula of Sumbawa Island in Indonesia at 8°S (Stothers 1984). Estimates of the injected SO_2 are uncertain and range from approximately 50-180 Tg (Oppenheimer 2003; Self et al. 2004). The mass of injected SO_2 can be converted into aerosol optical depth (AOD) by a simple parameterized approximation (Metzner et al. 2012). In the experiment, the volcanic aerosol forcing is prescribed by a time series of AOD and effective radius (Crowley et al. 2008; Crowley and Unterman 2012). The applied aerosol

forcing dataset is one of the two recommend volcanic forcing data sets for the PMIP3 intercomparison (Schmidt et al. 2010, 2012) with a maximum AOD of the Tambora eruption of 0.4, corresponding to approximately 55 Tg SO_2 with the conversion rate given by Gao et al. (2008). The time resolution of the volcanic forcing series is ten days and the forcing is provided as zonal mean values for four equal-area latitude bands (90°S-30°S, 30°S-0°, 0°-30°N, 30°N-90°N). The highest AOD values in this dataset can be found in the tropical latitude bands. The southern hemisphere tropical latitude band exhibits higher AOD values (0.4263 maximum) compared to the NH tropical latitude band (0.3355 maximum), indicating that the aerosols spread more to the south. The AOD estimates are based on sulfate records in Greenland and Antarctic ice cores. The compilation of this data set involves a series of processes including a calibration against satellite observations after the Pinatubo eruption which are described in detail in Crowley and Unterman (2012). The AOD in the model is distributed between 86-20 hPa over three stratospheric levels with a maximum at 50 hPa (Timmreck et al. 2009). The simulations were started from the CMIP5 pre-industrial control simulation of the MPI-ESM-LR with constant boundary conditions and greenhouse gas concentrations of the year 1850. For the pre-industrial control simulation, constant monthly mean ozone fields averaged over the years 1850-1860 are used (Cionni et al. 2011). For each of the 20 ensemble members I chose a different year of the pre-industrial control simulation and started the simulation on the 1^{st} of January of the respective year. The restart dates for the different ensemble members were chosen as such that there is no systematic bias towards a specific state of the tropical Pacific, i.e. the phase of ENSO, and the Atlantic Meridional Overturning Circulation. The eruption was set up in April in accordance with observational records (Stothers 1984). I analyze the monthly means of the first post-eruption winter and anomalies are calculated for each ensemble member with respect to a 20 year reference period of pre-industrial control simulation prior to the chosen eruption year. The significance is based on a two-tailed t-test.

Additionally, I use a ten member ensemble members of CMIP5 historical simulations with the MPI-ESM-LR over the time period 1850-2005. Details about the MPI-ESM-LR, its performance compared to observations and the stratospheric aerosol dataset by Stenchikov et al. (1998) are given in chapter 2. I analyze the largest two eruptions of the historical period, the eruptions of Krakatau and Pinatubo. Details about these two eruptions as well as the methods to obtain post-volcanic anomalies are given in chatper 2.3. I average the response to the eruptions of Krakatau and Pinatubo (**KP** in the following). In this way I have 20 ensemble members for KP (10 for Krakatau and 10 for Pinatubo) as well as 20 ensemble members for the Tambora eruption. Satellite based measurements give an estimation of the injected mass of SO_2 into the stratosphere by the Pinatubo eruption of about 17 Tg (Guo et al. 2004). While ice core data generally imply Krakatau produced a slightly smaller stratospheric aerosol loading compared to Pinatubo (Gao et al. 2008; Sigl et al. 2014), based on pyrheliometer data, Sato et al. (1993) estimated the radiative forcing by Krakatau to be slightly larger than that of Pinatubo. In the reconstruction of Sato et al. (1993), which is the basis of the Stenchikov data set used here, the AOD for the Krakatau eruption is 1.1 times that of Pinatubo. The spatial distribution of the AOD for Krakatau is close to the hemispheric mirror-image of the satellite-based Pinatubo

forcing (http://data.giss.nasa.gov/modelforce/strataer/), with fairly equal hemispheric partitioning of the AOD.

The prescribed monthly mean AOD at 0.55 μm and the simulated global top-of-the-atmosphere (TOA) shortwave anomalies for Krakatau, Pinatubo and Tambora reveal that the radiative forcing and the response of the TOA shortwave anomalies is somewhat larger for the Krakatau eruption than for the Pinatubo eruption (Fig. 4.1a-b). However, both quantities are approximately 3-4 times smaller compared to the Tambora eruption. The zonal mean AOD field of the Tambora eruption in October-November (ON) is comparable in the spatial structure to much better resolved AOD of the Pinatubo and Krakatau eruption (Fig. 4.1c). It is clear that the AOD fields of Krakatau and Pinatubo are not exactly the same, but are similar in the magnitude and the meridional gradient compared to the much larger Tambora AOD. The ensembles of Krakatau and Pinatubo overlap considerably for the global TOA shortwave anomalies, whereas the Tambora ensemble is well separated (Fig. 4.1b). I therefore assume that the global radiative impact of the Krakatau and the Pinatubo forcing is within the same range to justify combining these two eruptions into a single ensemble of simulations (KP) for the purpose of this study. However, different background conditions could be a non-negligible factor that can influence the surface temperature and ocean dynamics response to a volcanic eruption on decadal time scales (Zanchettin et al. 2013a). Nevertheless, for the short term stratospheric dynamical response it can be justified to combine eruptions in different background conditions as it was done for the assessment of the volcanic response in CMIP3 and CMIP5 simulations (Stenchikov et al. 2006; Driscoll et al. 2012).

The practise of analyzing the first two years after a volcanic eruption is mainly due to the limited number of observations. Because the ensemble is comparably large, and it is not a priori clear that the mechanisms in the first winter after the eruption are the same as in the second winter, I choose to focus on the first winter after the eruption, only. For comparison of the single eruptions of Tambora, Krakatau and Pinatubo with observations I use the ERA-Interim reanalysis (Dee et al. 2011) from 1980 to 2002. I exclude the two winters following the volcanic eruptions of El Chichón in 1982 and the two winter following Pinatubo in 1991 for a volcanically unperturbed dataset. With respect to volcanic signals, ERA-Interim agrees well with other reanalysis datasets (Manney et al. 2005).

4.3 Results

4.3.1 Temperature an zonal wind response

Observations have suggested that large tropical volcanic eruptions lead to a positive temperature anomaly in the tropical lower stratosphere and an intensification of the polar vortex in NH winter. I am interested not only in the mid-winter response, but also in the temporal evolution of zonal mean temperature and zonal wind. Therefore, I split the winter season into three parts and refer to them as the following: early winter (October-November mean), mid-winter (December-January mean) and late winter

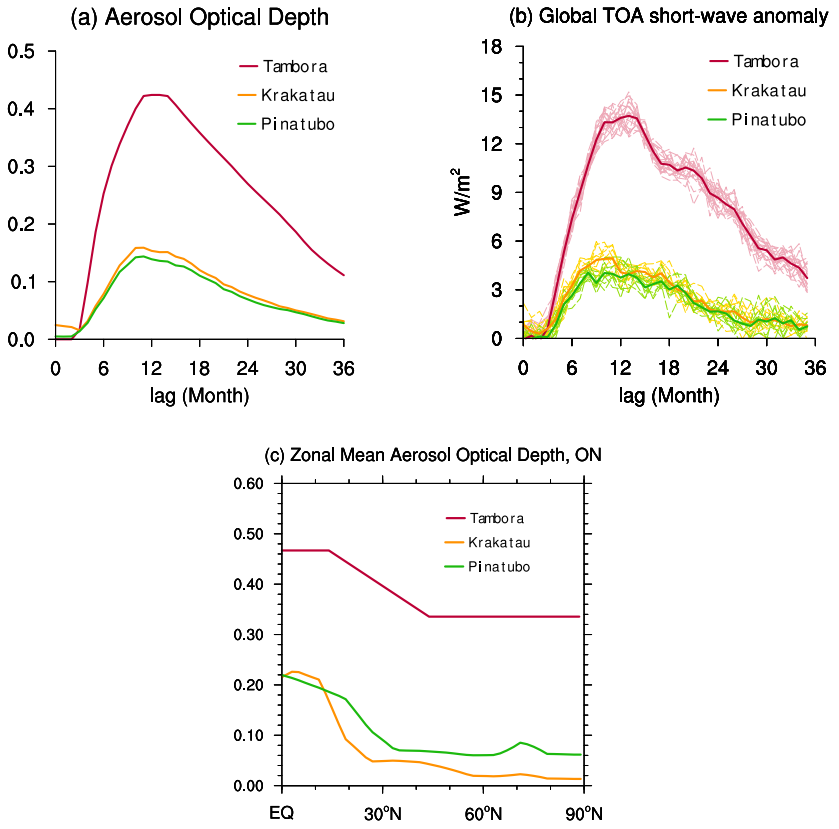

Figure 4.1: (a) Prescribed global averaged aerosol optical depth (AOD) at 0.55 μm for Tambora (red), Krakatau (orange) and Pinatubo (green) in the first 36 month after the eruptions. (b) Anomalies of the global averaged de-seasonalized top-of-the-atmosphere (TOA) short-wave radiation in $[W/m^2]$ in the first 36 month after the eruptions. Thin lines indicate individual ensembles and thick lines ensemble average. (c) Zonal mean AOD at 0.55 μm in October-November.

(February-March mean). Further splitting into single monthly means does not give qualitatively different results (not shown).

The Tambora-experiment and the KP-experiments simulate a significant warming in the tropical lower stratosphere from about 100 hPa up to 10 hPa and from the equator to 60°N during the whole winter following the eruption (Fig. 4.2). The positive temperature anomaly in the equatorial stratosphere of the Tambora experiment is approximately 19 K in early winter and peaks in late winter with approximately 21 K. The zonal mean temperature anomaly in the tropical stratosphere of the Tambora-experiment is about 4 times larger than the KP-experiments. The temperature anomaly in the KP-experiments reaches a maximum of about 5 K in late winter. This temperature anomaly in the KP-experiments is larger than the observed temperature anomaly after Pinatubo in the winter of 1991/1992 which is in the range of 2-3 K (Labitzke and McCormick 1992). The difference between the observed and the simulated temperature anomalies cannot fully be explained by the different magnitudes of the Krakatau and the Pinatubo eruptions that are averaged in the KP-ensemble. The temperature anomalies in the equatorial stratosphere are approximately only 0.5 K larger after the Krakatau eruption compared to the Pinatubo eruption. However, other sources of vari-

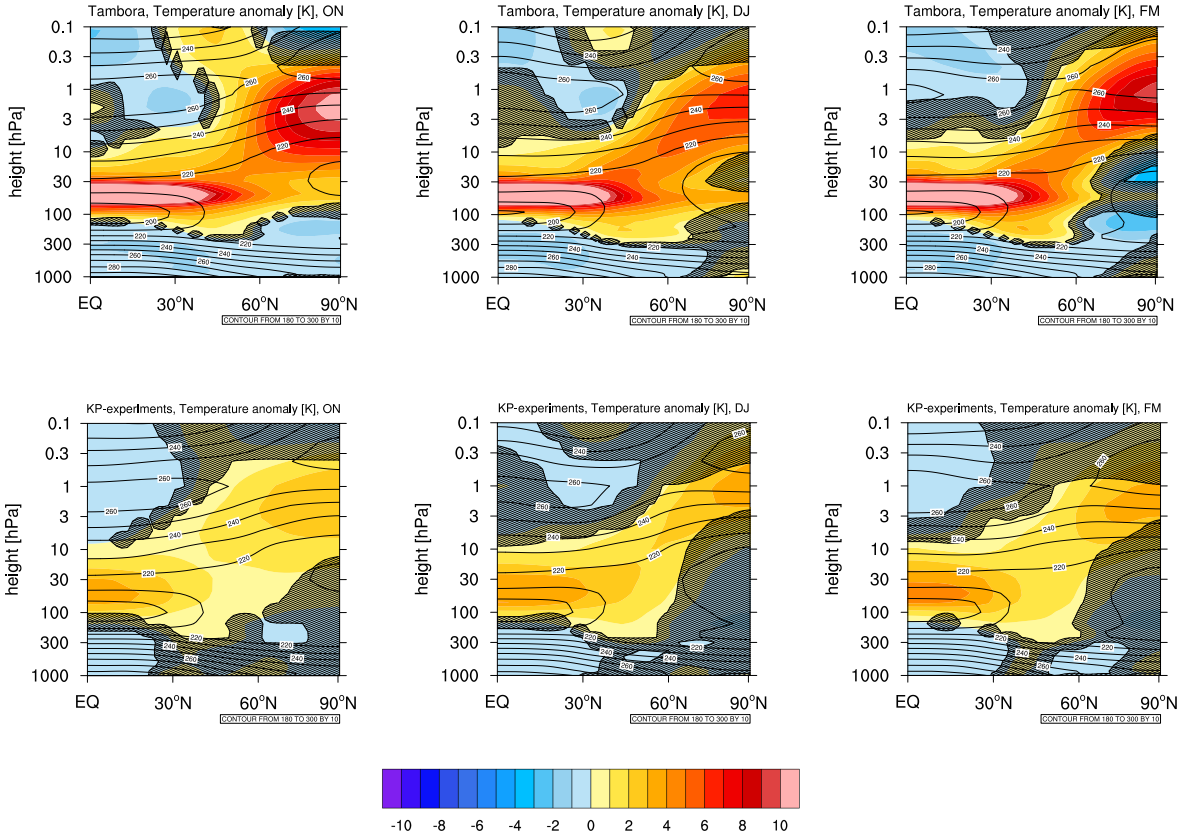

Figure 4.2: Ensemble average of the zonal mean temperature anomalies $[K]$ (shading) averaged over October-November (left), December-January (middle) and February-March (right) in the first NH winter for the Tambora- (top) and the KP-experiments (bottom). Contour lines display the climatological background conditions of the reference periods. Regions not significant at the 95% confidence level are hatched.

ability in the equatorial stratosphere, for instance the QBO and ENSO, or different ozone and water vapor concentrations, and feedback mechanisms can alter the temperature response of volcanic eruptions in the real atmosphere (Ramachandran et al. 2000). Thomas et al. (2009b) showed that it is crucial to include all known boundary conditions correctly to simulate the observed equatorial temperature response. They showed in model simulations that the easterly phase of the QBO after the Pinatubo eruption leads to a cooling in of 1-2 K at 30 hPa. Because our model set-up does not simulate a QBO, and also the AOD forcing fields have substantial uncertainties (Arfeuille et al. 2013), discrepancies to the observed temperature response are expected. In the upper stratosphere/lower mesosphere, a significant negative temperature anomaly in the equatorial region and a significant positive temperature anomaly over the poles occurs. Both temperature anomalies are due to the acceleration of the residual meridional circulation and the accompanied adiabatic heating and cooling anomalies, respectively. The contribution of longwave cooling seems to be of minor importance (Toohey et al. 2014). The maximum of the positive temperature anomaly in the polar upper stratosphere remains during the whole winter at approximately 3-1 hPa. Despite the differences in magnitude, the patterns of the zonal mean temperature anomalies are similar for all experiments.

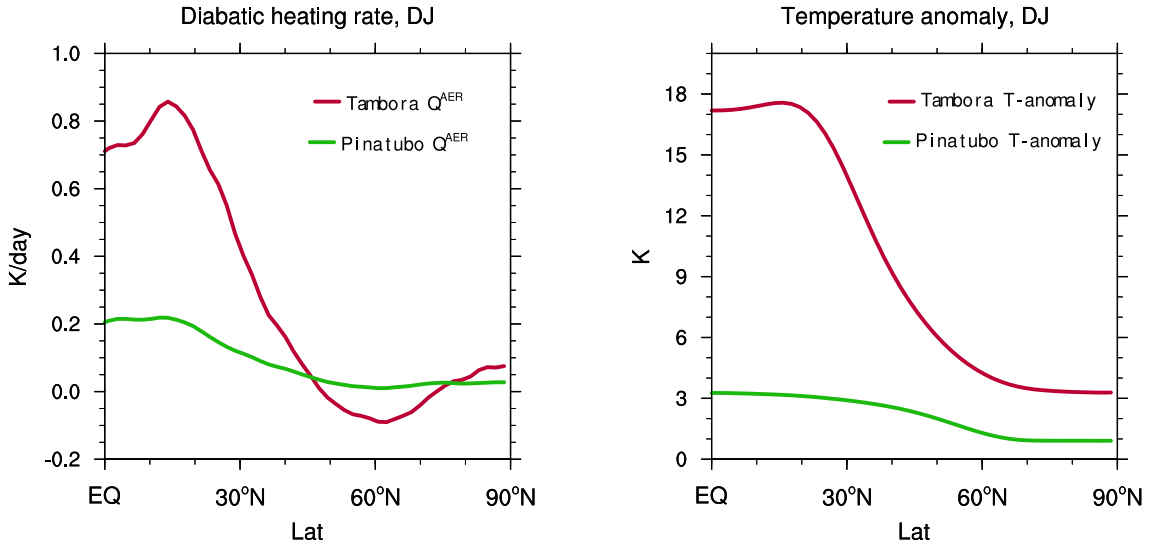

Figure 4.3: Left: 70-30 *hPa* DJ zonally averaged aerosol diabatic heating rates [*K/day*] in the first NH winter after the eruption of Tambora and Pinatubo. Right: Same but for the zonally averaged ensemble mean temperature anomalies [*K*].

The temperature response to volcanic eruptions is a result of radiative processes and other dynamical feedback mechanisms. The diabatic heating-rates due to aerosols (Q^{aer}) and the zonal mean temperature anomalies averaged between 70 and 30 *hPa* have a maximum in the equatorial latitudes (Fig. 4.3). I only show the diabatic heating rates for the Tambora eruption and the Pinatubo eruption, because only for those two eruptions the diabatic heating rates are available as model output. However, due to the very similar AOD fields, heating rates caused by aerosols from Krakatau and Pinatubo can be expected to be comparable. Despite the influence of other processes, such as dynamical cooling due to increased upwelling, tropical heating rates and temperature anomalies show qualitative agreement. Hence, the positive temperature anomaly in the tropical lower stratosphere, as seen in Figure 4.2, can be interpreted as the original perturbation and is mainly due to the short- and longwave radiation absorption by the volcanic aerosols. In the following I refer to the equatorial zonal mean temperature anomaly as the direct radiative response of the zonal mean temperature to volcanic aerosols.

The zonal mean zonal wind anomalies for the Tambora- and the KP-experiments show that in the NH, the maximum of the westerly winds in the upper stratosphere (0.3-1 *hPa*) in early and mid-winter is weakened due to adiabatic heating that is caused by the increased meridional circulation (Fig. 4.4). Only in late winter of the Tambora-experiment, the maximum wind speed of the polar vortex is significantly intensified. In the KP-experiments, a positive zonal wind anomaly in mid- and late winter can be obtainted, but is only locally significant. However, the magnitude of the intensification of the polar vortex is small compared to observations after El Chichón and Pinatubo (Kodera 1994). In the context of this study, an important feature is the positive zonal wind anomaly in early winter at approximately 30°N at 30 *hPa*. This zonal wind anomaly can be interpreted as the direct response of the wind field to the temperature perturbation by the volcanic aerosols. In early winter, the positive zonal wind anomaly

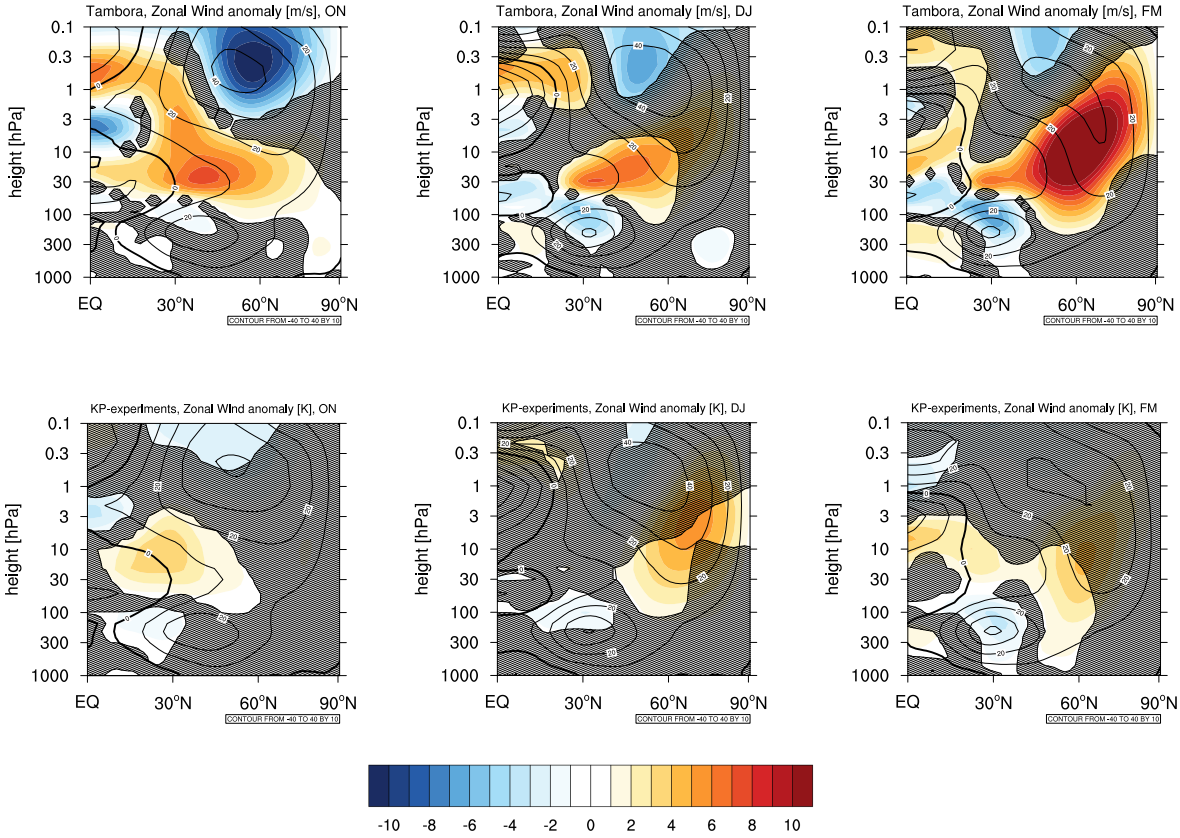

Figure 4.4: Ensemble average of the zonal mean zonal wind anomalies [m/s] (shading) averaged over October-November (left), December-January (middle) and February-March (right) in the first NH winter for the Tambora- (top) and the KP-experiments (bottom). Positive wind anomalies are defined as eastward. Contour lines display the climatological background conditions of the reference periods. Regions not significant at the 95% confidence level are hatched.

is significant in all experiments. In the case of the Tambora experiment, this zonal wind anomaly is persistent during the whole winter while in the KP-experiments it is significant only for early winter. It is worth mentioning that the positive zonal mean zonal wind anomaly in early winter at approximately 30°N is not a particular feature of the MPI-ESM-LR, but can be found in a large number of CMIP5 models (see chapter 5).

4.3.2 Meridional temperature gradient

The vertical change in the zonal wind due to temperature anomalies is dependent on the meridional temperature gradient and, due to the Coriolis force, on the latitude. The thermal wind relation implies that the zonal wind changes most where the meridional temperature gradient is steepest. Hence, I focus on the strength and position of the temperature anomaly and the corresponding meridional temperature gradient in the stratosphere.

To evaluate the model response, a comparison of the simulated zonal mean temper-

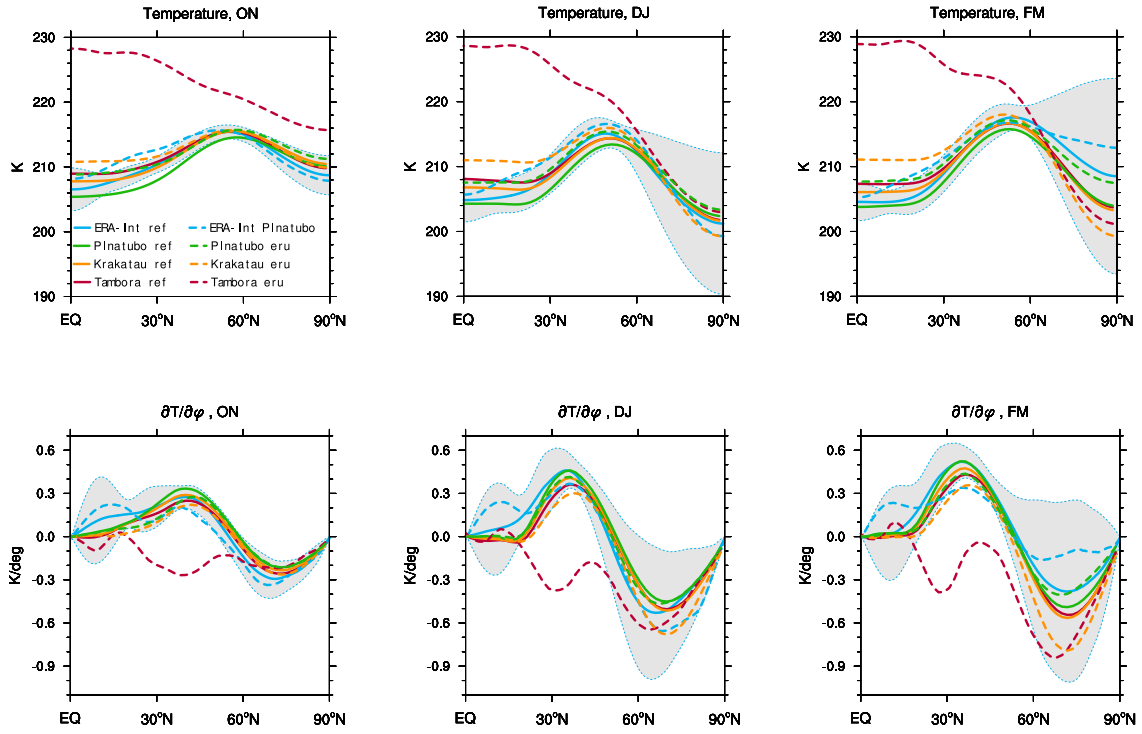

Figure 4.5: Ensemble averages of the zonal mean temperature $[K]$ (top) and temperature gradient $[K/°]$ (bottom) at 50 hPa averaged over October-November (left), December-January (middle) and February-March (right). The solid lines show the reference period without volcanic perturbations and the dashed lines the temperature in the NH winter following the respective eruption (red: Tambora; orange: Krakatau, green: Pinatubo). The blue solid line displays the temperature and its gradient averaged over the ERA-Interim period (1980-2001) with 2σ interval (grey shading) and the blue dashed line shows the respective quantities in ERA-Interim after the volcanic eruption of Pinatubo.

ature and its meridional gradient with ERA-Interim re-analysis at 50 hPa is shown in Figure 4.5. The model simulates lower temperatures in the sub-tropics and mid-latitudes for the Pinatubo reference period compared with the ERA-Interim volcanically unperturbed state. The temperatures lie outside the observed natural variability, indicated by the shaded interval of the ERA-Interim period in early winter, with a maximum difference of approximately 2 K, only. Due to the stratospheric cooling by ozone loss and increased anthropogenic greenhouse gases, the zonal mean temperature at 50 hPa is lower for the Pinatubo reference and ERA-Interim periods compared to the pre-industrial period of Tambora and Krakatau (Fig. 4.5, top row). The heating of the tropical stratosphere due to volcanic aerosols is apparent, since the zonal mean equatorial temperatures after the eruption (dashed lines) are higher compared to their corresponding reference periods (solid lines). The simulated meridional temperature gradient agrees well with the observed meridional temperature gradient obtained from ERA-Interim (Fig. 4.5, bottom row) and does not exceed the natural variability of the reanalysis dataset apart from a small region around 20°N in mid-winter. Hence, I assume that the present model set-up is capable of representing the background state of the zonal mean stratospheric temperature reliably. For the very large Tambora eruption, the temperature gradient changes the sign between 20°N-40°N. Under con-

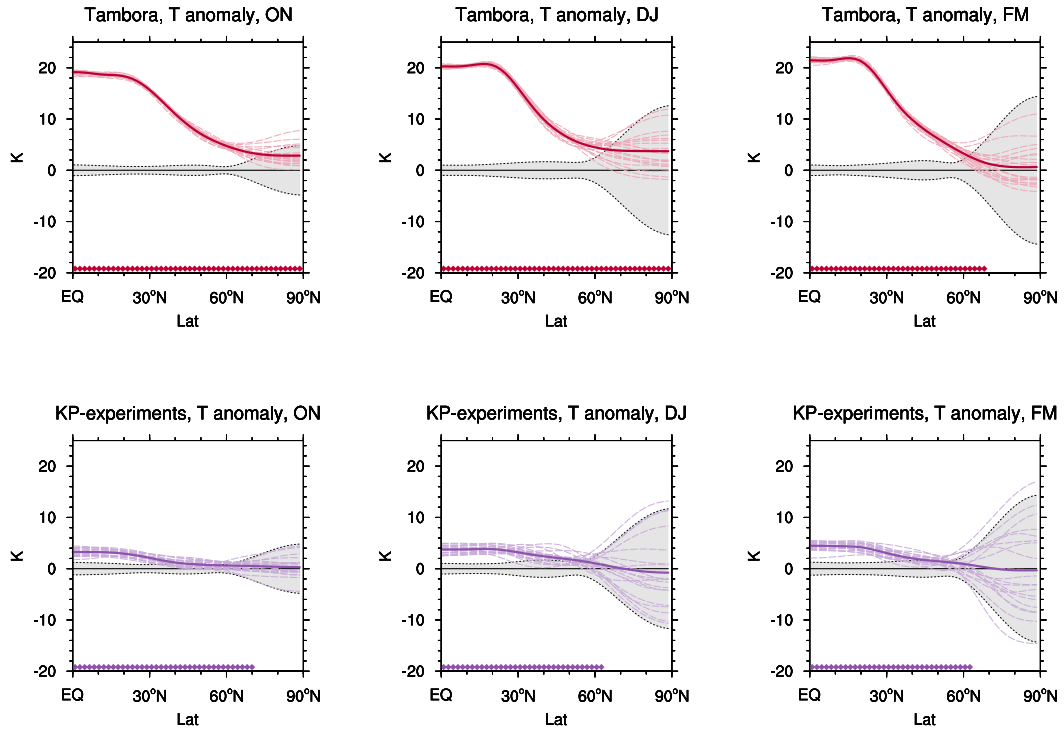

Figure 4.6: Zonal mean temperature anomalies $[K]$ at 50 hPa averaged over October-November (left), December-January (middle) and February-March (right) in the first post-eruption boreal winter for the Tambora- (top) and the KP-experiments (bottom). The thin dashed lines are the individual ensemble members and the thick solid line is the ensemble average. The grey shading displays the 2σ interval of the reference period of the respective experiment and bottom dots indicate whether the ensemble mean is significantly different from the reference period.

ditions without volcanic perturbations, the temperature at 50 hPa increases from the Equator northwards to approximately 50°N and afterwards decreases towards the pole. Because the Tambora eruption increases the temperature in low latitudes strongly, the local minimum at the equator disappears.

To identify the response of the zonal mean temperature to the volcanic forcing in more detail, Figure 4.6 illustrates zonal mean temperature anomalies at the height of the maximum heating in the equatorial region (50 hPa) for the Tambora and KP-experiments. The grey shaded area is the +/-2σ interval of the pre-eruption reference period for each experiment. The spread of the grey shaded area indicates the inter-annual variability of the zonal mean temperature, which is consistently small through the winter in the tropical stratosphere in absence of a QBO. At polar latitudes, the interannual variability is large compared to the tropics and increases through winter. In the Tambora experiment, the heating due to volcanic aerosols in the tropics leads to a positive zonal mean temperature anomaly of about 20 K from the equator to approximately 25°N. Northwards of 25°N, the positive zonal mean temperature anomaly decreases whereas the spread between the ensemble members increases. The positive temperature anomaly of the ensemble mean is significant at the 95% confidence level for all latitudes through winter apart from the polar latitudes in late winter as indicated by the markers at the bottom of the plot. For the KP-experiments, the shape

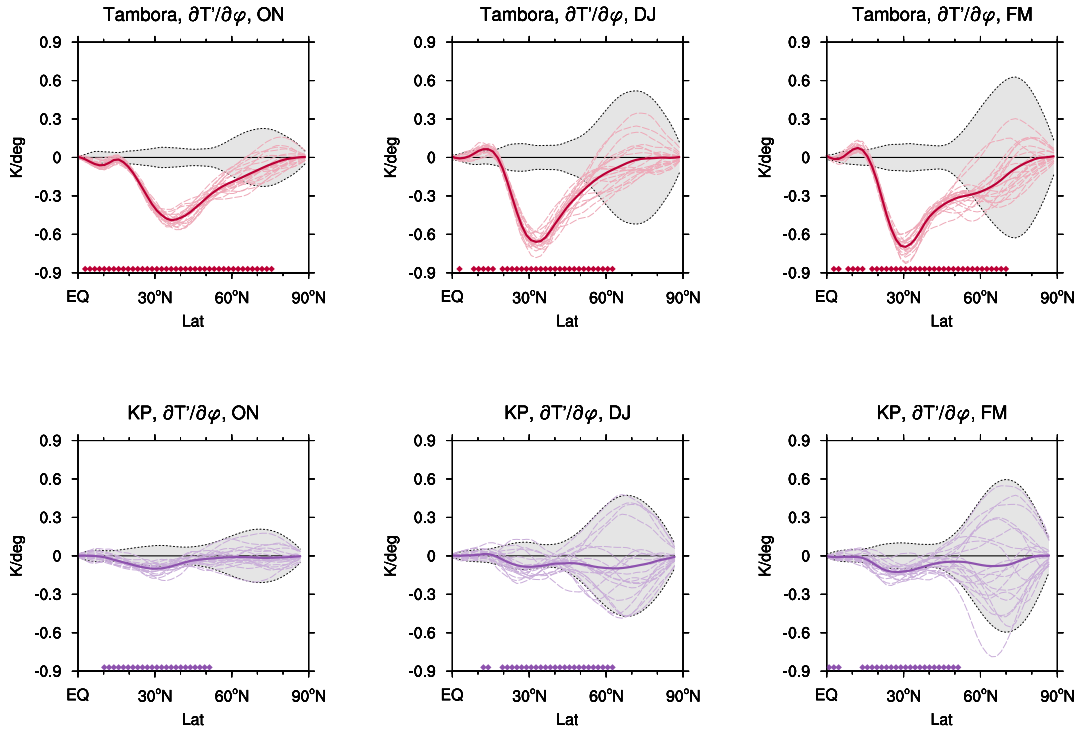

Figure 4.7: Same as Figure 4.6 but for the zonal mean temperature anomaly gradient $[K/°]$ at 50 hPa.

of the zonal mean temperature anomalies is similar to the Tambora experiment with positive anomalies from the Equator to 30°N and on average zero response in the polar latitudes. The maximum heating in the tropical stratosphere is 15 K smaller than in the Tambora experiment, but exceeds 95% confidence level of the reference period. The spread between the ensemble members in the NH polar region, however, is substantial in mid- and late winter. The ensemble mean shows no significant response at high latitudes. In the late winter, some ensemble members show significantly higher polar temperatures whereas others show the opposite. I will address this issue in more detail in section 4.3.3.

The thermal wind relation implies that the meridional temperature gradient across the polar vortex influences the strength of the polar vortex. The meridional temperature anomaly gradient, $\partial T'/\partial\varphi$, where φ is the latitude, for the Tambora-experiment and the KP-experiments (Fig. 4.7) shows negative values for decreasing temperature anomalies from the equator northwards. Independent of the eruption magnitude, the strongest ensemble mean meridional temperature anomaly gradient occurs around 30°N, where the heating due to the aerosols gets weaker from the tropics to the poles. For the Tambora experiment, the meridional gradient of every ensemble member at 30°N exceeds the confidence interval during the whole winter. The ensemble mean anomalies are significant from the equator up to 75°N in early winter, 60°N in mid-winter and 70°N in late winter, but the strongest signal can be obtained at extra-tropical latitudes. In the KP-experiments, the maximum meridional temperature anomaly gradient at 30°N is considerably smaller compared to the Tambora-experiment, but the ensemble mean exceeds the confidence interval from 10°N to 50°N in early and late winter and from

Table 4.1: Ensemble averaged zonal mean temperature anomaly gradient at 50 hPa $[K/°]$ +/- standard deviation between 20°N-40°N for Tambora, Krakatau and Pinatubo in October-November (ON), December-January (DJ) and February-March (FM).

	ON	DJ	FM
Tambora	-0.358 +/- 0.030 $K/°$	-0.522 +/- 0.052 $K/°$	-0.575 +/- 0.052 $K/°$
Krakatau	-0.087 +/- 0.034 $K/°$	-0.109 +/- 0.042 $K/°$	-0.132 +/- 0.038 $K/°$
Pinatubo	-0.088 +/- 0.036 $K/°$	-0.038 +/- 0.089 $K/°$	-0.088 +/- 0.055 $K/°$

10°N to 60°N in mid-winter. At 30°N in the extra-tropical stratosphere, significant westerly zonal wind anomalies are obtained in all experiments (Fig. 4.4). Thus, the response of the zonal wind field to the meridional temperature anomaly gradient is not a strengthening of the polar vortex, but a positive wind anomaly in the extra-tropical stratosphere. The position of the strongest meridional temperature anomaly gradient and the positive zonal mean zonal wind anomaly at 30°N in the KP-experiment are also obtained if the Krakatau and the Pinatubo eruption are considered separately. The temperature anomaly gradients for Krakatau and Pinatubo are similar during the winter compared to the strong Tambora eruption (see Table 4.1). Differences in the magnitude of the meridional temperature anomaly gradient between the Tambora and the KP-experiments may not solely be due to the different magnitudes of the forcing, but also to the different structures of the AOD reconstruction data sets. I will discuss this issue in more detail in section 4.4.

The positive wind anomaly in the sub-tropics implies an equator-ward shift of the zero-wind line and allows for more equator-ward wave propagation. For the case of the large Tambora eruption, this is illustrated in Figure 4.8 by the anomalies of the Eliassen-Palm Flux (EP-Flux) vectors at the location of positive zonal wind anomalies around 30°N. As a consequence, less waves break at high latitudes where the divergence

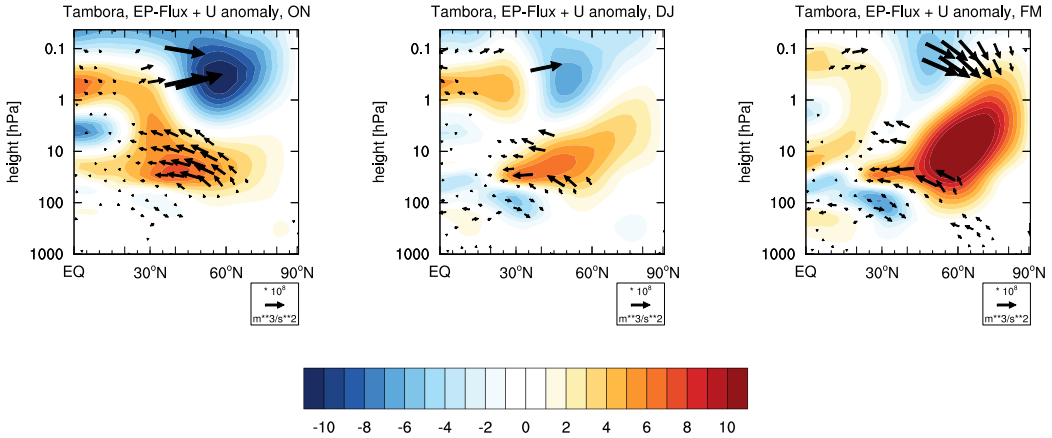

Figure 4.8: Shaded regions display the ensemble average zonal mean zonal wind anomalies $[m/s]$ averaged over October-November (left), December-January (middle) and February-March (right) in the first NH winter after the Tambora eruption (same as Figure 4.4, top row). Arrows show the ensemble average Eliassen-Palm Flux $[m^3/s^2]$. Only vectors which are significant at the 95% confidence level are shown. For better visibility, the EP-Flux vector is scaled by dividing by the basic density ρ_0.

of the EP-Flux (not shown) and thus the wave-driven deceleration of the polar vortex are reduced. Hence, the strengthening of the polar vortex in late winter is not solely an effect of the increased temperature gradient acting directly on the polar vortex, but rather an indirect effect due to a changed propagation of planetary waves. A similar behavior of the EP-Flux is obtained for the KP-experiments in early winter, but because the magnitude of the zonal wind perturbation at 30°N is smaller compared to the Tambora experiment, the change of the EP-Flux is also small (not shown). In mid- and late winter, where there is no significant change of the zonal mean zonal wind at approximately 30°N, the EP-Flux does not show significant response. It appears that because the original temperature anomaly only weakly affects the polar vortex directly and the response of the planetary waves is not significant, the response of the polar vortex is less robust.

4.3.3 Ensemble variability

In this section I investigate to what extent a tropical eruption influences the post-eruption ensemble variability of the polar stratosphere. I use the 50 hPa zonal mean temperature anomaly in the first year after the eruption and calculate the standard deviation of the 20 ensemble members for the Tambora- and KP-experiments. The interannual variability of the unperturbed stratosphere is represented by the standard deviation of 20 randomly chosen years of the pre-industrial control simulation and the pre-eruption reference period for the Tambora- and the KP-experiments, respectively. I repeat this resampling process 1,000 times and average over the standard deviations of the unperturbed stratosphere. The standard deviation of the ERA-Interim period, excluding winters influenced by volcanic eruptions, is also shown for reference (Fig. 4.9, bottom row). The unperturbed stratosphere of all experiments shows weak interannual variability in early winter at high latitudes. The interannual variability increases over the course of the winter reaching up to 7.5 K in late winter. Differences between the model and the reanalysis data occur in the tropics and mid-latitudes, where the re-analysis dataset shows higher interannual variability compared to the model. This can be explained by the absence of the QBO in the MPI-ESM-LR, which dominates the variability in the tropical stratosphere (Baldwin et al. 2001). At polar latitudes the MPI-ESM-LR captures the observed interannual variability throughout the winter well.

For the Tambora-experiment, significantly weaker ensemble variability in the equatorial stratosphere during the whole winter are obtained compared to the unperturbed variability (Fig. 4.9, top row). The diabatic heating of the volcanic aerosols reduces the ensemble variability, at least in the absence of the QBO. Striking is the significantly reduced ensemble variability in the northern polar stratosphere from mid-winter onwards. Even though there is no significant change in the temperature in this region in late winter, the decreased variability suggests that the polar stratosphere is constrained to a certain zonal mean temperature at 50 hPa. The KP-experiments exhibit two remarkable differences compared to the Tambora-experiment (Fig. 4.9, bottom row). First, the ensemble variability in the tropical stratosphere is not reduced compared to the control variability. The weak increase is related to the slightly different diabatic heating rates between the Krakatau and the Pinatubo experiments, which lead

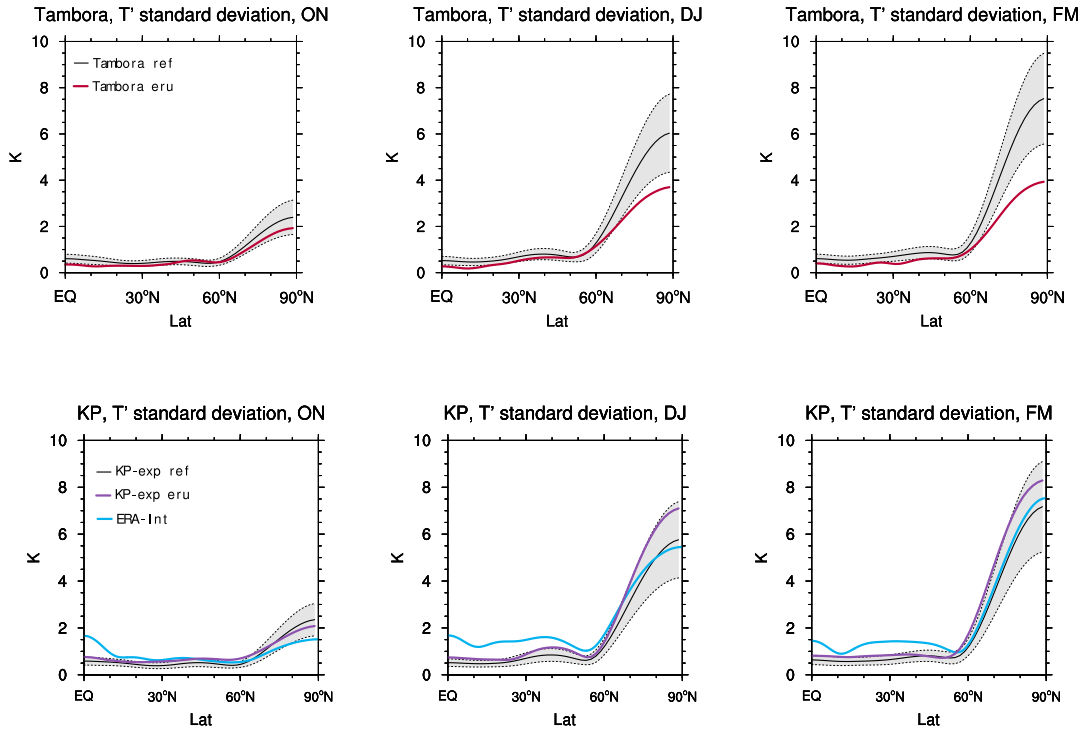

Figure 4.9: Standard deviation of the 50 hPa zonal mean temperature anomalies $[K]$ averaged over October-November (left), December-January (middle) and February-March (right) in the first NH winter for the Tambora- (top) and the KP-experiments (bottom). The solid black line displays the averaged standard deviation of a 20 member ensemble randomly drawn 1.000 times out of the reference period with the grey shading as 2σ interval. The blue solid line in the bottom figures shows the 50 hPa zonal mean temperature standard deviation of the ERA-Interim period excluding years with volcanic eruptions.

to slightly different temperature anomalies between the Krakatau and the Pinatubo eruptions. Second, the ensemble variability of the 50 hPa temperature anomaly at mid- and high latitudes is not decreased but increased compared to the unperturbed stratosphere.

To investigate response of the polar vortex variability to the applied forcing, I show the ensemble variability anomalies of the zonal mean zonal wind in Figure 4.10. I subtracted the interannual variability of the volcanically unperturbed period from the ensemble variability of the Tambora- and KP-experiments at all pressure levels and NH latitudes. I do not find any significant responses in the NH polar region in early winter, but mid- and late winter show a similar response (late winter shown in Fig. 4.10). A significant reduction of the polar vortex variability is apparent in the Tambora-experiment, which confirms the findings of the zonal mean temperature variability at 50 hPa in Figure 4.9. The reduced variability is significant between 100 hPa and 3 hPa north of 60°N. Hence, the polar vortex is constrained to a state of stronger-then-average zonal winds. The variability anomalies of the zonal mean zonal wind of the KP-experiment show the opposite response, with increased variability in the region of the polar vortex. The signal is slightly shifted equator-wards and only significant in a small region between 100 hPa and 30 hPa at 60°N. The increase in variability in the KP-ensemble is not due to the merging of the Krakatau and Pinatubo eruption,

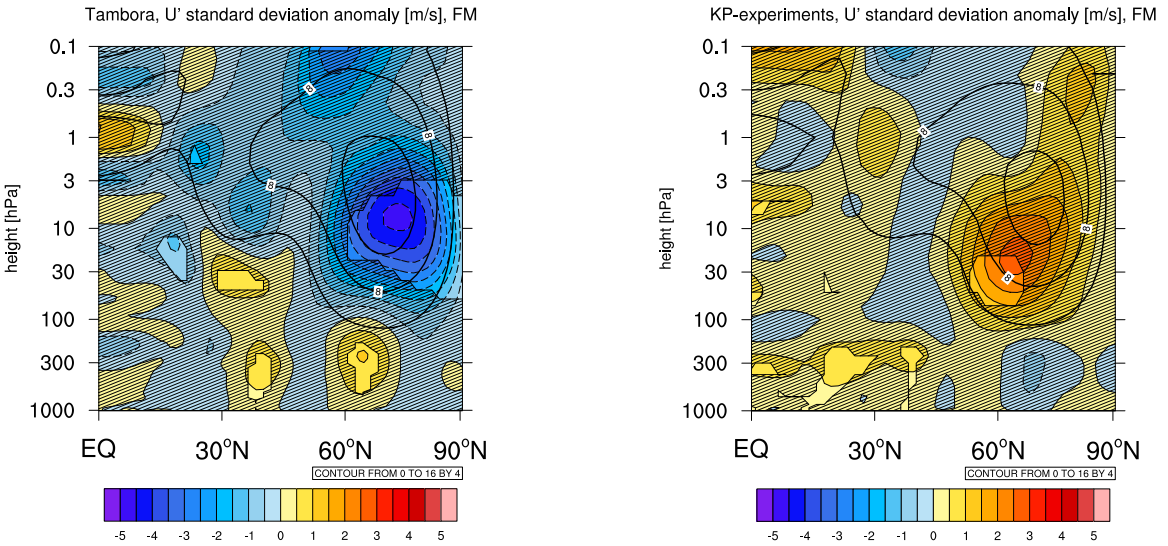

Figure 4.10: Standard deviation anomalies of the zonal mean zonal wind anomalies $[m/s]$ (colored) averaged over February-March in the first NH winter for the Tambora- (left) and the KP-experiments (right). Contour lines display the climatological background conditions of the reference periods. Regions not significant at the 2σ level are hatched.

because a similar behavior is found if one considers both eruption separately. The reason of the increased variability is at the moment unclear. Nevertheless, the different behavior of the Tambora- and KP-experiments, especially the reduced variability of the Tambora-ensemble, indicates that only the very strong Tambora forcing produces a robust stronger-than-average NH polar vortex.

The increased ensemble variability in the KP-experiments in the NH polar stratosphere, with respect to the interannual variability of the unperturbed reference period, helps to explain the limited response of climate models to volcanic eruptions in the CMIP5 historical period. The presented results show that at least the MPI-ESM-LR is able to reproduce the observed intensification of the polar vortex as expected based on observations, but only for very strong eruptions the model is constrained to a state of a stronger vortex. In contrast to the Tambora simulations, an eruption of the strength of Krakatau or Pinatubo is, in this model set-up and with 10 ensemble members, not large enough to force the polar stratosphere into a state of a stronger vortex. Even if the ensemble average suggests an intensified polar vortex, the impact of the volcanic eruption is not discernable from the internal variability of the polar NH stratosphere. Thus, for smaller eruptions compared to Tambora, like Krakatau or Pinatubo, the model internal variability masks the response to the forcing of the volcanic aerosols.

4.4 Discussion

In addition to the magnitude of the volcanic eruption, it is likely that the spatial structure of the forcing plays a significant role in controlling the dynamical response (Toohey et al. 2014). In contrast to the Stenchikov AOD field used in the KP-experiments, the AOD field of Crowley used for the Tambora-experiment is only available in four latitude bands (90°S-30°S, 30°S-0°, 0°-30°N, 30°N-90°N). To avoid unrealistically steep gradients, the original values for the AOD are linearly interpolated between 15°N-45°N, 15°S-15°N and 15°S-45°S. But with only four latitude bands, the model will create different heating gradients compared to the AOD field of Stenchikov, where the AOD does not linearly decrease from the equator to the North Pole. However, observations following the Pinatubo eruption suggest that the bulk of the aerosols remained in the tropical middle stratosphere. The tropical stratosphere can be regarded as a temporary reservoir for aerosols entering the stratosphere through the tropical tropopause (Trepte and Hitchman 1992). The position of the AOD gradient of the Crowley dataset for the Tambora eruption agrees with satellite measurements after the tropical Pinatubo eruption that showed that the aerosols cloud was bounded between 20°S and 30°N (McCormick and Veiga 1992; Trepte et al. 1993). As I have shown in Figure 4.1c, the position of the zonal mean AOD gradient of the Tambora eruption is in reasonable agreement with the position of the zonal mean AOD gradient of the much finer resolved Krakatau and Pinatubo eruptions. Actually, the AOD gradient is constant in the Tambora experiment between 15°N and 45°N. That implies that the position of the maximum temperature anomaly is not solely due to the exact location of the AOD gradient but might also be influence by the solar zenith angle and possible feedback mechanisms. This idealized Tambora setup shows, that the exact location of the AOD gradient might not be so important. Nevertheless, the spatial pattern of the AOD depends on the exact latitude and season of the eruption (Toohey et al. 2013; Sigl et al. 2014), but as all three eruptions take place in spring/summer season, I assume that the influence of the season is not significant in the experiments for the processes I investigated in this study. Even for Pinatubo —the best observed eruption in history— the volcanic aerosol forcing datasets suffer from uncertainties due to gaps in the satellite record from sparse sampling of the satellite instrument (Stenchikov et al. 1998). Furthermore, the large optical depth in the initial months after the eruption reduced atmospheric transmission below detectability (Russell et al. 1996), which might lead to an underestimation of the true AOD. Updates to the retrieval of the satellite products have led to significant changes in the space-time morphology of the estimated aerosol extinction after the Pinatubo eruption (Arfeuille et al. 2013) and a new forcing set has been made available. A comparison between the dataset of Stenchikov used here and the new forcing set by Arfeuille et al. (2013) (SAGE 4λ) with respect to their impact on the NH winter circulation was done in the study by Toohey et al. (2014), where they did not find a significant difference in the NH winter polar vortex response between these two datasets.

Re-analysis data suggest a stronger polar vortex after volcanic eruptions, which is accompanied by low temperatures and low geopotential height over the NH polar cap (Driscoll et al. 2012; Charlton-Perez et al. 2013). In the Tambora experiment with

the MPI-ESM-LR, the intensification of the polar vortex in late winter is not due to low temperatures/geopotential heights at the pole, but high temperatures/geopotential heights over the tropical region extending towards the North Pole. The temperature anomalies in the KP-experiments are not sufficiently strong to influence the polar vortex directly but induce a positive zonal wind anomaly in the extra-tropical region. In this context it is important to mention that the effects of ozone is not adequately accounted for in our simulations (see chapter 2.1). The ozone depletion after a volcanic eruption leads to a colder polar stratosphere in the following winter (Stenchikov et al. 2002). In the case of the Pinatubo eruption with ozone depleting substances in the stratosphere, the meridional temperature gradient will not be affected by the tropical heating alone, but the cooling due to ozone depletion at polar latitudes might influence the polar vortex directly. On the other hand, negative ozone anomalies in the tropical stratosphere after a tropical volcanic eruptions damp the heating due to the volcanic aerosols (Thomas et al. 2009a). A modelling study by Muthers et al. (2014) with the coupled atmosphere-ocean model SOCOL3-MPIOM shows that for a Tambora-like eruption the influence of different ozone climatologies on the NH continental winter warming at the surface is significant. With our model setup it is not possible to quantify the impact of ozone on the tropical and high latitude temperature anomalies. Dedicated experiments with and without ozone changes would be necessary to quantify how much ozone contributes to the simulated temperature changes.

A robust result of the Tambora-experiment and the KP-experiments, as well as for Krakatau and Pinatubo separately, is the positive zonal wind anomaly in the stratosphere at approximately 30°N. This result agrees with findings of Stenchikov et al. (2002) who state that the stratospheric radiative forcing from tropical volcanic aerosols is confined to lower latitudes and does not act directly on the polar vortex. A zonal wind anomaly in the extra-tropical region changes the background conditions for the propagation of tropospheric planetary waves (Shepherd and McLandress 2011). Because the variability of the polar vortex strength is largely controlled by planetary wave drag (Newman et al. 2001; Polvani and Waugh 2004), changes of the background conditions for planetary waves to propagate into the stratosphere will have an impact on the polar vortex. An indirect effect of the diabatic heating on the polar vortex can be seen in the Tambora-experiment of the MPI-ESM-LR, where planetary waves are deflected towards lower latitudes and consequently deposit less momentum into the polar region. Whether or not there is an indirect effect of the volcanic eruptions on the polar vortex in the real atmosphere is difficult to examine, because of the limited number of observed eruptions. Additionally, in the real atmosphere other factors of variability alter the propagation of waves, for instance the QBO which is not present in our model set-up, and ENSO that in individual simulations is in accidental phase-correlation with the volcanic eruptions. Concerning the phase of ENSO, I find no bias towards a specific phase in the Tambora ensemble but a slight domination of La Niña phases in the KP-ensemble. I expect that this small bias does not impact our results qualitatively. However, the combination of ENSO and volcanic forcing might not be linear (Graf et al. 2014) and disentangling the effects would need additional experiments which is beyond the scope of this study. In a model with an internal generated QBO, the QBO itself may also strengthen or dampen the positive zonal wind anomaly at 30°N. Therefore, the deflection of planetary waves may be altered dependent on the

phase of the QBO. Re-analysis data show evidence of an increased wave flux into the stratosphere following the last three large tropical eruptions (Graf et al. 2007), which might be biased because of coinciding El Niño events, but might as well support the hypothesis of changed background conditions for the propagation of planetary waves. Toohey et al. (2014) found in MPI-ESM-LR simulations an enhanced stratospheric residual circulation resulting from enhanced resolved wave activity in mid-latitudes. In polar latitudes, the adiabatic heating due to the enhanced residual circulation dominates over the diabatic heating of the volcanic aerosols. Therefore, Toohey et al. (2014) concluded that the meridional temperature gradient at polar latitudes is primarily an indirect response to the aerosol diabatic heating at the equator.

As outlined in the chapter 1, coupled climate models fail to reproduce on average the robust surface winter warming pattern observed after large tropical volcanic eruption (Driscoll et al. 2012). Also the intensified polar vortex, which is observed even after the smaller eruption of El Chichón is not captured by the CMIP5 ensemble (Charlton-Perez et al. 2013). This study focuses on the stratospheric response. Nevertheless, an analysis of the near surface temperature and sea level pressure anomalies after the Tambora- and KP-experiments has been conducted. For the KP-experiments, I do not find any significant changes of the mean sea level pressure and the near surface temperature, apart from the surface cooling in low latitudes. This is not surprising, because no significantly stronger polar vortex is simulated, so one would not expect a response of the NAO. For the Tambora experiment, the surface temperature shows a significant increase over the central Arctic. The sea level pressure increases in the northern Atlantic and decreases North of Iceland. However, a deeper investigation of the surface signal after the Tambora eruption is beyond the scope of this study.

4.5 Summary and conclusions

I investigated the impact of large tropical volcanic eruptions on the NH polar stratosphere in the MPI-ESM-LR. I compared two ensembles of simulations of different eruption strengths and focus on the first post-eruption winter. One 20-member ensemble of simulations covers the large Tambora eruption and a second ensemble (KP-experiments) consists of a 10-member ensemble of simulations of the Krakatau eruption and a 10-member ensemble of simulations of the Pinatubo eruption. Krakatau and Pinatubo simulations are combined because these two eruptions are of similar eruption strengths and significantly weaker compared to the Tambora eruption.

All model experiments show the expected positive zonal-mean temperature anomalies in the equatorial stratosphere due to the absorption of radiation by the volcanic aerosols. The temperature anomalies in this region are four times larger after the Tambora eruption compared to the KP-eruptions. The zonal wind anomalies show only in late winter after the Tambora eruption a significant intensification of the polar vortex. After the smaller KP-eruptions, the strengthening of the polar vortex is weak compared to observations, and only locally significant.

I focused on two important factors to explain the different results of the Tambora-experiment compared to the KP-experiments: First, the position of the maximum

meridional temperature gradient in the stratosphere after a volcanic eruption, and, second, the volcanically induced effect on the ensemble spread of the NH stratospheric temperature and zonal wind anomalies. The main results are summarized as follows:

1. The strongest change of the stratospheric temperature gradient is not in the region of the polar vortex, but occurs equator-wards at approximately 30°N, at the edge of the bulk of the tropical aerosol cloud. Consequently, I find significant zonal wind anomalies in both experiments at 30°N between 50-10 hPa, especially in early winter.

2. I find a reduced ensemble spread in the northern polar stratosphere for the very large Tambora eruption. In the case of the smaller KP eruptions, the ensemble spread of the stratospheric temperature and zonal wind anomalies is in some areas even significantly enlarged.

I find that the intensified polar vortex in the Tambora-experiment is not solely due to the direct effect of the increased meridional temperature gradient by the heating of the volcanic aerosols in the tropical stratosphere. The direct effect is rather a positive zonal wind anomaly around 30°N that changes the conditions for wave propagation, leading to a deflection of planetary waves to lower latitudes. These waves will deposit less momentum in the region of the NH polar vortex and therefore wave-driven deceleration of the zonal wind at high latitudes is hampered. The reduced ensemble spread and the higher zonal wind speed in the polar stratosphere imply that the model is forced into a state of a significantly intensified polar vortex. For the smaller eruptions of Pinatubo and Krakatau, the increased meridional temperature gradient does only weakly influence the polar vortex directly and the indirect effect by the deflection of waves towards lower latitudes is less robust. The large spread between the individual ensemble-members of the KP simulations reveals that internal variability plays a dominant role for the state of the polar vortex in the post-eruption winter. To what extent the indirect effect acts in the real atmosphere is hard to quantify, because of the lack of stratospheric observations after large tropical volcanic eruptions. Moreover, other sources of variability, for instance the QBO and ENSO, alter the proposed mechanism of the deflection of planetary waves. However, at least in the MPI-ESM-LR the internal variability masks the impact of an eruption of the size of Pinatubo or Krakatau. The reason for this masking is twofold: First, the MPI-ESM-LR shows a slightly too large interannual variability compared to observations in early winter. This overestimation of variability might have an impact on the evolution of the polar vortex in mid- and late winter. Second, the polar vortex in the MPI-ESM-LR seems to be relatively insensitive also to other forcings such as the QBO, solar variability, and ENSO (Schmidt et al. 2013). The two eruptions of Krakatau and Pinatubo are the strongest tropical eruptions since 1850. Therefore, the lack of a significant impact of volcanic eruptions on the NH polar vortex in the CMIP5 historical period could be due to the dynamical effects of the volcanic forcing being not discernable from internal variability.

Concerning the main focus, the impact in the NH winter stratosphere, this study cannot give a final answer to the question why models seem to underestimate the response to large tropical volcanic eruptions. However, I have identified a dynamical mechanism

that links the sub-tropical gradient in the heating rate anomaly with the strength of the polar vortex. The fact that it robustly strengthens the polar vortex only for a very large eruption (Tambora) may hint to an imperfect representation of wave-mean flow interactions in the model. To what extent this proposed mechanism plays a dominant role in the real atmosphere is difficult to quantify due to the very limited number of eruptions in the satellite era. Another candidate leading to the underestimation of the vortex strengthening in climate models is the negligence of ozone anomalies. Further research should hence be directed into these two directions: wave-mean flow interactions and ozone anomalies in post-eruption winter.

Chapter 5

Polar vortex response to volcanic eruptions: the impact of early winter polar vortex variability and strength

5.1 Introduction

For the major part of this thesis, I focus on the response to volcanic eruptions of one comprehensive climate model, the MPI-ESM. However, the apparent inability to capture the observed dynamical response to volcanic eruptions is not just an issue of this particular model, but has been identified in a large number of coupled climate models. In a comprehensive study, Driscoll et al. (2012) analyzed 13 coupled climate models that participated in CMIP5 and concluded that the models generally fail to simulate a strengthened NH polar vortex, a positive NAO, and the continental winter warming pattern, at least in an average of the nine largest tropical eruptions from 1880 to 2005. Driscoll et al. (2012) are, however, not able to give a conclusive explanation to why the models underestimate the impact of volcanic eruptions. In this chapter I investigate a possible reason for this shortcoming of the climate models. I hypothesize that the variability and strength of the polar vortex in early winter could be key to simulate a stronger polar vortex after volcanic eruptions.

To represent the variability and strength of the NH polar stratosphere reliably, the climate models must have a well-resolved stratosphere (Charlton-Perez et al. 2013). The coupled climate models that participated in CMIP5 resolve the stratosphere reasonable well with only few models that have a model lid near 10 hPa. Moreover, 15 out of 45 models in the CMIP5 archive have a model top above 1 hPa (high-top models). While the high-top models have a significantly better representation of the stratospheric variability on daily and interannual time scales compared to low-top models, neither high-top nor low-top models simulate the observed decadal variability in the NH polar stratosphere reliably (Charlton-Perez et al. 2013). Charlton-Perez et al. (2013) claimed that this underestimation of decadal variability is likely due to the fact that neither ensemble can reproduce the dynamical response to volcanic eruptions. Because there is no substantial difference between high-top models and low-top models with regard to their simulation of the dynamical response to volcanic forcing, the absence of a well-resolved stratosphere is apparently not the cause of the why models seem to underestimate the response to volcanic eruptions.

According to Kodera and Kuroda (2002), the mean evolution of the polar vortex during winter can be characterized in three stages. In early winter, the wind speed increases monotonically and almost identically each year. This stage can be considered to be primarily radiatively controlled. In late winter, the polar vortex gets weaker and the polar stratosphere warms. Here, planetary waves largely determine the state of the vortex and therefore the vortex is dynamically controlled. Between these two stages, there is a transition phase from the radiatively to the dynamically controlled state. Volcanic eruptions can change the dynamically controlled stage by altering the wave propagation and the upward wave flux from the troposphere into the stratosphere (Toohey et al. 2014). However, as shown in chapter 4 for the MPI-ESM-LR, the change of wave propagation is only significant for very large eruptions as Tambora. It is still unclear whether fewer waves enter the stratosphere after volcanic eruptions due to a weaker tropospheric meridional temperature gradient (Stenchikov et al. 2004) or more waves enter the stratosphere as observed after the latest eruptions (Graf et al. 2007). But certainly volcanic eruptions act on the radiatively controlled stage by changing the equator-to-pole temperature gradient in the stratosphere. Therefore, volcanic eruptions should have the strongest impact in early winter when the variability of the polar vortex is small, as seen in chapter 4.

However, climate models show a considerable spread in the simulated variability of the polar vortex in early winter. This potentially implies that for those models with a large early winter variability, the polar vortex is not solely radiatively but also already dynamically controlled. In this case, the response of the polar vortex to volcanic eruptions might be weakened, because the polar vortex will not only respond to the radiative forcing of the volcanic aerosols, but also to wave perturbations in contrast to the study of Kodera and Kuroda (2002) which is based on reanalysis data. In this chapter I examine the response of the NH polar stratosphere to the tropical volcanic eruption of Krakatau, El Chichón and Pinatubo in the CMIP5 ensemble with respect to the NH early winter polar vortex interannual variability and polar vortex strength. First, I introduce the CMIP5 models which are used in this study (section 5.2). Then I will assess the models with regard to their ability to represent the mean state and variability of the NH polar vortex in boreal winter (section 5.3.1) before investigating the influence of the polar vortex variability (section 5.3.2) and polar vortex strength (section 5.3.3) on response of the models to the volcanic forcing. At the end of this chapter, I summarize and conclude the main finding (section 5.4).

5.2 Data and Methods

I analyze the CMIP5 historical simulations (1850-2005) in which the models are forced with observed greenhouse gas concentrations, solar irradiance variability, land use change, ozone depletion, and tropospheric and stratospheric aerosols (Taylor et al. 2011). The set of CMIP5 models which are analyzed in this study are listed in Table 5.1, as well as the model lid, the volcanic forcing dataset which is applied in the different models, and the vertical resolution of the models to indicate high-top and low-top models. The threshold to distinguish high-top and low-top models is usually

Table 5.1: Models used in this study as well as their upper model lid height, numbers of vertical levels, volcanic forcing dataset, and number of ensemble members.

Model Name	Modelling Group	Lid Height	Vertical Levels	Volcanic Forcing	Ensemble Size
BCC-CSM1-1	Beijing Climate Center	2.9 hPa	26	Amman	3
CESM1-CAM5	National Center for Atmospheric Research	5.1×10^{-6} hPa	30	Interactive	3
CanESM2	Canadian Centre for Climate Modelling	1 hPa	35	Sato	5
CCSM4	National Center for Atmospheric Research	2.2 hPa	27	Ammann	6
CNRM-CM5	Centre National de Recherches Meteorologique	10 hPa	31	Sato	10
CSIRO-Mk3-6-0	Commonwealth Scientific and Industrial Research Organisation	4.5 hPa	18	Sato	10
GISS-E2-R	NASA Goddard Institute for Space Studies	0.1 hPa	40	Sato	6
GFDL-CM3	NOAA Geophysical Fluid Dynamics Laboratory	0.01 hPa	48	Stenchikov	5
HadGEM2-ES	Met Office Hadley Centre	40 km	38	Sato	4
MIROC-ESM	Japan Agency for Marine-Earth Science and Technology	0.0036 hPa	80	Sato	3
MPI-ESM-LR	Max Planck Institute for Meteorology	0.01 hPa	47	Stenchikov	10
MPI-ESM-MR	Max Planck Institute for Meteorology	0.01 hPa	95	Stenchikov	3
MRI-CGCM3	Meteorological Research Institute	0.01 hPa	48	Interactive	5
NorESM1-M	Norwegian Climate Centre	3.54 hPa	26	Ammann	3
CESM1-WACCM	National Center for Atmospheric Research	5.1×10^{-6} hPa	66	Interactive	7

set at 1 hPa (Cagnazzo and Manzini 2009; Charlton-Perez et al. 2013). For the volcanic forcing, in most of the models either the reconstruction of volcanic aerosols by Ammann (2003), its update (Ammann et al. 2007) or the reconstruction by Sato et al. (1993), updated by Stenchikov et al. (1998) is applied. The volcanic forcing dataset of Ammann (2003) and Ammann et al. (2007) provide monthly distribution of aerosol optical depth (AOD) for 64 latitude bands. The effective radius is 0.42 μm and the distribution size is fixed for all volcanic eruptions. The volcanic forcing dataset of Stenchikov et al. (1998), which is used in the MPI-ESM, is described in detail in chapter 2.1.1. The MRI-CGCM3 does not prescribe the volcanic forcings, but interactively computes the conversion from SO_2 amount to stratospheric aerosol by including the aerosol model MASINGAR mk-2 (Tanaka et al. 2003). MASINGAR-mk2 uses volcanic SO_2 emissions provided by Stothers (1996), Bluth et al. (1997), Andres and Kasgnoc (1998), and Stothers (2001) and is interactively coupled with the atmospheric component of MRI-CGCM3. Also the CESM1-CAM5 and the CESM1-WACCM do not use a prescribed AOD forcing dataset, but prescribe surface area density of the volcanic aerosols and calculate the heating rates via conversion of the surface area density to voloume density of H_2SO_4/H_2O aerosols (Marsh et al. 2013).

I investigate the response of the NH polar vortex to the eruptions of Krakatau, El Chichón and Pinatubo. The Krakatau and the Pinatubo eruptions are of comparable size and the strongest eruptions in the historical simulations, thus I expect these eruptions to yield the clearest signal in the respective post-eruption winters. The El Chichón eruption is approximately 1/3 of the Pinatubo magnitude, but since it is besides Pinatubo the only major tropical eruption for which satellite observations exists,

I thus can compare the El Chichón eruption to reanalysis data. Further details about the three eruptions are given in chapter 2, as well as the method of calculation the post-eruption anomalies. For the multi-model mean, the models have been interpolated to a common grid of the models with the lowest vertical (Nor-ESM1-M) and horizontal (HadGEM2-ES) resolution to avoid upscaling errors. To obtain the multi-model mean, I average the ensemble mean of each individual model with equal weight.

5.3 Results

5.3.1 Model evaluation of the polar vortex mean state, variability and response to volcanic eruptions

It is important to assess the CMIP5 models with regard to their ability to represent the mean state and the variability of the NH polar vortex in boreal winter before statements about the response to volcanic eruptions can be made. Since I focus on the radiatively controlled and the transition to the dynamically controlled stage of the NH winter, I show early winter (October-November mean —ON) and mid-winter (December-January mean —DJ) results for the respective analyses. Late winter (February-March) is omitted, because in this stage the polar stratosphere is to a large extent dynamically controlled.

The zonal mean zonal wind averaged over the time period from 1970 until 2001 in ON and DJ for each individual model is shown in Figure 5.1. There are differences among the models in terms of absolute magnitude as well as development of the NH polar vortex. While most models simulate the observed transition from weaker westerlies in early winter to a maximum wind speed in mid-winter (GFDL-CM3, HadGEM2-ES, MIROC-ESM, MPI-ESM-LR, MPI-ESM-MR MRI-CGCM, Nor-ESM1-M), another set of models do not show strong differences between early and mid-winter polar vortex strength, but rather constant wind speeds (Can-ESM2, CSIRO-Mk3-6-0, CESM1-WACCM). The GISS-ES-R model does not show a distinct polar vortex at all. However, the multi-model mean of the CMIP5 ensemble agrees reasonably well with ERA-40 reanalysis data (Fig. 5.2) in terms of vortex strength as well as the position of the vortex, in both early and mid-winter.

The distinction between the radiatively and the dynamically controlled stages is manifested by the change of the interannual variability in the NH polar stratosphere from early to mid-winter. The most obvious difference among the models, however, is in the equatorial stratosphere, where some models (GFDL-CM3, MIROC-ESM, MPI-ESM-MR and CESM1-WACCM) simulate a Quasi-Biennial Oscillation (QBO) and therefore show larger variability in this region and consequently compare better with observations (Fig. 5.3). In northern high latitudes the models differ more strongly among each other in terms of their interannual variability compared to the inter-model difference in the zonal mean zonal wind. While most of the models reproduce the observed temporal evolution of the variability during winter, with comparably small values in early winter and an increase during mid-winter, the absolute magnitude of the simulated

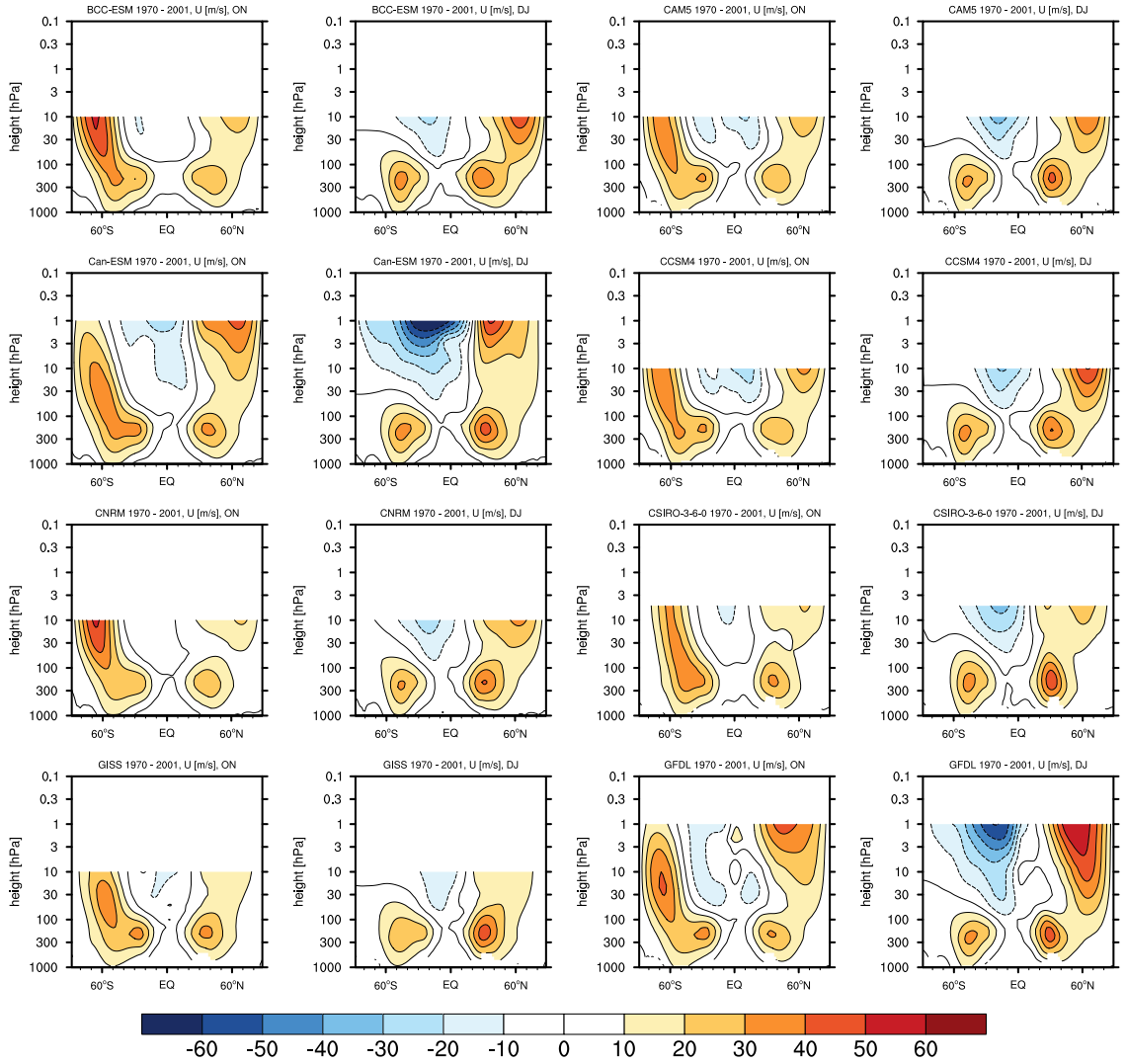

Figure 5.1: Ensemble mean of each individual model of the zonal mean zonal wind averaged over the time period from 1970-2001 from the historical simulations in early (ON) and mid-winter (DJ). Positive values denote westerly winds.

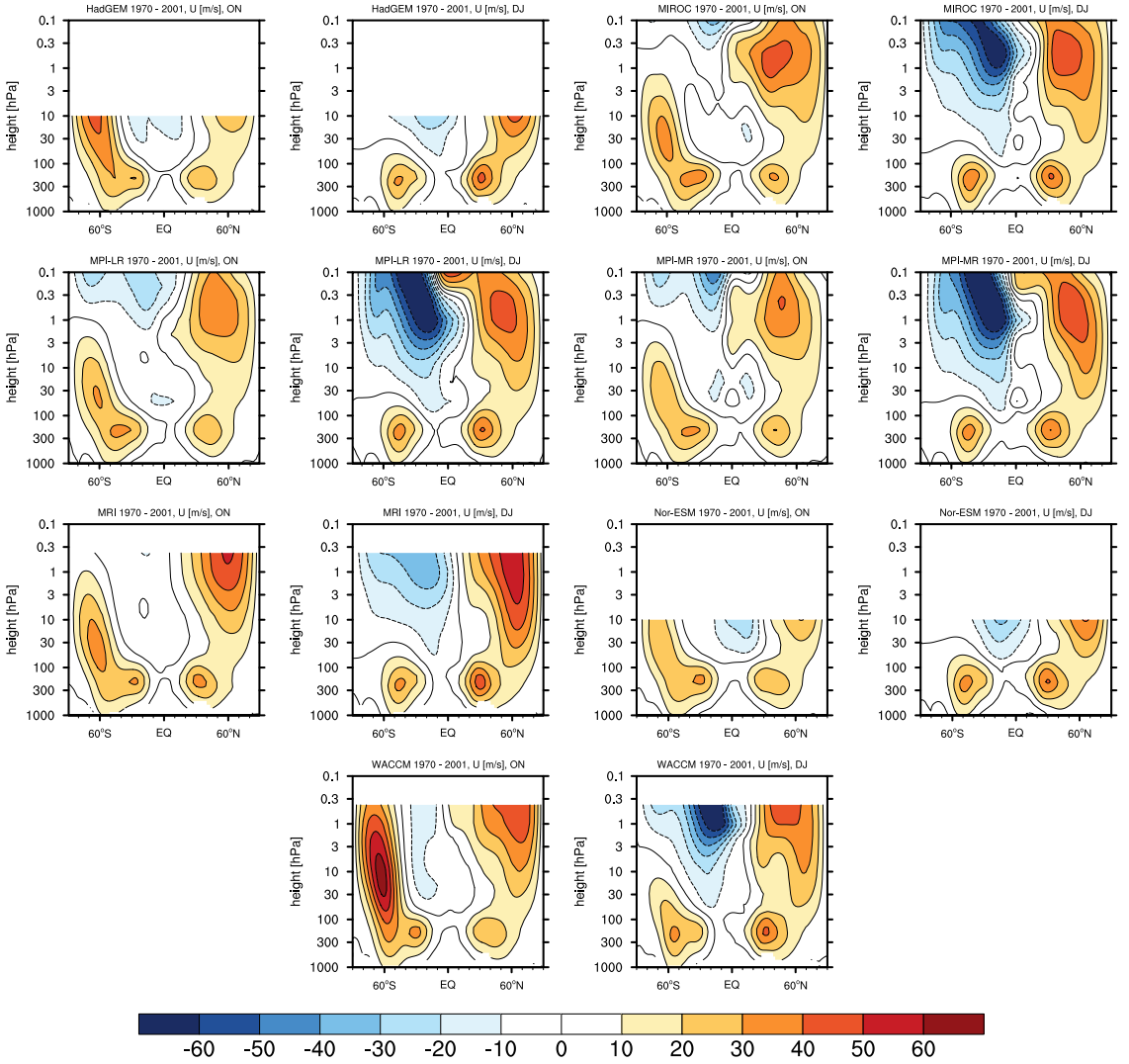

Figure 5.1 (Cont.): Ensemble mean of each individual model of the zonal mean zonal wind averaged over the time period from 1970-2001 from the historical simulations in early (ON) and mid-winter (DJ). Positive values are defined as eastward.

interannual variability differs among the models. Some models show only a comparably small interannual variability in both ON and DJ (CSIRO-Mk3-6-0, GISS-E2-R, Nor-ESM), while other models show large year to year variations (CESM1-WACCM, MRI-ESM, MPI-ESM-MR, HadGEM2-ES, Can-ESM2). Re-analysis data show that the interannual variability is relatively small in early winter and increases substantially during mid-winter (Fig. 5.4), confirming the hypothesis of a radiatively controlled early winter versus a more transitional phase in mid-winter. This is also reflected in the appearance of Sudden Stratospheric Warming events (SSW), which in observations primarily appear in mid- and late winter (Butler and Polvani 2011). Different coupled climate models show different distributions of the frequency of occurrence of SSW. Especially low-top models underestimate the frequency of SSW and shift the majority of occurrence to late winter (Charlton-Perez et al. 2013). The comparison of the multi-model mean and the ERA-40 reanalysis data reveals, apart from the obvious difference in the equatorial stratosphere due to the lack of a QBO in most models, a slight over-

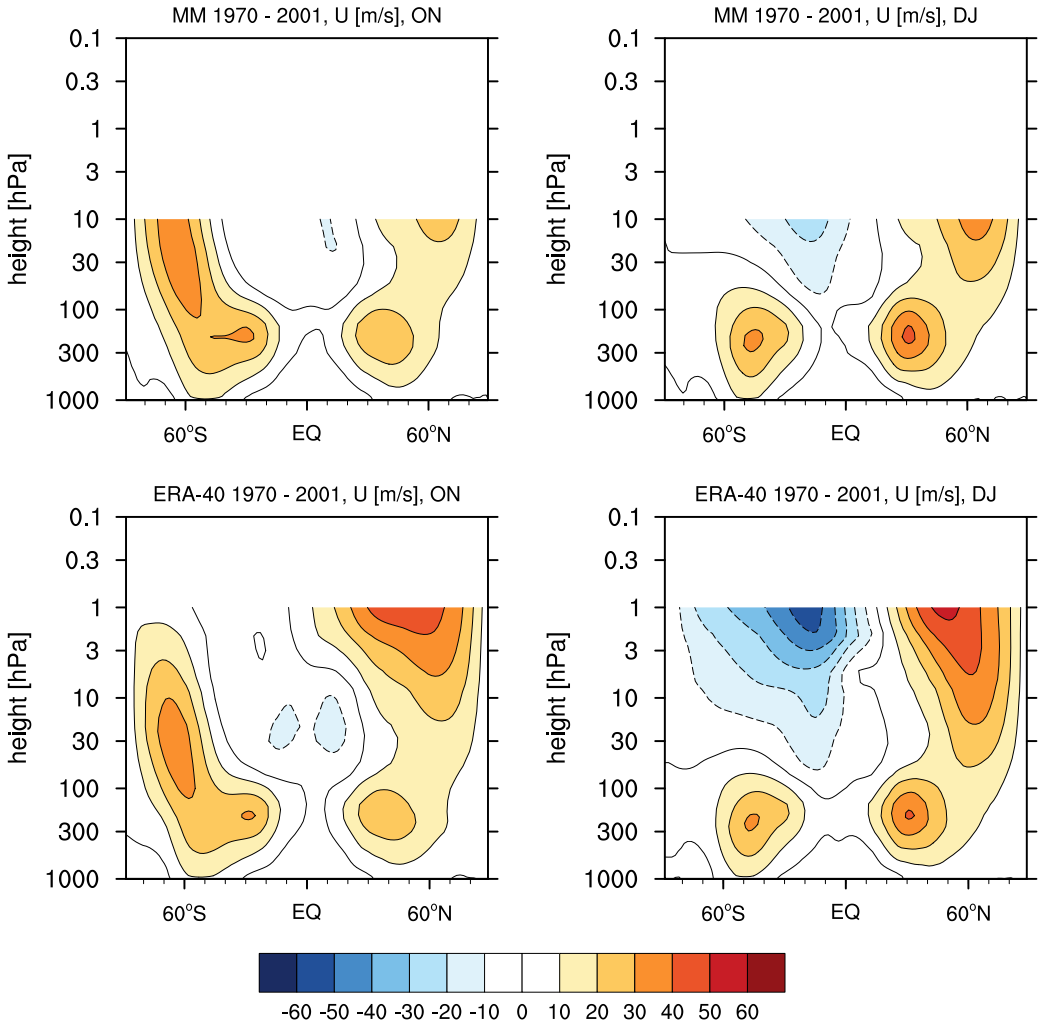

Figure 5.2: Top Panel: Multi-model mean of zonal mean zonal wind averaged over the time period 1970-2001 of the historical simulations for ON (left) and DJ (right). Bottom Panel: same as top panel but for ERA-40 reanalysis. Positive values are defined as eastward.

estimation of the interannual variability in NH high latitudes in early winter by the models. In mid-winter, however, most of the models underestimate the variability in the NH polar stratosphere.

Driscoll et al. (2012) stated that almost all climate models simulate a smaller impact of tropical volcanic eruptions on the NH polar vortex than suggested by the observations of the last two volcanic eruptions. However, given a strong forcing, such as the Krakatau and Pinatubo eruptions, the multi-model mean in fact shows a strengthening of the polar vortex (Fig. 5.5). Of the individual models, only the CSIRO-Mk3-6-0, the GISS-E2-R and Nor-ESM1-M simulate no effect after either of these two strong eruptions, whereas all other models, to some degree, show an intensified polar vortex in mid-winter (see Appendix B.1-3). For the smaller El Chichón eruption, the multi model mean indeed does not capture the very strong polar vortex intensification as seen in ERA-40 (Fig. 5.5, bottom left). But one must be careful in concluding a general failure of climate models from this mismatch, because obviously nature offers only one single realization of the polar vortex response to each volcanic eruption. The polar vortex

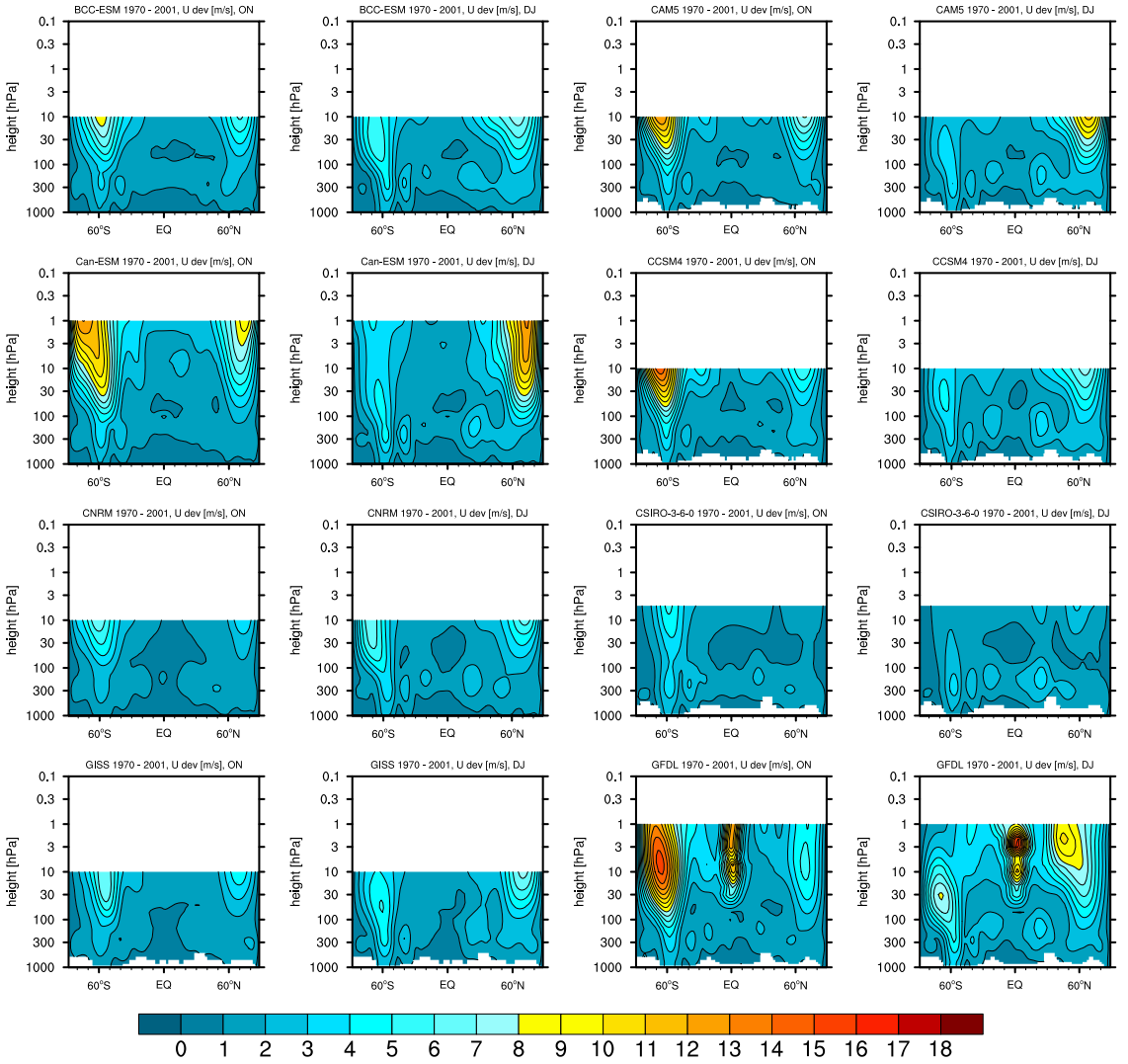

Figure 5.3: Ensemble mean of each individual model of the standard deviation of the zonal mean zonal wind averaged over the time period from 1970-2001 from the historical simulations in early (ON) and mid-winter (DJ).

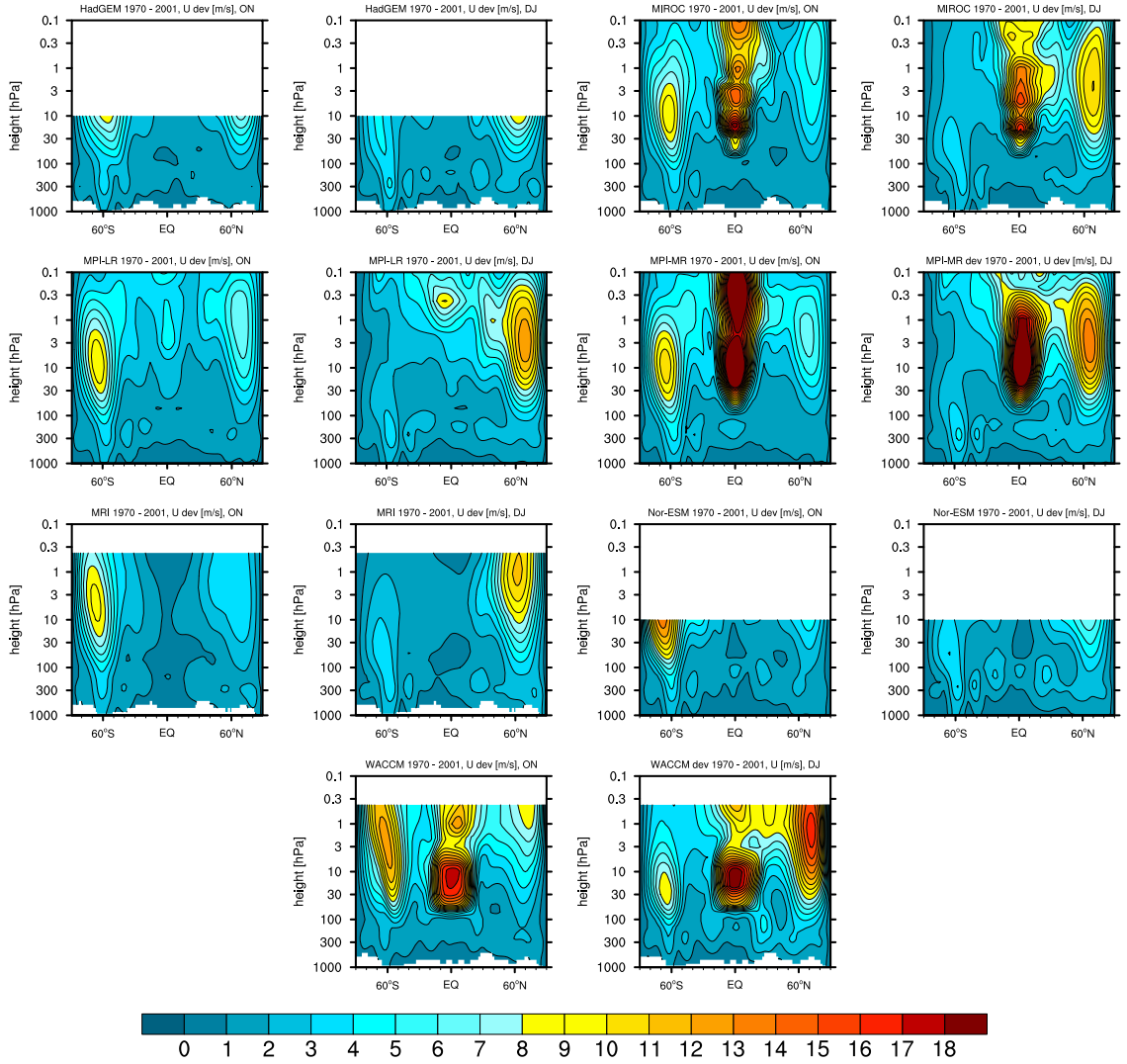

Figure 5.3 (Cont.): Ensemble mean of each individual model of the standard deviation of the zonal mean zonal wind averaged over the time period from 1970-2001 from the historical simulations in early (ON) and mid-winter (DJ).

will be influenced not only by the volcanic eruption, but other factors such as the phase of the QBO and ENSO are also important. Moreover, the polar vortex exhibits a large internal variability (see chapter 1), so even under identical external forcing conditions, the polar vortex can respond differently just due to its chaotic nature (Scott and Polvani 2006; Waugh and Polvani 2010).

This is exemplified by the observed polar vortex response to the Pinatubo eruption. Although the magnitude of the Pinatubo eruption is approximately 3 times the size of the El Chichón eruption, the polar vortex anomaly in the ERA-40 reanalysis is much smaller in the first winter after Pinatubo compared to the first winter after El Chichón (Fig. 5.5). In fact, the multi-model mean polar vortex anomaly after the Pinatubo is in good agreement with the reanalysis data, with the exception that the positive zonal wind anomaly extends to the troposphere in ERA-40, which is not the case for the multi-model mean. Hence, I do not find evidence for a general failure of coupled

climate models to reproduce the volcanic response of the NH polar vortex. Possibly, the models underestimate the impact of smaller eruptions such as El Chichón on the polar vortex, but conclusive statements are difficult due to the limited number of observed eruptions. Given a large forcing, the coupled climate models do on average show a strengthened polar vortex as reanalysis data suggests. The apparent contradiction to the study of Driscoll et al. (2012) may arise from the different method of analyzing the post-eruption response. While I selected three eruptions and calculated the post-eruption response individually, Driscoll et al. (2012) averaged over the nine strongest tropical eruptions since 1880. They included eruptions with even smaller magnitude as El Chichón, which might weaken the signal beyond detectability.

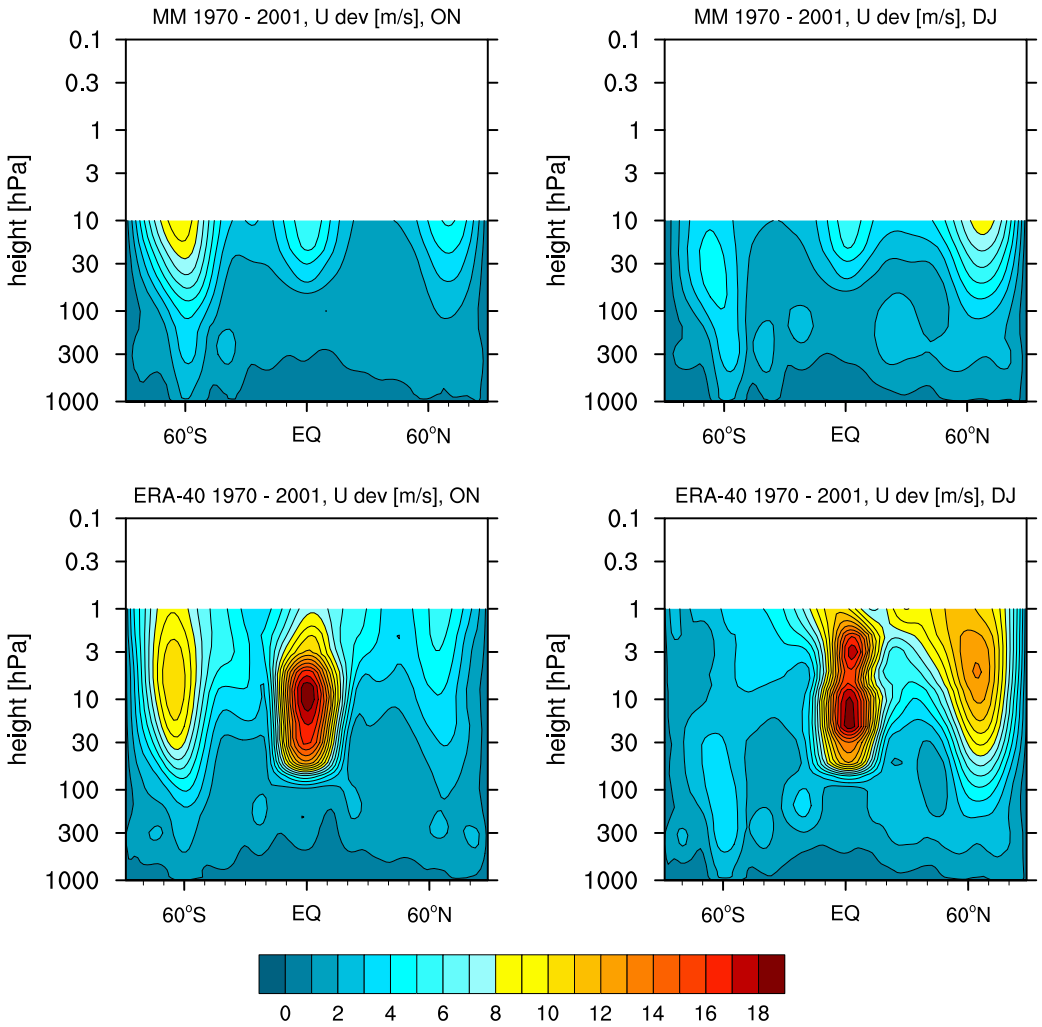

Figure 5.4: Top Panel: Multi-model mean of the standard deviation of the zonal mean zonal wind over the time period 1970-2001 for ON (left) and DJ (right). Bottom Panel: ERA-40 reanalysis standard deviation of the zonal mean zonal wind over the same time period.

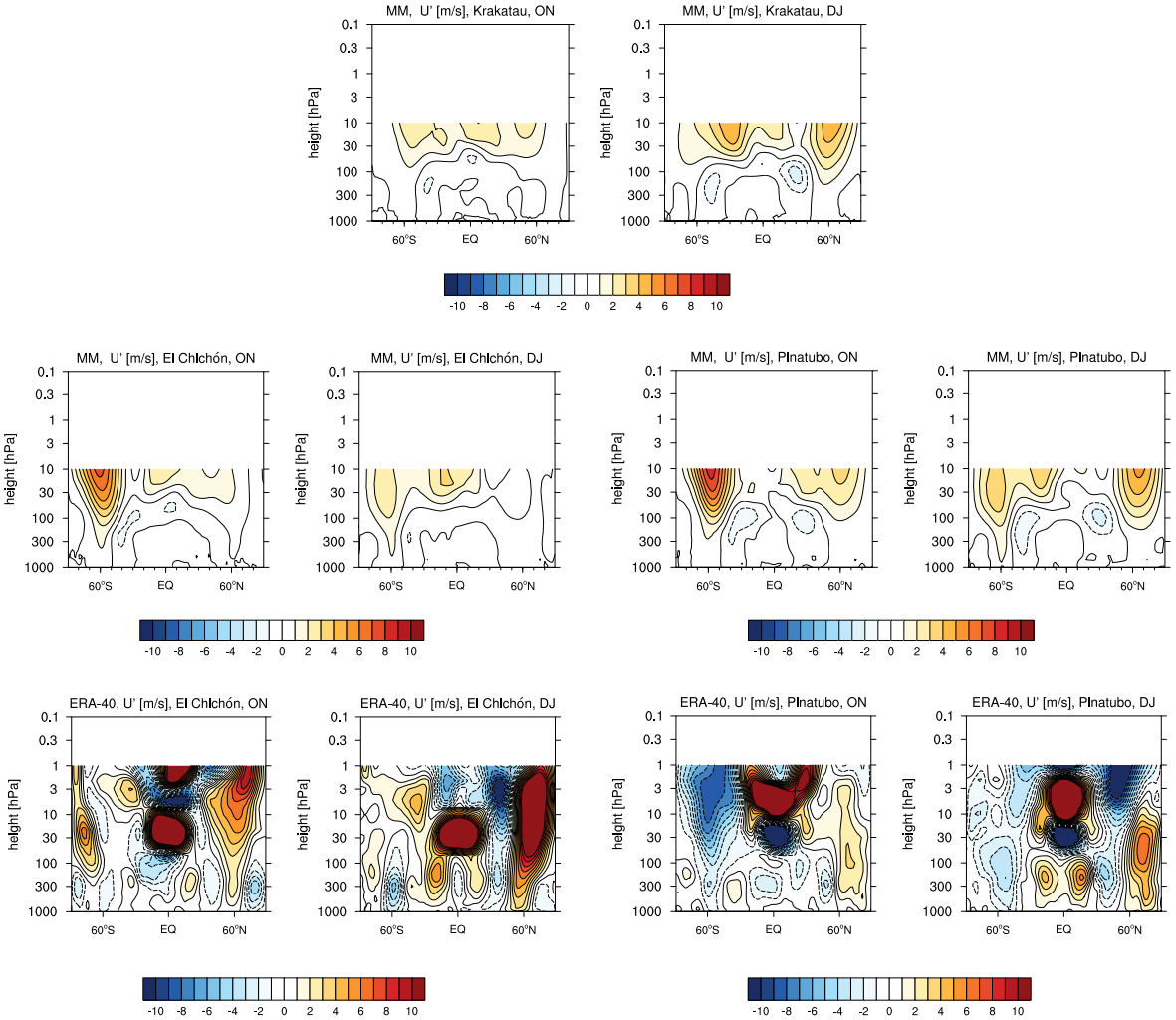

Figure 5.5: Multi-model mean of zonal mean zonal wind anomalies in ON and DJ of the first NH winter after the eruptions of Krakatau (top), El Chichón (middle left) and Pinatubo (middle right). ERA-40 reanalysis zonal mean zonal wind anomalies in ON and DJ of the first NH winter after the eruptions of El Chichón (bottom left) and Pinatubo (bottom right). Positive values denote westerly anomalies.

5.3.2 Influence of early winter NH polar vortex variability on the response to volcanic eruptions

The models show, on average, a slight overestimation of the interannual variability in early winter and an underestimation of the interannual variability in mid-winter in high northern latitudes. As a measure for the interannual variability of the polar vortex, I define as an index the standard deviation of the zonal mean zonal wind between 55°N and 65°N at 10 *hPa* to be consistent with the definition of the strength of the polar vortex in numerous studies (e.g. Matthes et al. (2006); Butler and Polvani (2011)). In the climatology from 1970-2000, where I excluded winters after volcanic eruptions, all models underestimate the interannual variability of the polar vortex in mid-winter (Fig. 5.6). Only the MPI-ESM-MR shows variability of comparable magnitude with reanalysis data. In early winter, most of the models have a slight tendency to over-

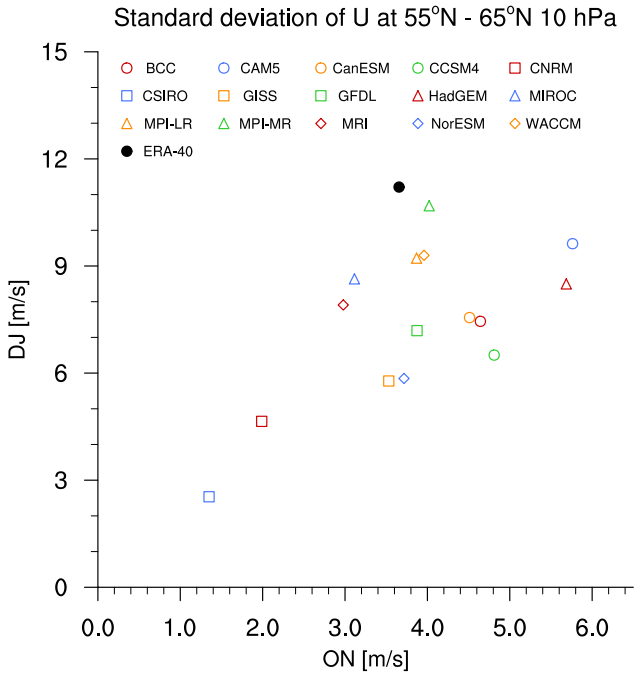

Figure 5.6: Ensemble mean of the standard deviation of the zonal mean zonal wind averaged from 55°N to 65°N at 10 *hPa* from 1970 to 2000 in ON (x-axis) and DJ (y-axis) for individual models (colored markers). The black dot indicates the ERA-40 standard deviation of the zonal mean zonal wind at the same location over the same time period.

estimate the interannual variability. The CESM1-CAM5 and the HadGEM2-ES show the largest variability of all models in early winter. The CSIRO-Mk3-6-0 and CNRM-CM5, on the other hand, underestimate the variability throughout the winter, hence the evolution and strength of the polar vortex is similar each year.

To test whether the hypothesis of an influence of the early winter variability on the response to volcanic eruptions is true, the polar vortex variability index in early winter is plotted against the polar vortex anomaly in the first post-eruption mid-winter after the eruptions of Krakatau, El Chichón and Pinatubo (Fig. 5.7). A negative correlation, i.e. larger interannual variability of the models corresponds to a weaker response to volcanic forcing, would corroborate the hypothesis that a too large variability of the polar vortex in early winter weakens the response to volcanic eruptions. However, for neither of the three eruptions considered, I find a significant correlation between the interannual variability and the post-eruption polar vortex anomaly. Contrary to the assumption, after the eruptions of El Chichón and Pinatubo a positive correlation implies that models with a larger interannual variability in ON actually show a stronger response to volcanic eruptions in DJ. Hence, the hypothesis that the overestimation of the interannual variability of the polar vortex in early winter can explain the failure of coupled models to reproduce the dynamically response to volcanic eruptions must be discarded.

Note that there is for some models a large difference in their response to the volcanic eruptions of Krakatau and Pinatubo, even though both eruptions are of similar magnitude. For example, the MPI-ESM-MR simulates a strengthening of the polar vortex of approximately 6 *m/s* after Krakatau but a much larger anomaly of more than 15

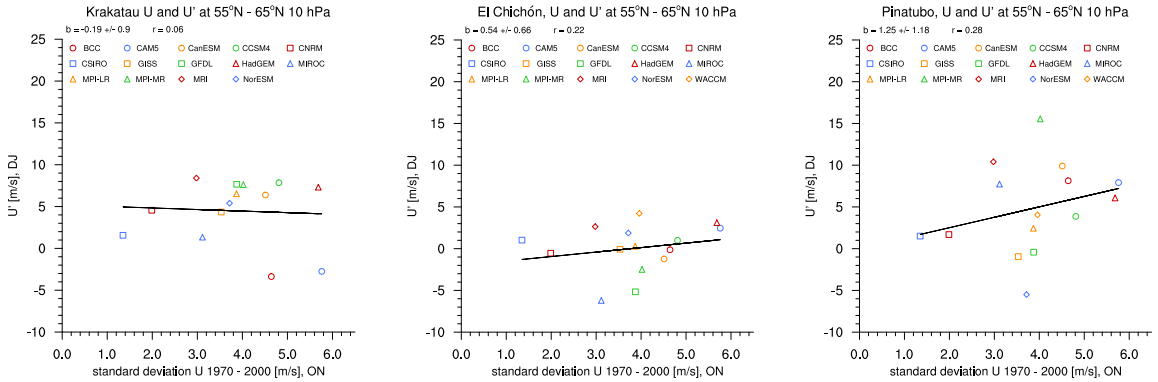

Figure 5.7: Correlation of the ensemble mean standard deviation of zonal mean zonal wind averaged from 55°N to 65°N at 10 *hPa* from 1970 to 2000 in ON (x-axis) with the ensemble mean zonal mean zonal wind anomalies at the same location after the eruptions of Krakatau (left), El Chichón (middle) and Pinatubo (right) in DJ (y-axis). **b** is the linear regression coefficient including the standard deviation and **r** is the Pearson's correlation coefficient.

m/s after Pinatubo. The BCC-CSM1-1 and the CESM1-CAM5 both show a negative polar vortex response to the Krakatau eruption but a strengthening of the polar vortex after Pinatubo, whereas the Nor-ESM1-M exhibits the opposite behavior. As there is no systematic difference in the response between the Krakatau and the Pinatubo eruption, e.g. all models tend to show a stronger response to the Pinatubo eruption than to the Krakatau eruption, the different climatic background states of Krakatau in 1883 and Pinatubo in 1991 seem to be of minor importance. But the four models mentioned above have only three ensemble members, hence three realizations of each individual eruption. The considerable difference the individual ensemble mean response of these four models show after the comparable eruptions of Krakatau and Pinatubo highlights the importance of other factors such as ENSO and internal variability. For small ensembles, similar volcanic forcing can yield very different responses of the NH polar vortex, which will be discussed in more detail in chapter 6.

5.3.3 Influence of early winter NH polar vortex strength on the response to volcanic eruptions

Climate models which exhibit a large interannual variability of the polar vortex seem to be more susceptible to volcanic forcing, i.e. they simulate a stronger polar vortex anomaly after the eruptions of El Chichón and Pinatubo. A large interannual variability of the zonal mean zonal wind in the region of the polar vortex implies that the magnitude of the polar vortex varies considerably between single winters. Potentially, the polar vortex strength in early winter is more important than the variability itself in determining the response to volcanic eruptions. For example, a weaker-than-average polar vortex in early winter could mean that the vortex is already dynamically controlled and not susceptible to slight changes in radiative forcing by the volcanic eruption. Hence, it is reasonable to investigate if the polar vortex response to volcanic eruptions depends on the strength of the polar vortex in early winter.

Before analyzing the individual winters after the eruptions of Krakatau, El Chichón

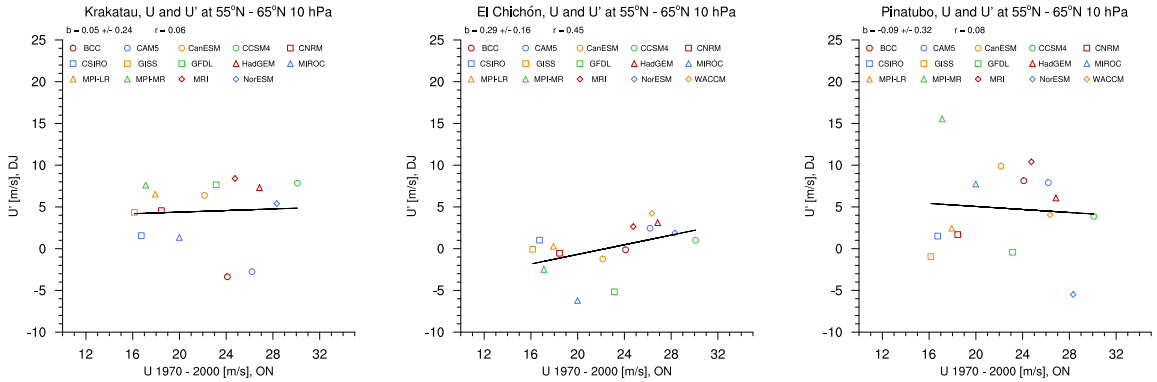

Figure 5.8: Correlation of the ensemble mean zonal mean zonal wind averaged from 55°N to 65°N at 10 *hPa* from 1970 to 2000 in ON (x-axis) with the ensemble mean zonal mean zonal wind anomalies at the same location after the eruptions of Krakatau (left), El Chichón (middle) and Pinatubo (right) in DJ (y-axis). **b** is the linear regression coefficient including the standard deviation and **r** is the Pearson's correlation coefficient.

and Pinatubo, it is crucial to test whether a climatological strong polar vortex influences the ensemble mean polar vortex response to volcanic eruptions. Figure 5.8 shows the ensemble mean polar vortex response to the eruptions of Krakatau, El Chichón and Pinatubo dependent on the climatological polar vortex strength in early winter from 1970-2000 where winters after volcanic eruptions are excluded. Only after the comparably weak eruption of El Chichón, I find a significant positive correlation between the polar vortex strength in early winter and the post-eruption polar vortex anomaly in mid-winter. However, in the case of El Chichón, the polar vortex anomaly itself is close to zero (Fig. 5.2). For the stronger eruptions of Krakatau and Pinatubo, no significant correlation can be obtained, which implies that the mean vortex strength of a particular model does not influence the response to volcanic eruptions. Thus, a strong climatological vortex in ON does not lead to a better representation of the volcanic response per se.

However, for single winters, the response of the polar vortex to volcanic eruptions in mid-winter might depend on the polar vortex strength in early winter, which cannot be seen in the ensemble mean. Before investigating the the relation between early and mid-winter polar vortex strength in winters after volcanic eruptions, it is necessary to test whether the polar vortex strengths in early and mid-winter are correlated in volcanically unperturbed winters. Because the polar vortex strength differs among the models by almost a factor of two (see Fig. 5.8), the individual climatological mean of the polar vortex strength in ON and DJ of each model is subtracted to allow for an inter-model comparison. The correlation of the polar vortex strengths in ON and DJ for the period 1970-2000 (winters after volcanic eruptions are excluded) across all models is shown in Figure 5.9. A weak correlation with a regression coefficient of 0.22 and a correlation coefficient of 0.11 implies that the vortex strength in mid-winter is fairly independent on the vortex strength in early winter. The ERA-40 reanalysis data (black dots) do not enter the calculation of the linear regression, but confirm the weak correlation of early and mid-winter polar vortex strength. Also for individual models, the correlation is weak and not significant, which shows that the weak correlation in

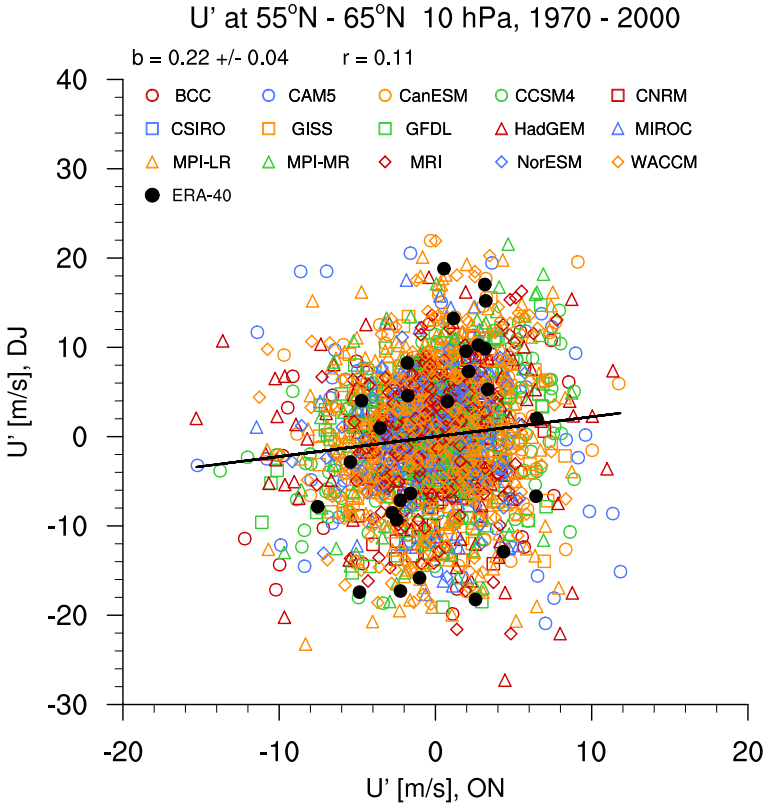

Figure 5.9: Correlation of the zonal mean zonal wind anomalies averaged from 55°N to 65°N at 10 *hPa* from 1970 to 2000 in ON (x-axis) with the same quantity in DJ (y-axis). Anomalies are calculated with respect to the climatological mean of each individual model and the ERA-40 reanalysis, respectively. **b** is the linear regression coefficient including the standard deviation and **r** is the Pearson's correlation coefficient.

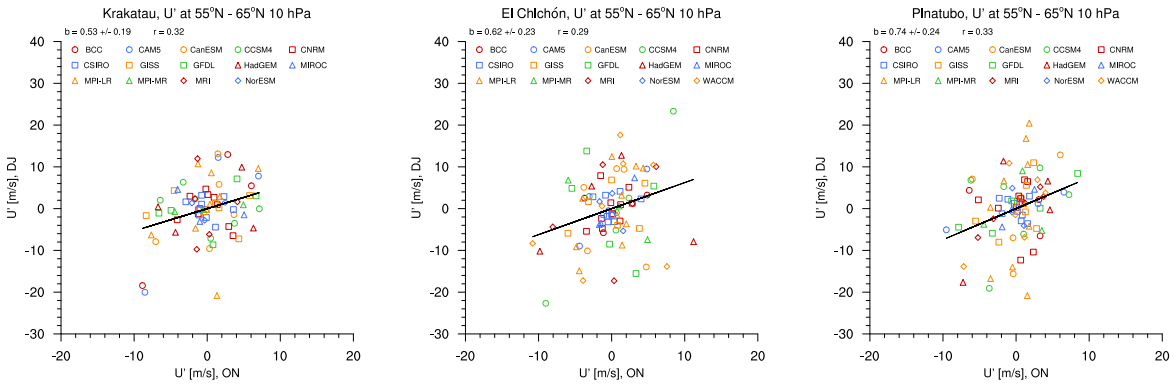

Figure 5.10: Correlation of the zonal mean zonal wind anomalies averaged from 55°N to 65°N at 10 *hPa* after the volcanic eruptions of Krakatau (left), El Chichón (middle) and Pinatubo (right) in ON (x-axis) with the same quantity in DJ (y-axis). Anomalies are calculated with respect to the mean anomalies after the respective eruptions of each individual model. **b** is the linear regression coefficient including the standard deviation and **r** is the Pearson's correlation coefficient.

the multi-model ensemble is not obtained due to opposing correlations in individual models (not shown). The linear regression and correlation coefficients do not change

significantly, when the reference periods that are used to calculate the post-eruption anomalies instead of the 1970-2000 period are considered (see Appendix C.1). Thus, the different climatic background state of the Krakatau reference period (1860-1883), due to lower greenhouse gas concentration in the atmosphere compared to the 1970-2000 period, does not alter the correlation of early and mid-winter polar vortex strength.

For the correlation of early and mid-winter polar vortex strengths in post-eruption winters, the polar vortex anomalies are normalized by subtracting the mean polar vortex anomaly after the eruptions of each individual model (Fig. 5.10). In this way artificial correlations due to the different magnitude of the volcanic response of each model are avoided. For each of the three eruptions, Krakatau, El Chichón and Pinatubo, I find significant correlations of the polar vortex strength in ON and the polar vortex strength in DJ. The regression coefficient is larger than 0.5 and the correlation coefficient is approximately 0.3. These findings imply that the response to volcanic eruption in mid-winter depends to some extent on the state of the polar vortex in early winter. In other words, under the influence of a volcanic eruption, a strong early winter polar vortex is likely to stay strong at least to the end of mid-winter. Note that this relation is substantially weaker in winters without volcanic perturbation. Here, I only find a weak correlation between the state of the NH polar stratosphere in early and mid-winter. Hence, the volcanic eruption perturb the polar vortex in a way, which allows a positive wind anomaly to be persistent from early to mid-winter, whereas a positive wind anomaly in ON without volcanic eruption does not necessarily lead to a stronger vortex in DJ. Validating this result with observations is unfortunately difficult, due to the limited number of stratospheric observations after volcanic eruptions. However, Mlynczak et al. (1999) find in satellite observations after the eruption of Pinatubo a larger relaxation time in the stratosphere compared to year prior to the eruption, which supports the model findings of a longer lifetime of the volcanic polar vortex anomalies.

5.4 Summary and conclusion

In order to find a possible explanation why coupled climate models in general seem to underestimate the NH polar vortex response to large tropical volcanic eruptions, I have investigated the impact of the volcanic eruptions of Krakatau, El Chichón and Pinatubo in the CMIP5 ensemble. Based on the study of Kodera and Kuroda (2002), I hypothesized that the overestimation of the interannual variability of the polar vortex in early winter is potentially the reason for the reported general failure to capture the NH dynamical response to volcanic eruptions (Driscoll et al. 2012; Charlton-Perez et al. 2013).

Before investigating the response to volcanic eruptions, I assessed the CMIP5 models with respect to their climatological polar vortex strength and interannual variability. I found that the multi-model mean agrees well with the observations in terms of polar vortex strength and position in the climatology from 1970-2000. The interannual variability of the zonal mean zonal wind differs substantially among the CMIP5 models. In the multi-model mean, the interannual variability is overestimated at high latitudes in early winter but underestimated during mid-winter in comparison with reanalysis

data. Larger biases of the variability are obtained in the tropical stratosphere, because only 4 of the 15 models simulate a QBO, which is the dominant source of variability in this region.

The response of the polar vortex depends on the choice which volcanic eruption is considered. For the comparably small El Chichón eruption, a strengthening of the polar vortex is not simulated in the multi-model mean, which seems to be in contradiction to reanalysis data. Interestingly, for the larger eruptions Krakatau and Pinatubo the multi-model mean shows a positive anomaly of the polar vortex. This finding challenges the assumption of a general failure of climate models to reproduce the dynamical response of the NH polar vortex to volcanic eruptions. Given a large enough volcanic forcing, the models do on average simulate a stronger polar vortex in mid-winter. Moreover, the ERA-40 reanalysis data shows a much weaker positive polar NH vortex anomaly in the first winter after the Pinatubo eruption, compared to the smaller El Chichón eruption. With only two eruptions where observations of the NH stratosphere exist, one must be careful in attributing the polar vortex anomaly to the volcanic forcing, because other factors such as the phase of the QBO and ENSO as well as the large internal variability of the polar stratosphere will also be important. I cannot rule out the possibility that coupled climate models underestimate the polar vortex response to volcanic eruptions, but a general failure of the models is not supported by my analysis.

In contradiction to the hypothesis that an overestimation of the interannual polar vortex variability in early winter leads to an underestimation of the volcanic response, no significant correlation between polar vortex variability in ON and polar vortex anomaly in DJ in post-eruption winters can be obtained. On the contrary, for the El Chichón and the Pinatubo eruptions, models with a larger interannual variability in early winter simulate a stronger response of the polar vortex in mid-winter. Hence, the hypothesis that the overestimation of the interannual variability of the polar vortex in early winter can explain the possible underestimation of the dynamically response to volcanic eruptions in coupled models must be discarded. Based on the definition of the interannual variability applied in this chapter, I don't find evidence that models with lower interannual variability in early winter simulate a stronger response to volcanic eruptions.

A large interannual variability of the polar vortex means that polar vortex strength varies substantially from year to year. It is possible that a climatological weak polar vortex in early winter hints towards a dynamically controlled state of the vortex, and in such a state the vortex might be not susceptible to slight changes in radiative forcing by the volcanic eruption. However, in the ensemble mean there is no evidence that models with a comparably strong climatological polar vortex in early winter simulate a stronger response to volcanic eruptions in mid-winter. Interestingly, for individual winters the post-eruption polar vortex anomaly in mid-winter significantly depends on the polar vortex strength in early winter. If the polar vortex is already strong in early winter after volcanic eruptions, the polar vortex will on average also be strong in mid-winter and vice versa. This correlation does not depend on the climatological strength of the polar vortex of each individual model, but on the polar vortex anomaly relative to the models individual mean response to volcanic eruptions. Importantly, this

relation between early and mid-winter polar vortex anomalies is substantially weaker in volcanically unperturbed winters. Here, the polar vortex strength in mid-winter only weakly depends on the polar vortex strength in early winter. It seems as if the volcanic eruption perturb the polar vortex in a way that allows a wind anomaly to be more persistent, which is not the case without volcanic perturbation. A larger relaxation time of the stratosphere, which supports the model findings of a longer lifetime of the zonal wind anomalies, was also found in satellite observations after the eruption of Pinatubo (Mlynczak et al. 1999), but the reasons for this phenomenon are still not resolved.

However, the inter-model spread in the response to the three volcanic eruptions analyzed in this chapter highlights the substantial contribution of internal variability and possibly other factors such as ENSO. Validation of the presented findings, especially correlations which are significant only for a large number of ensemble members, with the two eruptions for which stratospheric observations exist, is at least problematic. But conclusively, I find that coupled models simulate a strengthening of the polar vortex for a strong volcanic forcing such as Krakatau or Pinatubo. If the absent response to the smaller El Chichón eruption is due to an underestimation of the dynamical impact of climate models to volcanic eruptions could not be verified, but an overestimation of the interannual variability or the strength of the polar vortex is not the cause.

Chapter 6

How many ensemble members are needed to indentify a significant impact of volcanic eruptions?

6.1 Introduction

The simulated response of coupled climate models to tropical volcanic eruptions is often small in comparison with observations and to a large extent insignificant, especially for variables in regions which inherit a large internal variability such as the NH polar vortex strength (Driscoll et al. 2012; Charlton-Perez et al. 2013). The MPI-ESM-LR shows a significantly strengthened polar vortex only for very strong eruptions like Tambora (see chapter 4), but does not capture a strengthened polar vortex and a shift to a positive phase of the NAO after the largest eruptions in the CMIP5 historical simulations from 1850-2005 as observations suggest (see chapter 3). Hence, even when combining different eruptions to increase the sample size, a substantial uncertainty in the response remains. This uncertainty is due to three main sources: forcing uncertainty, model uncertainty, and internal variability. In this section, I use a very large 100 member ensemble of the MPI-ESM-LR to quantify the uncertainty in the response to volcanic eruptions arising from internal, interannual variability. The guiding question is: What is the minimum number of ensemble members needed to detect a statistical significant response to volcanic eruptions?

For future climate projections, the forcing uncertainty arises from incomplete knowledge of the future concentration pathways of greenhouses gases (Tebaldi and Knutti 2007; Hawkins and Sutton 2009). In the case of volcanic eruptions, the forcing uncertainty is due to incomplete knowledge of the aerosol loading and distribution after historical eruptions before the satellite era (Gao et al. 2008; Arfeuille et al. 2014). But even for the Pinatubo eruption, the best observed large eruption, there are uncertainties due to sparse sampling of the satellite instruments (Stenchikov et al. 1998) and the fact that large aerosol optical depths right after the eruption reduced transmission below the detection level (Russell et al. 1996). Model uncertainty arises because different models with different dynamical cores and different parametrizations may simulate different response to the same external forcing, e.g. a volcanic eruption. Because for CMIP3 and CMIP5 all model centers were free to decide on which forcing dataset to use and how to implement it in the model, a quantitative statement on how much the

model uncertainty contributes to the total uncertainty was not possible. A CMIP6 activity, the volcanic forcing model intercomparison project (VolMIP) (Zanchettin et al. 2015), where a number of different coupled climate models simulate the response to the same volcanic perturbation, will help to pin down the model uncertainty in the future. Internal, or natural variability arises in the atmosphere, ocean or the coupled system in the absence of any external forcing, and occurs because of non-linear dynamical processes (Madden 1976; Feldstein 2000). The NH polar stratosphere is a region prone to large variability on interannual, interseasonal and weekly time scales (Waugh and Polvani 2010). The internal interannual variability arises on the one hand from variations within the climate system but remote from the polar stratosphere itself, such as the quasi-biennial oscillation (QBO) (Labitzke and Loon 1988; Anstey and Shepherd 2013) or El Nino Southern Oscillation (ENSO) (van Loon and Labitzke 1987; Sassi et al. 2004; Manzini et al. 2006), and on the other hand from nonlinearities within the polar stratosphere (Holton and Mass 1976; Scott and Polvani 2006) as described in chapter 1.2.1.

An assessment of the response to volcanic eruptions with a large multi-model ensemble has been conducted by Driscoll et al. (2012) for different models in the CMIP5 archive. The underlying assumption is that the multi-model mean potentially shows a more robust response to the volcanic forcing compared to a single model, because of the reduction of model uncertainty and internal variability (e.g. Tebaldi and Knutti (2007) for climate change signal). But individual models provide only a small number of ensemble members and due to different volcanic forcing datasets used by different climate models, it is difficult to quantify the contribution of internal variability, model and forcing uncertainty in the total uncertainty. Here, I concentrate on a large ensemble of one particular model to provide an estimate of the contribution of internal variability (Deser et al. 2010). I use 100 ensemble members of historical simulations of the MPI-ESM-LR to quantify the uncertainty due to internal, interannual variability. The question I address is: How many ensemble members are needed to identify a significant NH winter response to volcanic eruptions? Although I focus on the NH winter stratosphere, I will also examine the response and uncertainty of surface temperature and tropospheric circulation.

6.2 Data and Methods

I use 100 ensemble members of the historical simulation from 1850-2005 with the MPI-ESM-LR version 1.1. A major difference to the CMIP5 version of the MPI-ESM, used throughout this thesis and described in chapter 2, is the implementation of the new version of the atmosphere component (ECHAM6.3). In addition to several bug fixes, a new radiation code is applied in ECHAM6.3 that leads to changes in the temperature fields. As these simulations are only recently completed, a full evaluation of the model performance with respect to observations has not been done yet. With regard to the middle atmosphere in the NH high latitudes, the MPI-ESM-LR version 1.1 compares well with the previous version of the MPI-ESM described by Schmidt et al. (2013). However, the NH polar vortex is weaker compared to observations and shows a larger interannual variability (see Appendix D.1 and D.2).

The 100 ensemble members of the historical simulation in the MPI-ESM-LR version 1.1 are forced with identical observed greenhouse gas and ozone concentrations, solar insolation and aerosol optical depths which is prescribed by an extended version of the Pinatubo aerosol data set by Stenchikov et al. (1998) described in chapter 2.1.1, and differ only in their initial conditions. In this chapter, I will mainly focus on the eruption of Pinatubo in 1991 and the respective reference period from 1985-1986 to 1990-1991. Details of the Pinatubo eruption, the eruption of El Chichón and the multi-eruption mean of the nine largest eruptions in the historical period, which will be investigated briefly, are described in chapter 2.

The minimum number of ensemble members needed to identify a significant response is determined based on a resampling method. First, the anomaly in dependence of the ensemble size is calculated by formula 6.1.

$$A_n = \frac{\sum_{i=1}^{n} V_i}{n} - \frac{\sum_{j=1}^{n \cdot m} R_j}{m \cdot n} \tag{6.1}$$

A is the anomaly of a certain variable of interest (strength of the polar vortex, global mean surface temperature, etc.), **V** is the state of that variable after the volcanic eruption, **R** is the same variable in the reference period, **n** is the number of ensemble members, and **m** is the number of reference years for the given eruption. The anomaly is calculated by averaging **n** randomly drawn ensemble members after the volcanic eruption and subtracting the average of **m** times **n** randomly drawn years of the reference period. Drawing the reference years randomly implies that autocorrelation does not significantly impact the results. To test this assumption, I performed the analysis with a fixed ensemble member relation. That means, I sample a random **V** and use the reference years of the same ensemble members to calculate the anomaly **A**. However, the choice how to sample the reference years does not change the results presented in this chapter. The calculation of **A** is repeated 5,000 times to obtain a distribution of anomalies for each **n** from 1 to 100. The minimum number of ensemble members needed to identify a significant volcanic response is defined by the **n** where both, the upper and lower 90% or 98% confidence intervals of the anomaly distribution are greater or lower than zero. In that case, the anomaly averaged over the 5,000 draws is defined as significantly different from zero at the 95% or 99% confidence level.

6.3 Results

6.3.1 Northern Hemisphere polar vortex response

The dynamical response which is expected after large volcanic eruptions based on observations is a significant strengthening of the NH polar vortex in boreal winter. Thus, the variable of interest is the strength of the polar vortex, which I define as the zonal mean zonal wind at 55°N-65°N and 10 *hPa* averaged over DJF in accordance with previous studies (Matthes et al. 2006; Butler and Polvani 2011). I calculate a distribution dependent on the ensemble size of the polar vortex anomaly after the eruption

of Pinatubo by resampling of formula 6.1 5,000 times and obtain a mean response as well as confidence intervals (Fig. 6.1). Because the polar vortex anomaly is expected to be positive, only the lower 90% and 98% confidence intervals are shown. The lower confidence intervals indicate that 95% or 99% of the polar vortex anomalies are larger and only 5% or 1% are weaker than the respective interval. The mean response is a strengthening of the polar vortex of about 3-4 *m/s* which is independent of the ensemble size (Fig. 6.1a). This is expected because the mean of 5,000 resamples should not change significantly if only one ensemble members is drawn or more ensemble members are drawn and averaged. The confidence intervals, however, change substantially with increasing ensemble size. Only for ensembles larger than 15 members, the positive polar vortex anomaly is significantly different from zero at the 95% confidence level and almost double the ensemble size is needed for the 99% confidence level. Most of the coupled climate models in the CMIP5 archive have an ensemble size of 3 to 5 members of the historical simulations and none has an ensemble size larger than 10 members. The findings of Figure 6.1 for the MPI-ESM-LR indicate that such a small ensembles may show no significant response of the polar vortex to the Pinatubo eruption which can be interpreted as a failure of the coupled model, even though the model actually can reproduce a strengthening of the polar vortex but the large internal variability masks the response to the volcanic forcing.

To circumvent the small ensemble size, most assessments of volcanic eruption do not rely on a single eruption only, but average over a number of large tropical volcanic eruptions (Stenchikov et al. 2006; Driscoll et al. 2012). The benefit of a larger sample size by including different volcanic eruptions comes with the caveat of introducing forcing uncertainty, because different eruptions have different forcing fields arising from different eruption magnitudes, latitudes and seasons, which all can potentially influence the polar vortex response (Timmreck et al. 2012; Toohey et al. 2014). Moreover, the eruptions which are included are mostly of smaller magnitude than the Pinatubo eruption and given the large internal variability of the polar vortex, a smaller forcing will be even more difficult to detect. As I have shown in chapter 3, the MPI-ESM-LR does not show a significantly strengthened polar vortex averaged over the nine largest eruptions in the historical simulations, but for a larger forcing as Tambora, the polar vortex is intensified (see chapter 4). The mean response of the polar vortex in the MPI-ESM-LR to the El Chichón eruption in 1982, which is the about 1/3 the magnitude of Pinatubo and the only other eruption than Pinatubo where satellite observations are available, is not significantly different from zero even with an ensemble of 100 members (Fig. 6.1b). Averaging the two eruptions of El Chichón and Pinatubo shows a mean polar vortex anomaly of approximately 2 *m/s*, but only significantly different from zero at the 95% confidence level with more than 20 ensemble members (Fig. 6.1c). Thus, doubling the sample size by adding a smaller eruption to the Pinatubo reduces the mean response as expected, but also increases the number of ensembles needed to identify a significant response of the polar vortex. Including all nine large tropical volcanic eruption as in Driscoll et al. (2012) and in chapter 3 of this thesis, shows a mean strengthening of the polar vortex of approximately 1-2 *m/s* which is significantly different from zero for more than 12 ensemble members at the 95% confidence level (Fig. 6.1d). Hence, adding more eruptions including for example Krakatau, which has a similar magnitude as Pinatubo, reduces the ensemble size needed to identify a

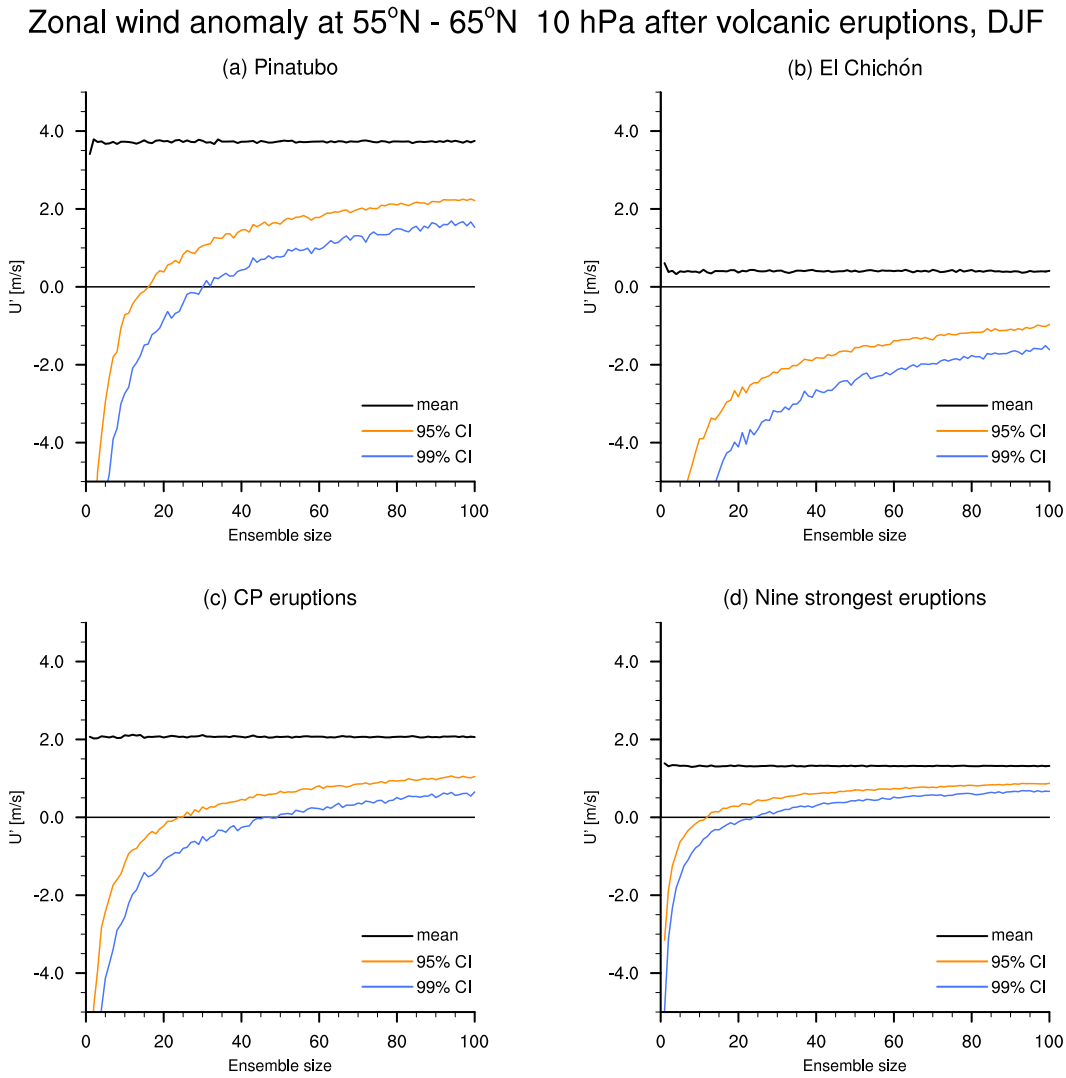

Figure 6.1: Ensemble average of the zonal mean zonal wind anomaly between 55°N and 65°N at 10 *hPa* in the first post-eruption DJF (a) after the eruption of Pinatubo, (b) after the eruption of El Chichón, (c) averaged over the eruptions of El Chichón and Pinatubo and (d) averaged over the nine strongest eruptions since 1880 (see Table 3.1) dependent on the ensemble size of the MPI-ESM-LR. Black line is the mean response and the red and blue line are the 95% and 99% confidence intervals, respectively.

significant response of the polar vortex compared to Pinatubo alone, but only by 3 members.

Increasing the sample size narrows the uncertainty of the mean polar vortex signal, but the mean signal itself is reduced as smaller eruptions are included in the sample. This poses the question whether there is an "ideal" composite of eruptions for which the volcanic signal can be detected most robustly. Figure 6.2 shows the change in the mean polar vortex anomaly as well as the change in the minimum number of ensemble members needed to detect a significant polar vortex anomaly at the 95% confidence level when successively smaller eruptions are included in the sample. The magnitude of the volcanic eruptions is defined as tropical AOD (20°N-20°S) in the first winter (DJF) after the volcanic eruption. The numbers on the x-axis corresponds to the numbers of

Table 6.1: The nine strongest, tropical volcanic eruptions since 1880 ranked according to their magnitude defined by the tropical (20°N-20°S) Aerosol Optical Depth in the first post-eruption winter (DJF).

Rank	Volcano	Tropical AOD
1	Krakatau	0.182
2	Pinatubo	0.156
3	El Chichón	0.107
4	Santa María	0.092
5	Agung	0.072
6	Tarawera	0.055
7	Bandai	0.039
8	Fuego	0.022
9	Quizapu	0.008

volcanic eruptions which are averaged to obtain the polar vortex anomaly as well as the numbers of ensemble members needed to detect the respective anomaly significantly. At each step, the next smaller eruption is added to the composite. The volcanic eruptions and their respective maximum tropical AOD ranked according to their strength is given in table 6.1. When only the strongest eruption (Krakatau) is considered, the mean polar vortex response is a strengthening of approximately 4.5 m/s and 11 ensemble members are necessary to identify a significant response. Adding the Pinatubo eruption to the sample only slightly reduces the mean polar vortex anomaly, but because the sample size is doubled the minimum number of ensemble size decreases to 7 members. Including the third-strongest eruption (El Chichón) substantially weakens the mean polar vortex anomaly to 2.7 m/s which leads to an increase in the minimum ensemble size to 9 members. Adding even smaller eruptions further weakens the polar vortex anomaly, with the notable exception of Quizapu in 1933, the smallest of the nine eruptions. However, as this eruption does not produce a significant positive temperature anomaly in the lower tropical stratosphere (not shown), other mechanisms must be responsible for the strengthening of the polar vortex. Nevertheless, the most robust response to volcanic eruptions in the MPI-ESM-LR is achieved when only the two strongest eruptions, Krakatau and Pinatubo, are considered. As shown in chapter 5, also the multi-model mean of the CMIP5 models show a stronger polar vortex after these two eruptions. This at least questions the conclusions of the apparent failure of coupled climate models to reproduce the stratospheric dynamical response to volcanic eruptions drawn from composites which include smaller eruptions.

An ensemble size of 12 members, which is needed in the MPI-ESM-LR when all nine tropical eruptions are considered, is still larger than available for any of the coupled climate models in the CMIP5 archive. Of course, the exact number of ensemble members which are needed to identify a significant response of the polar vortex given here is valid only for the MPI-ESM-LR. Other climate models use different volcanic forcing fields which may influence the response of the polar vortex. Additionally, the polar vortex itself and especially the internal variability of the NH winter polar stratosphere will be different among the CMIP5 models, as shown in chapter 5. Therefore, the necessary ensemble size to detect a significant signal will also differ from one model to the other. A large ensemble, similar to the 100 members of the MPI-ESM-LR, would

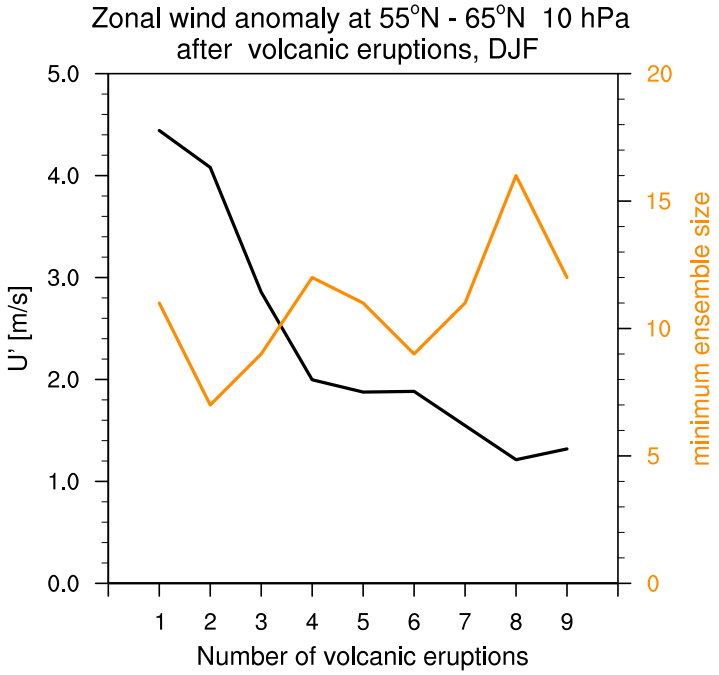

Figure 6.2: Ensemble average of the zonal mean zonal wind anomaly between 55°N and 65°N at 10 *hPa* in the first post-eruption DJF averaged over successively smaller eruptions as ranked in Table 6.1 (black line) and minimum ensemble size neccesarry to detect a zonal mean zonal wind anomaly significantly different from zero at the 95% confidence level (orange line).

be necessary to give quantitative statements for every single model. But the findings presented for the MPI-ESM-LR display that results gained from small ensemble sizes, even when including multiple eruptions, may not describe the true response of the model, especially in regions of large internal variability as the NH polar vortex.

6.3.2 Zonal mean temperature and zonal wind response

Of course the NH polar vortex is not the only region and the zonal mean zonal wind not the only variable which is influenced by a tropical volcanic eruption. For a more comprehensive analysis of the volcanic response and the ensemble size needed to identify a significant response, I focus on the Pinatubo eruption in the first post-eruption winter (DJF). The ensemble mean anomaly of all 100 members is shown in black contour lines for the zonal mean temperature and zonal mean zonal wind in Figure 6.3. In the same way as for the polar vortex strength, I calculate for every grid point the minimum number of ensemble members for which the respective anomaly is different from zero at the 95% confidence level. The minimum number of ensemble members is indicated by the color shading in Figure 6.3 and can be interpreted as a measure of quantitative uncertainty. White color means that even with 100 ensemble members the anomaly is not statistically significant at the 95% confidence level. Choosing a different confidence level (for example 99%) increases the number of ensemble members in almost every region, sometimes even below significance, but does not change the overall conclusions.

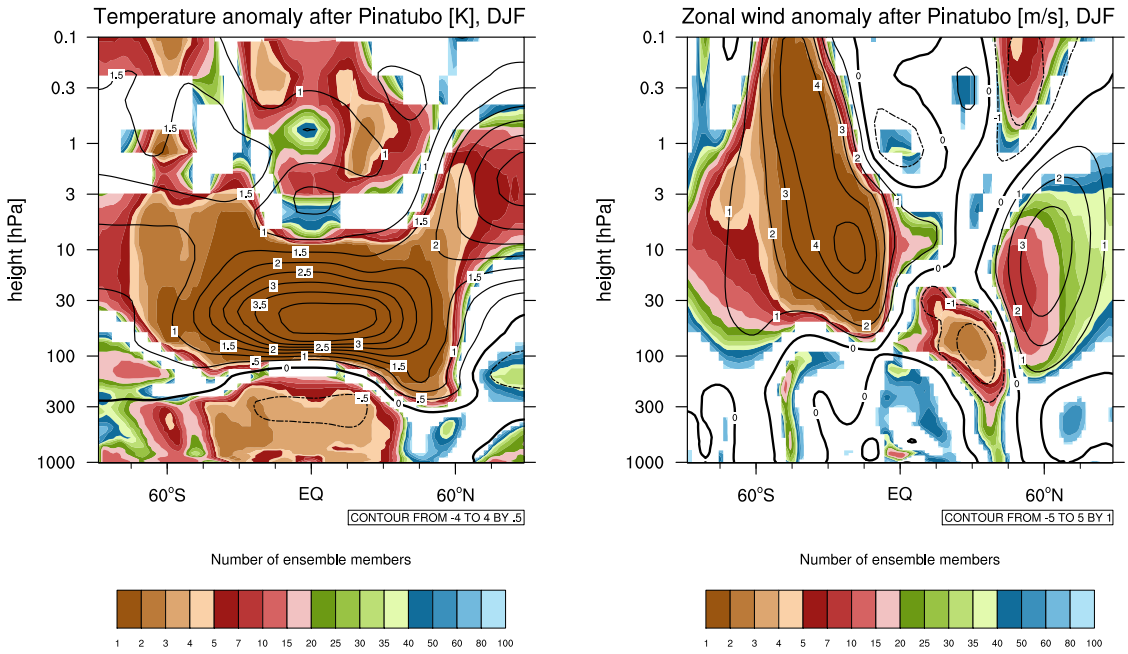

Figure 6.3: Ensemble average of the zonal mean temperature anomaly $[K]$ (left) and zonal mean zonal wind anomaly $[m/s]$ (right) in first post-eruption DJF after the Pinatubo eruption (contour lines). The shading indicates the minimum number of ensemble members nedded to detect the anomaly significantly at the 95% confidence level.

The warming of about 4 K in the tropical lower stratosphere after the Pinatubo eruption exceeds the 95% confidence level with 2 ensemble members, only (Fig. 6.3, left). This is not surprising, because in absence of the QBO the internal variability of the tropical stratosphere is small and the forcing of the volcanic eruption acts directly on the radiation. Also the cooling of the troposphere is significant in low latitudes with already 3-10 ensemble members, because the increase in albedo due to the volcanic aerosol layer directly influences the radiation. Since the internal variability of the troposphere is larger and the temperature anomaly is smaller compared to the tropical stratosphere, more ensemble members are needed to detect a significant tropospheric cooling. The positive temperature anomaly of 3.5 K at high NH latitudes at approximately 3 hPa results from adiabatic, dynamical heating by increased downwelling over the pole (Toohey et al. 2014), but even though the anomaly is almost as strong as the lower tropical heating, more than 5 ensemble members are needed to exceed the 95% confidence level. This is explained by the larger internal variability of the NH polar stratosphere compared to lower latitudes in DJF (see chapter 1).

The weakening of the southern hemisphere DJF easterlies is the strongest response of the MPI-ESM-LR to the eruption of Pinatubo and is significant with only 2 ensemble members (Fig. 6.3, right). Many climate models show this zonal wind anomaly in the austral summer hemisphere after a volcanic eruption, which might be due to the increased meridional temperature gradient in the lower stratosphere (see chapter 5). However, why the weakening of the SH easterlies is less clear in the reanalysis data after the El Chichón and Pinatubo eruption is not fully understood yet. The weakening of the subtropical jet in the NH can be explained by the decreased temperature gradient

in the troposphere, due to cooling of the low latitudes (Rind et al. 1992; Zanchettin et al. 2012). The maximum of this negative zonal mean zonal wind anomaly exceeds the 95% confidence level with 3-5 ensemble members. Even a significant near surface signal at approximately 40°N, although smaller than -0.5 m/s, can be significantly detected, but a large ensemble of more than 30 ensemble members is necessary. How many ensemble members are needed to exceed the 95% confidence threshold for the zonal mean zonal wind in the NH polar stratosphere crucially depends on the latitude. The maximum anomaly of about 3-4 m/s is approximately at 55°N-65°N and 10 hPa, and is already discussed in the previous section. Equatorward of the maximum, the numbers of ensemble members needed decreases to 7-15, whereas poleward of the maximum up to 40 members are necessary for the same anomaly magnitude. This is due to the internal variability which is larger north of 60°N than south of 60°N (Schmidt et al. 2013) and therefore more ensemble members are needed to detect a significant response to the Pinatubo eruption. But the model is able to simulate a significantly strengthened polar vortex, albeit only with an ensemble larger than what most couple climate models offer in the CMIP5 archive. Even the magnitude of the polar vortex anomaly is comparable with reanalysis data after Pinatubo (Toohey et al. 2014).

However, a much stronger polar vortex anomaly was observed after the eruption of El Chichón, where the MPI-ESM-LR does not to simulate a significant anomaly (Fig. 6.1b). Missing and/or incorrect processes in the model, for example coupled chemistry or the QBO, or to uncertainties in the prescribed volcanic forcing can contribute to a too weak response of the polar vortex, which is an important question for future research. But given the large internal variability of the NH polar stratosphere, it is impossible to attribute the observed polar vortex anomaly after El Chichón to the volcanic forcing alone. The observations of the polar vortex after volcanic eruptions are available only for the two eruptions of El Chichón and Pinatubo. Even if one includes two winters after the eruptions, the sample size of four post-eruption winters is very likely too small make conclusive statements about the magnitude of the polar vortex anomaly that is expected after volcanic eruptions. Reanalysis data suggests that the true atmosphere shows an even larger internal interannual variability of the polar vortex in DJF compared to the MPI-ESM-LR (see chapter 5, Fig. 5.6), which implies that more eruptions would be necessary to detect a significant signal in the real atmosphere compared to the MPI-ESM-LR. However, it is possible that the polar vortex in the real atmosphere is more susceptible to volcanic forcing than the climate models, i.e. for the same eruption magnitude the polar vortex is robustly strengthened in the real atmosphere but not in the models. But testing the sensitivity of the polar vortex to volcanic eruptions in the real atmosphere is difficult. First, because of the limited number of observations in the stratosphere after volcanic eruptions and second, because all eruptions will differ among each other not only in their magnitude, but also in their exact location, their eruption season and their climatic boundary conditions, which all might influence the response of the polar vortex (Timmreck et al. 2012). But assuming that the sensitivity of the real atmosphere to volcanic eruptions is equal to the sensitivity to volcanic eruptions in the MPI-ESM-LR, it is not possible to conclude that the model underestimates the dynamical response of the NH polar vortex with only two observed eruptions, given the large internal variability of the NH winter stratosphere. For the MPI-ESM-LR, the observed averaged polar vortex anomaly of 8 m/s after the

two winters following El Chichón and Pinatubo is well within the 95% quantile for an ensemble of four members for the same eruptions (Fig. 6.1c).

6.3.3 Surface response

The expected dynamical response to tropical volcanic eruption is however not solely based on the sparse observation of the stratosphere, but to a much larger part on changes of surface temperature and tropospheric circulation. Instrumental and proxy records of the surface temperature and the sea level pressure after volcanic eruptions cover a much larger timespan than satellite observations and apparently show a significant shift of the NAO to a positive phase and the volcanic winter warming in northern Europe (Shindell et al. 2004; Fischer et al. 2007; Christiansen 2008). The shift of the NAO is assumed to originate from the downward propagation of a strong polar vortex signal in the stratosphere (Graf et al. 1993; Kodera 1994), which is supported, but due to the small sample size, not proven by the eruptions of El Chichón and Pinatubo. Still, observations as well as model studies indicate that the signal of a stronger polar vortex in winters without volcanic perturbation can significantly impact surface climate (Baldwin and Dunkerton 2001; Reichler et al. 2012). The shift of the NAO and the subsequent winter warming pattern is not reproduced by the coupled climate models in the CMIP5 archive (Driscoll et al. 2012), but whether this is due to uncertainties in the volcanic forcing or due to internal variability is not known. In the same way as for the zonal mean temperature and zonal wind, I use the 100 ensemble members of the MPI-ESM-LR to investigate whether a large ensemble reproduce the observed surface temperature and circulation response and if so, how many ensemble members are needed to significantly detect the changes.

The cooling of the tropical latitudes after the Pinatubo eruption, due to less incoming solar radiation, is in the order of 0.2-0.6 K (Fig. 6.4, top panel). Although the magnitude of the anomaly is small, the temperature anomaly is already significantly different from zero with 2-7 members in the Atlantic, Indian, and western Pacific Ocean. In southern Asia, more than 7-20 ensemble members are needed to detect a significant negative surface temperature anomaly. However, because some model centers provide only 3-5 ensemble members for the historical simulation, even the cooling in the tropics might not be significant for their particular model. No significant surface temperature signal can be found in the central Pacific, most likely due to the large variability of ENSO that can complete mask the volcanic cooling. In the NH high latitudes, a warm temperature anomaly extends from northern Europe and Siberia into the Arctic Ocean, where a maximum of 1.4 K occurs. Over Canada and the Middle East a negative temperature anomaly of -0.5 K is apparent. The temperature anomaly pattern is not inconsistent with observations and proxy records after volcanic eruption, but there are no long temperature proxy-data of the Central Arctic. However, only the anomaly over the central Arctic can be significantly detected and at least 10-25 ensemble members are needed at the 95% confidence level. In some regions, including the negative temperature anomaly in Canada, even up to 35-50 members are necessary. The continental winter warming over Northern Europe and Siberia is not significantly different from zero even with 100 ensemble members.

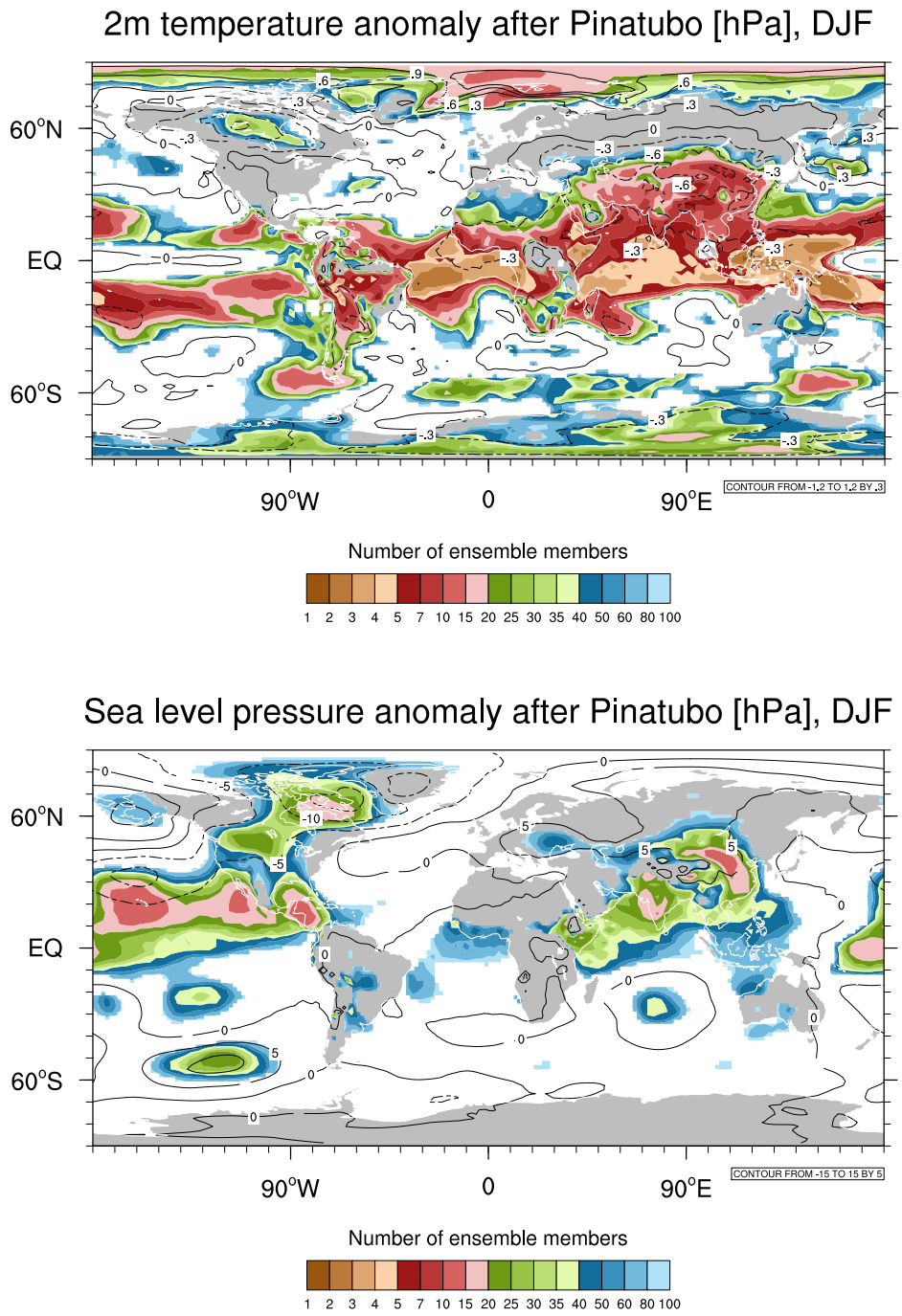

Figure 6.4: Ensemble average of the near-surface temperature anomaly $[K]$ (top) and sea level pressure anomaly $[hPa]$ (bottom) in first post-eruption DJF after the Pinatubo eruption (contour lines). The shading indicates the minimum number of ensemble members nedded to detect the anomaly significantly at the 95% confidence level.

Changes in the surface circulation are less significant than changes in surface temperature as seen in the sea level pressure anomaly (Fig. 6.4, bottom panel). Anomalies that can be significantly detected with the smallest ensemble size are found in the tropics, but even here more than 10 members are neccessary. A positive surface pressure anomaly over the Indian subcontinent is likely due to the negative temperature

anomaly in the same region and intensifies the climatological high pressure system over the Asian continent in boreal winter. In the NH, only the negative surface pressure anomaly over the Canadian Archipelago can be significantly detected, but 15-50 members are necessary. The nonsignificant negative anomalies over Greenland and positive anomalies in the northern Atlantic suggest a northward shift of the climatological SLP pattern. The positive pressure anomaly over Central-Eastern Europe, which is significant for an ensemble of at least 50 members, might lead to the advection of warm, maritime air masses to the central Arctic, explaining the positive temperature anomalies in that region. However, the response of the NH pressure field to the Pinatubo eruption is very limited and in large parts not significant. A positive phase of the NAO is not supported by the MPI-ESM-LR, even with a large ensemble, and is therefore in contrast to the significant signal in the observations and proxy-records (Christiansen 2008). Although the MPI-ESM-LR shows a stronger polar vortex after the Pinatubo eruption with a large enough ensemble of approximately 15-30 members, the signal in the polar stratosphere does not propagate downward and significantly impact the surface climate.

However, it has been shown that the previous model version of the MPI-ESM-LR captures the stratosphere-troposphere coupling reasonably well (Bunzel et al. 2013). First analyses of the current version suggest that this is also the case for the MPI-ESM-LR version 1.1 (Gerber 2015, personal communication). Possibly the positive polar vortex anomaly after Pinatubo of about 3-4 m/s is too small to significantly influence the tropospheric circulation. To investigate the downward coupling, usually large polar vortex anomalies such as major stratospheric warmings, which can decelerate the polar vortex by 40 m/s (Ayarzagüena et al. 2011), are investigated. For such events, the polar vortex anomaly can possibly influence the troposphere significantly, but the comparably smaller anomaly after the Pinatubo eruption might not be distinguishable from internal variability at the surface. Splitting the winter into single month rather than focusing of DJF might yield different results, because the anomalies of the polar vortex need some time to propagate to the surface (Baldwin and Dunkerton 2001; Manzini et al. 2006). Therefore, a time lag of about one month between the polar vortex anomaly and the tropospheric response can possible improve the significance of the volcanic signal at the surface. It is not evident, that a too weak response of the NH polar vortex is the reason for the failure of the model to show significant surface anomalies. Given the large internal interannual variability of the NH polar vortex, the model is not in disagreement with the sparse stratospheric satellite observations after El Chichón and Pinatubo. Unfortunately, only more observed events of volcanic eruptions in order to pin down more accurately the response of the polar vortex can help to solve this problem.

6.4 Summary and conclusion

I used a 100 member ensemble of historical simulation with the MPI-ESM-LR to quantify the uncertainty in the response to volcanic eruptions arising from internal, interannual variability. I focused on the NH polar vortex response in the stratosphere, but I also investigated the surface response to the Pinatubo eruption in the NH winter. The

guiding question is: How many ensemble members are necessary to detect a significant response to volcanic eruptions?

A strengthening of the polar vortex of 3-4 m/s in the first winter after the Pinatubo eruption can be significantly detected with an ensemble larger than 15 members. The necessary ensemble is larger than what coupled climate models in the CMIP5 archive provide. Although the exact number of necessary ensemble members will be model dependent, a too small ensemble can potentially show no significant response to a volcanic eruption due to the large internal variability of the polar stratosphere. Adding smaller eruptions to increase the post-volcanic composite and to reduce the uncertainty of the volcanic signal due to internal variability may weaken the response of the polar vortex by so much, that actually more ensemble members are needed for a statistical significant signal. For a significant polar vortex response averaged over the eruptions of El Chichón and Pinatubo even more than 20 ensemble members are necessary, although the sample size is doubled. For an even larger composite of the nine largest eruptions since 1850, as used in the assessment of Driscoll et al. (2012), the strengthening of the polar vortex is significantly different from zero for 12 ensemble members. Thus, increasing the sample size for the sake of better statistics does not necessarily improves the detectability very much compared to a single, strong eruption. The most robust signal of a strengthened polar vortex can be obtained in the MPI-ESM-LR if only the two strongest eruptions, Krakatau and Pinatubo, are averaged. Including smaller eruptions weakens positive polar vortex anomaly by so much that more ensemble members are needed to significantly detect the impact of volcanic eruptions. Of course the multi-model mean consists of more than 12 members in total, but averaging different models with different volcanic forcing datasets and different implementations of these forcing datasets introduces another sources of uncertainty (model and forcing uncertainty) which impacts the detectability of the signal as well.

In the absence of the QBO in the model, the positive temperature anomaly due to absorption of near infra-red radiation by the volcanic aerosol layer in the lower tropical stratosphere in the first winter after the Pinatubo eruption is significantly different from zero with two ensemble members, only. In regions with larger interannual variability, for example the tropical troposphere or the upper polar stratosphere, between 3-10 ensemble members are necessary. The most significant response of the zonal mean zonal wind to the Pinatubo eruption is the weakening of the easterlies in the SH, which is detectable with two ensemble members and is due to the increased meridional temperature gradient in the lower stratosphere. A weakened tropospheric equator-to-pole temperature gradient causes a weakening of the subtropical jet in the NH, which is significant with at least 3-5 ensemble members. How many ensemble members are necessary to detect the strengthening of the polar vortex depends crucially on the latitude considered and reaches from 7 at the southward flank of the positive wind anomaly to more than 40 members at high latitudes, where the internal variability is larger. However, the MPI-ESM-LR is able to significantly simulate a strengthened polar vortex after the eruption of Pinatubo, albeit with an ensemble larger than what most of the models in the CMIP5 archive provide. The magnitude of polar vortex anomaly is not inconsistent with observations after the eruptions of El Chichón and Pinatubo, but the small sample size of the observations prevent conclusive statements.

The surface response of a shift of the NAO to a positive phase and a continental winter warming, which is robust in observation due to the larger number of records for past eruptions, is not captured by the MPI-ESM-LR. There are no significant anomalies of the sea level pressure in the North Atlantic which project on the NAO and a warming of Northern Europe and Scandinavia is even with 100 ensemble members not significantly simulated. The only significant temperature anomaly in the high northern latitudes is a warming of the central Arctic Ocean, which might be related to advection of warm air masses and possible subsequent positive sea-ice feedbacks. As there are no paleo reconstruction of the central Arctic temperatures, a comparison with observations to validate the warming is not possible.

Conclusively, given a large enough ensemble the MPI-ESM-LR is able to reproduce a stronger polar vortex after volcanic eruption with a magnitude not inconsistent with observations. However, since the observational sample size is limited to two eruptions, I cannot rule out the possibility of a two weak response of the model. Especially because the MPI-ESM-LR does not show a significantly stronger polar vortex after the El Chichón eurption in a large ensemble in contrast to observations. However, due to the large internal variability of the NH polar stratosphere, this might as well be just by chance. The simulation of the surface signal are, however, in contrast to the more robust observational and proxy-records. Three possible hypotheses to explain this discrepancy are: first, although the polar vortex is strengthened, the stratosphere-troposphere coupling is too weak or does not project onto the NAO to significantly influence the surface climate as observed. Second, the polar vortex strengthening itself is too weak, perhaps due to missing processes as interactive chemistry or uncertainties in the volcanic forcing, to impact the troposphere. Third, the stratospheric pathway is not the only mechanism which influence the NH climate after volcanic eruptions. Possibly the surface cooling in the tropics or the weakening of the subtropical jet are responsible for shifting the NAO to a positive phase in observations. A tropospheric pathway was found by Wegmann et al. (2014) in simulations of the Tambora eruption, but in their study they focused on the NH summer season to explain the"year without a summer" in 1816. The sample size of the stratospheric observation is too small to confidently state that a downward propagation is the main cause of the positive phase of the NAO. In this case, the MPI-ESM-LR, as well as most of the coupled climate models in the CMIP5 archive, miss tropospheric teleconnections which yet would have to be identified.

As nature offers only "one realization", the detectability of the volcanic signal in the real atmosphere is problematic, especially in regions with large internal variability such as the NH polar vortex. Attributing the polar vortex anomalies after the two available observed events of El Chichón and Pinatubo to the volcanic forcing is difficult, because the polar vortex will also be influenced by other factors such as ENSO, the QBO, solar irradiance and interannual variability. As demonstrated by the large ensemble needed to identify a significant response to a strong eruptions such as Pinatubo, one must be careful in validating the model response to the very limited observational record in the stratosphere after volcanic eruptions.

Chapter 7

Conclusion and Outlook

7.1 Summary and conclusions

In this thesis I investigated the NH winter response to strong tropical volcanic eruptions using the comprehensive Earth System Model MPI-ESM. The study focused on the dynamical impact of volcanic eruptions on the NH polar vortex, which is expected to be stronger in the first two post-eruption winters. A stronger polar vortex can subsequently change the surface climate by influencing the NAO, which is the leading mode of variability in the NH winter troposphere. Coupled climate models seem to generally fail in capturing the dynamical response to strong volcanic eruptions, i.e. they underestimate the intensification of the NH polar vortex and do not show the volcanic winter warming pattern at the surface as observed (Stenchikov et al. 2006; Driscoll et al. 2012). Whether this failure is due to missing and/or incorrect processes in the models or a lack of understanding about the mechanism how volcanic eruptions influence the NH stratosphere is unclear. The overarching question of the thesis —why climate models underestimate the dynamical response to volcanic eruptions— motivated four lines of investigation, aiming to answer the following more specific questions:

1) **Does an increased vertical resolution and a better representation of stratospheric processes improve the response to volcanic eruptions?**

I compared two configurations of the MPI-ESM with regard to their NH winter response to the nine strongest tropical volcanic eruptions in the CMIP5 historical simulations (1850-2005). The configurations differ in their horizontal resolution in the ocean and in their vertical resolution in the atmosphere, where the MPI-ESM-LR has 47 layers in contrast to the MPI-ESM-MR with 95 layers. Owing to the higher vertical resolution, the MPI-ESM-MR spontaneously generates a QBO in the tropical stratosphere. I find that the simulated positive temperature anomaly in the tropical stratosphere after the nine strongest eruptions from 1850 to 2005 is realistically captured in both configurations, but modulated in the MR configuration by the phase of the QBO. The QBO induces a secondary circulation which leads to adiabatic temperature changes in the tropical stratosphere. Due to a bias in the volcanic composite towards the west phase of the QBO in the MR configuration, the maximum temperature anomaly in the tropics is stronger and shifted to higher altitudes compared to the temperature anomaly in the LR configuration.

I find no evidence that enhanced vertical resolution and better representation of stratospheric processes, such as the QBO, improves the dynamical response to tropical volcanic eruptions, i.e. the strengthening of the NH polar vortex and the subsequent shift of the NAO to a positive phase. Strengthening of the NH polar vortex is not significant, with the exception of the second post-eruption winter in the MR configuration. Because the positive temperature anomaly of the tropical stratosphere in the second post-eruption winter is a factor of 2 smaller compared to the first post-eruption winter, and a similar effect is absent in the LR configuration, it is rather unlikely that the volcanic eruption is the cause of the stronger polar vortex. There is no known physical reason why the response of the polar vortex to volcanic eruptions in the second winter should be larger compared to the first winter, when the forcing is stronger in the first winter. In the SH austral summer, the variability is much smaller than in the NH during boreal winter and the zonal mean zonal wind signal reflects the temperature anomaly much more accurately. Here, both configurations show a stronger zonal mean zonal wind anomaly in the first post-eruption austral summer.

A significant shift of the NAO to a positive phase is not simulated by either the LR or the MR configuration. The shift of the NAO is assumed to arise from a stronger polar vortex after volcanic eruptions, which is not captured in either configuration. Hence, sea level pressure anomalies in the North Atlantic sector are largely not significant. Consequently, the volcanic winter warming pattern is absent in both configurations and the only consistent and significant surface temperature signal is the cooling of the tropical latitudes due to the reflection of incoming solar radiation.

2) How much does the response of the polar vortex to tropical volcanic eruptions depend on the magnitude of the eruption and what is the mechanism how volcanic eruptions influence the polar vortex?

I performed ensemble simulations of the very large Tambora eruption and compared these to the averaged response of the eruptions of Krakatau and Pinatubo (KP) with respect to their dynamical influence on the NH polar vortex in the first post-eruption winter. The Krakatau and Pinatubo eruptions, which are the largest eruptions of the CMIP5 historical simulations from 1850 to 2005, show a strengthening of the polar vortex, albeit weak in comparison with observations after the eruptions of El Chichón and Pinatubo. With the larger Tambora forcing however, the polar vortex is significantly strengthened in late winter. The ensemble variability is significantly reduced, which implies that the ensemble members respond similarly to the volcanic forcing. Thus, the very large forcing of the Tambora eruption damps the internal variability. This finding is important as it highlights that the MPI-ESM-LR does not in generally fail to reproduce the dynamical impact of tropical volcanic eruptions, but given a large enough forcing the expected response of the NH polar stratosphere can be obtained.

My analysis shows that the intensification of the polar vortex is not solely due to the direct effect of an increased meridional temperature gradient by the heating of the volcanic aerosols in the tropical stratosphere as often postulated. The meridional temperature gradient changes most equatorward of the polar vortex, at approximately

30°N. The temperature gradient anomaly induces a positive wind anomaly at 30°N between 50 *hPa* and 10 *hPa*, which is most pronounced in early winter. The positive wind anomaly implies an equatorward shift of the zero-wind line, which is critical for the propagation of waves. Planetary waves respond to the change in the wind field by propagating to lower latitudes and deposit less momentum in the region of the NH polar vortex. Therefore, wave-driven deceleration of the zonal wind at high latitudes is hampered. This dynamical mechanism links the sub-tropical gradient in the heating rate anomaly with the strength of the polar vortex. Thus, it is important in the context of the response to volcanic eruption not to focus solely on the meridional temperature gradient itself. Coupled climate models need to represent wave-mean flow interactions correctly in order to simulate successfully the strengthening of the polar vortex after volcanic eruptions.

Although the positive wind anomaly at 30°N in early winter is statistically significant after the eruptions of Krakatau and Pinatubo, for these smaller eruptions the indirect effect by the deflection of waves towards lower latitudes is less robust. In contrast to the Tambora experiment, the ensemble variability of the NH polar stratosphere in the KP experiment is not reduced, which implies that internal variability dominates over the forced response in the region of the polar vortex. The fact that the indirect, wave-driven mechanism significantly strengthens the polar vortex only for very large eruptions may hint at an imperfect representation of wave-mean flow interactions in the model. To what extent this proposed mechanism plays a dominant role in the real atmosphere is difficult to quantify due to the very limited number of eruptions in the satellite era. The two eruptions of Krakatau and Pinatubo are the strongest tropical eruptions since 1850. Therefore, the lack of a significant impact of volcanic eruptions on the NH polar vortex in the CMIP5 historical period could be due to the dynamical effects of the volcanic forcing being not discernable from internal variability in small ensembles.

3) Does the interannual variability of the NH polar vortex in early winter influence the response to volcanic eruptions?

Kodera and Kuroda (2002) find in reanalysis data that the polar vortex shows a comparable small interannual variability and is largely radiatively controlled in early winter, whereas in mid- and late winter the interannual variability is larger and planetary waves determine the state of the polar vortex. Climate models show a considerable spread in their representation of early winter polar vortex interannual variability. For models with large variability in early winter, the polar vortex might not be solely radiatively controlled but also already dynamically controlled. In this case, the response of the polar vortex to volcanic eruptions might be weakened, because the polar vortex will not only respond to the radiative forcing of the volcanic aerosols, but also to wave perturbations. I investigated whether the overestimation of the interannual variability of the polar vortex in early winter can explain the limited dynamical response to volcanic eruption in the CMIP5 ensemble.

I analyzed 15 models that participated in CMIP5 with respect to their stratospheric NH polar vortex response to the volcanic eruptions of Krakatau, El Chichón and Pinatubo.

The multi-model mean shows a stronger polar vortex in the first post-eruption winter after the eruptions of Krakatau and Pinatubo, which at least questions the assumption of a general failure of coupled climate models to reproduce the dynamical response of the NH polar stratosphere to volcanic eruptions. Given a large forcing, the coupled models on average simulate a strengthened polar vortex of a comparable magnitude as reanalysis data suggests in the first winter after the Pinatubo eruption. For the comparably smaller eruption of El Chichón, the multi-model mean does not show a response of the polar vortex, which seems to be in contradiction to the reanalysis data. However, one must be careful in attributing the polar vortex anomaly in the reanalysis data solely to the volcanic forcing, because of the very small sample of observed volcanic eruptions. The polar vortex in post-eruption winters will be influenced by other factors such as the El Niño events, which occurred after El Chichón and Pinatubo, and the phase of the QBO. The large interannual variability of the polar vortex in wintertime makes it very difficult to unambiguously differentiate the forced response from chaotic noise.

The hypothesis that an overestimation of the interannual polar vortex variability in early winter leads to an underestimation of the volcanic response must be discarded, because I dont find evidence that models with lower interannual variability in early winter simulate a stronger response to volcanic eruptions. On the contrary, for models that show a larger interannual variability of the polar vortex in early winter, the response to the El Chichón and Pinatubo eruption is actually stronger. Because a large interannual variability of the polar vortex means that polar vortex strength varies substantially from year to year, I further tested whether a climatological strong polar vortex in early winter favors a stronger response to volcanic eruptions. However, there is no correlation between the ensemble mean climatological polar vortex strength in early winter and the ensemble mean polar vortex anomaly in mid-winter after volcanic eruptions.

Interestingly, for the individual ensemble members of each model, the polar vortex anomaly in mid-winter after volcanic eruptions depends on the polar vortex anomaly in early winter after volcanic eruptions. If the post-eruption polar vortex is stronger-than-average in early winter, it is likely to be stronger-than-average also in mid-winter, and vice versa. It is important that the positive correlation between early winter polar vortex anomaly and mid-winter polar vortex anomaly is considerably stronger in winters after volcanic eruptions compared to winters without volcanic perturbation. In volcanically unperturbed winters, the strength of the polar vortex in mid-winter depends only weakly on the strength of the polar vortex in early winter. This implies that the volcanic eruptions influence the polar stratosphere in a way which allows a polar vortex anomaly to be more persistent compared to a volcanically unperturbed winter. However, the physical explanation for this behavior is still not resolved.

4) **How many ensemble members are necessary to detect a significant response to volcanic eruptions?**

Throughout this thesis, the simulated response to tropical volcanic eruptions is often small and insignificant, especially for quantities which exhibit large internal variability.

Here, I use a 100 member ensemble of historical simulations by the MPI-ESM-LR to quantify the uncertainty in the NH response to volcanic eruptions arising from internal, interannual variability. I find that even for the largest tropical eruption in the 20^{th} century (Pinatubo 1991) an ensemble of more than 15 members is necessary to detect a significant strengthening of the polar vortex in the first post-eruption winter. Increasing the post-eruption sample size by adding smaller eruptions than Pinatubo narrows the uncertainty of the mean response, but also weakens the mean signal by so much that potentially more ensemble members are necessary to detect a significant response. A composite of the nine largest tropical eruptions, as used in one assessment of the volcanic signal in CMIP5 models, only marginally reduces the number of ensemble members needed to detect a significant response in the MPI-ESM-LR compared to focusing only on Pinatubo.

The number of ensemble members needed to detect a significant signal after volcanic eruptions depends on the signal to noise ratio, i.e. the magnitude of the anomaly and the internal variability. Hence, a small ensemble is sufficient for large perturbations in regions with comparably low internal variability: e.g. the heating of the lower tropical stratosphere after the Pinatubo eruption is significant with 2 ensemble members due to the large temperature anomaly and the low variability in absence of the QBO in this model configuration. The tropical troposphere exhibits a larger internal variability compared to the tropical stratosphere, therefore the surface cooling in the tropics after Pinatubo is significant for 2-7 members, dependent on the exact location. Observations after volcanic eruptions suggest a positive NAO and a continental winter warming in northern Europe and Siberia, but no significant response is simulated by the MPI-ESM-LR even with 100 ensemble members. As the shift to a positive phase of the NAO and the according temperature response is robust in observations, I conclude that the model fails to reproduce the dynamical impact of tropical volcanic eruptions in the troposphere. Previous model versions of the MPI-ESM-LR, as well as first analyses of the current version, suggest that the stratosphere-troposphere coupling is reasonably well captured. Thus, is it not clear why a strengthened polar vortex after the Pinatubo eruption does not influence tropospheric climate. However, the magnitude of the anomalies which are usually investigated to study the downward coupling are much larger compared to the anomalies simulated after the Pinatubo eruption. Major stratospheric warming events can decelerate the NH polar vortex by approximately 40 m/s within one month (Ayarzagüena et al. 2011) compared to the 4 m/s acceleration of the polar vortex in DJF after the Pinatubo eruption. Therefore, the strengthening of the polar vortex might be too small have a significant impact on the troposphere in the MPI-ESM-LR. Furthermore, the anomaly in the polar stratosphere needs approximately 15-30 days to propagate from the polar vortex at 10 hPa to the surface (Baldwin and Dunkerton 2001; Manzini et al. 2006). Hence, splitting the DJF season into single months and analyzing the stratospheric and tropospheric anomalies with a time lag might yield different results.

In contrast to the surface signal, where longer instrumental and paleo-records exist, the observed polar vortex signal after volcanic eruptions is limited to the winters after El Chichón and Pinatubo. As nature only offers "one realization", the attribution of the polar vortex anomaly to the forcing of the volcanic eruptions is problematic if not impossible. Based on the small sample size of observations, even if two winters

after El Chichón and Pinatubo are taken into account, a sensible validation of the polar vortex response in the model is difficult due to the large internal variability of the NH polar stratosphere in boreal winter. Also in observations, the polar vortex is not strengthened in every case and continuously throughout the winter after volcanic eruptions, as highlighted by the minor stratospheric warming occurring in the winter 1991/1992 after the Pinatubo eruption. Simulations with a very large ensemble provide three important insights: First, for a sufficiently a large ensemble, the MPI-ESM-LR simulates a significantly strengthened polar vortex after the Pinatubo eruption as well as after the nine strongest tropical eruptions of the CMIP5 historical period. Second, the polar vortex response after volcanic eruptions in a too small ensemble can lead to false conclusions about the ability of the model (see chapter 3). An absent signal in a small ensemble might be assigned to model failure although the response is still considerably influenced by internal variability. Third, given the large variability of the polar stratosphere, one must be careful in validating the climate model response to the one realization of the real atmosphere. The stronger polar vortex in the observations after volcanic eruption is influenced by other factors, such as the phase of ENSO, the QBO, variations in the solar irradiance, or might just occur by chance due to internal variability.

Investigation of the four research questions made clear that this study cannot offer a final answer why coupled climate models seem to underestimate the dynamical response to tropical volcanic eruptions. However, important and new insights concerning the mechanism through which volcanic eruptions influence the NH winter climate have been gained. In particular, wave-mean flow interactions after tropical volcanic eruptions, given a large enough forcing, have a significant impact on the NH polar vortex and challenge the simplistic view of a direct influence of an enhanced meridional stratospheric temperature gradient from the equator to the pole as the dominant effect after volcanic eruptions. Eruptions of the magnitude of Pinatubo or Krakatau show the same indirect influence on the polar vortex, but possibly due to deficiencies in the wave-mean flow interaction in the model, the internal variability of the NH polar stratosphere prevents the indirect effect to have a significant impact in small ensembles of a single model. But a general failure of coupled climate models to reproduce the dynamical impact of tropical eruption on the NH polar vortex, as claimed by previous studies, is not supported by this thesis. Given a large enough forcing, such as Krakatau and Pinatubo, the multi-model mean simulates a strengthened polar vortex.

For the first time, this study quantifies the uncertainty in the response to volcanic eruptions arising from internal variability. Notably, the comparably large ensemble of at least 15 members needed to detect a significant response of the NH polar vortex in winter to the Pinatubo eruption highlights the substantial uncertainty due to internal variability. An ensemble of 15 members of historical simulations would be larger than any single model provided to the CMIP5 archive, which at least questions the apparent inability of climate models to reproduce the dynamical impact of volcanic eruptions. Of course, the multi model ensemble consists of more than 15 members, but due to different volcanic forcing datasets and different model physics, additional sources of uncertainty

will affect the volcanic signal. The large ensemble which is needed to identify the polar vortex response to volcanic eruptions has implications for conclusions drawn about the non-improvement in the MPI-ESM-MR. With three members only, the ensemble of historical simulation of the MPI-ESM-MR is too small to state with certainty that an enhanced vertical resolution does not improve the response of the polar vortex after volcanic eruptions, even if multiple eruptions are combined to increase the sample size. Moreover, the occurrence of the QBO in the MPI-ESM-MR adds another source of uncertainty, because the impact of volcanic eruptions might be different under different QBO phases. Hence, an ensemble of at least 15 members per QBO phase would be desirable. Many open questions remain concerning the impact of tropical volcanic eruptions on the NH polar vortex, which will be difficult the answer without more observations. The indirect effect via wave-mean flow interactions is significant in the MPI-ESM-LR, and a westerly zonal mean zonal wind anomaly in early winter, which allows for wave propagation towards lower latitudes, can also be found in a number of different CMIP5 models (see chapter 5). But whether this mechanism plays a role in the real atmosphere is impossible to say with only two eruptions observed since the start of global satellite coverage 1979. The internal variability of the polar vortex is substantial, as shown by the results of the 100 member ensemble, and because strong volcanic eruptions occur not very frequently, validation of climate models with respect to their ability to reproduce the dynamical impact of volcanic eruption will be a challenge for many years to come.

7.2 Outlook and ongoing work

Apart from the insufficient observational record, which is of course nothing which can be tackled, there are still a number of possible ways to go forward in research of volcanic impacts on climate. First, the assessment of the dynamical response to volcanic eruptions in the CMIP3 and CMIP5 models (Stenchikov et al. 2006; Driscoll et al. 2012) lacks a consistent volcanic forcing dataset. Because every modeling center was free to choose which dataset to use, the spread in the simulated response arises not only from model uncertainty but also from uncertainty in the forcing. Experiments with a single volcanic forcing set that is used in every coupled model would help to pin down the model uncertainty, which will be done in VolMIP (Zanchettin et al. 2015), an endorsed initiative of the upcoming CMIP6. Moreover, focusing on one single eruption would be beneficial, because averaging over eruptions of different magnitude, at different latitudes and in different eruption seasons might have an influence on the dynamical response as well (Toohey et al. 2011). Preferable would be large ensembles with an idealized forcing which can be easily modified to different magnitudes, eruption heights or seasons.

The analysis of volcanic eruptions in a coupled climate model often faces the caveat of prescribed and two dimensional ozone fields. Stenchikov et al. (2002) showed in a model study, that the depletion of ozone in the polar stratosphere after volcanic eruptions can substantially increase the polar vortex strength. However, it has been argued that for ozone depletion after volcanic eruptions to have a significant impact on the strength of the polar vortex, chlorine and other halogen species need to be

abundant in the stratosphere, which is only the case for the eruptions of El Chichón and Pinatubo (Marshall et al. 2009). Still, the impact of ozone depletion after volcanic eruptions has not been quantified in a coupled earth system model with interactive chemistry due to computational constraints. A comprehensive study of the effect of ozone depletion after volcanic eruptions with interactive chemistry in a coupled climate model, possibly under different climate states, i.e. different amounts of anthropogenic ozone depleting substances in the stratosphere, can help to solve a long lasting issue whether the effect of ozone needs to be accounted for or not.

In the same vein, simulations of volcanic eruptions in a coupled climate model with an interactive aerosol module can be beneficial for understanding the possible feedbacks of the circulation on the aerosol distribution. In contrast to prescribing a 2-dimensional aerosol field, as done in most of the CMIP5 models, an interactive 3-dimensional aerosol field can respond to circulation and the changed aerosol distribution can feedback on the circulation again. Some models, like the MRI-CGCM3 (Mizuta et al. 2012; Yukimoto et al. 2012), already use an interactive aerosol module and simulated the strengthening of the polar vortex well compared to the multi-model mean. However, the relatively small ensemble of 3 members prevents final conclusions whether this improvement is due to the interactive calculation of aerosol distribution or just by chance. Toohey et al. (2014) used a two-step approach, where an aerosol model first calculated the volcanic aerosol distribution and the optical properties serve in a second step as input to a coupled earth system model. They find that relatively small changes in the aerosol distribution yield very different responses in the polar vortex, indicating that accurate representation of space-time structure is crucial. Especially concerning the indirect effect of volcanic eruption on the NH polar vortex via wave deflection towards lower latitudes, a comprehensive study with an interactive aerosol module would be beneficial. Since for the indirect mechanism to work, the exact position of the heating gradient is vital, it would be interesting to study if the positive wind anomaly at 30°N substantially changes the aerosol distribution, the temperature anomaly gradient and subsequently the propagation of waves. But again, large ensembles are necessary in order to make certain the volcanic signal is distinguishable from internal variability.

Appendix

A Meridional stratospheric temperature difference

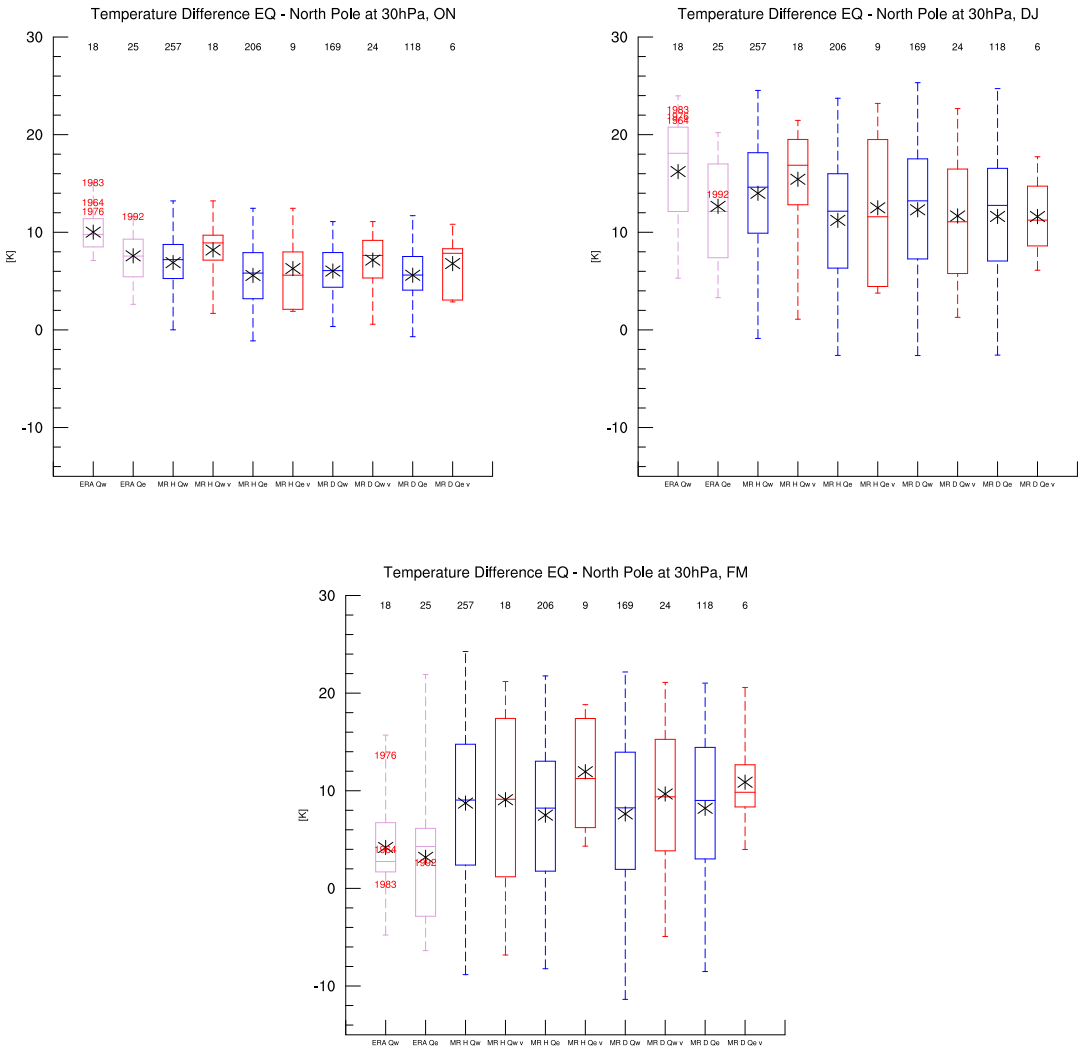

Figure A.1: Whisker-Box plot of the temperature difference between the equator (20°S-20°N) and the northern polar cap (60°N-90°N) at 30 *hPa* in October-November (upper left), December-January (upper right) and February-March (bottom). The temperature difference is shown for the ERA-40 reanalysis data (pink boxes) as well as for the historical (MR H) and decadal hindcase (MR D) simulatons of the MPI-ESM-MR. The red numbers display the winters after the volcanic eurptions of Agung (1963), Fuego (1976), El Chichón (1983) and Pinatubo (1992) in the ERA-40 reanalysis data. For the MPI-ESM-MR simulations, the blue boxes indicate winters without volcanic eruptions while the red boxes indicate the winters after the volcanic eruptions of Agung, Fuego, El Chichón and Pinatubo. The temperature difference is shown for the QBO west phase (Qw) and the QBO east phase (Qe), defined as the zonal mean zonal wind between 5°S-5°N at 30 *hPa*. The black numbers on the top indicate the number of winters which are used to obtain the temperature difference distribution represented by the Whisker-Box plot. The whiskers indicate the maximum and minimum temperature difference, the upper and lower lines of the box are the upper and lower quartile of the temperature difference distribution, the middle line is the median and the black star is the mean.

B Response of zonal mean zonal wind in CMIP5 models to volcanic eruptions

Krakatau

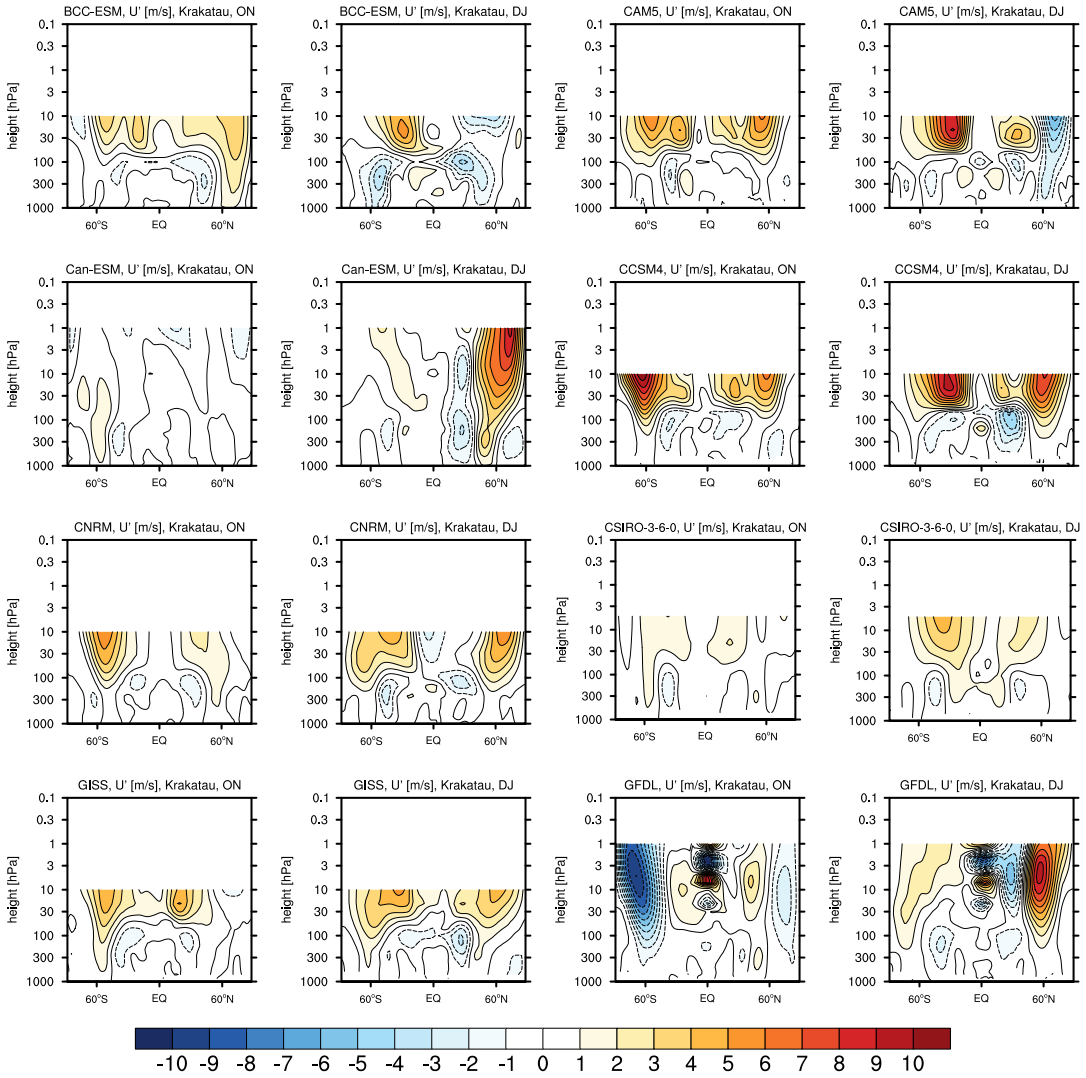

Figure B.1: Ensemble mean of the zonal mean zonal wind anomalies averaged over October-November (ON) and December-January (DJ) for CMIP5 models given in Table 5.1 after the eruption of Krakatau. Positive anomalies are defined as eastward.

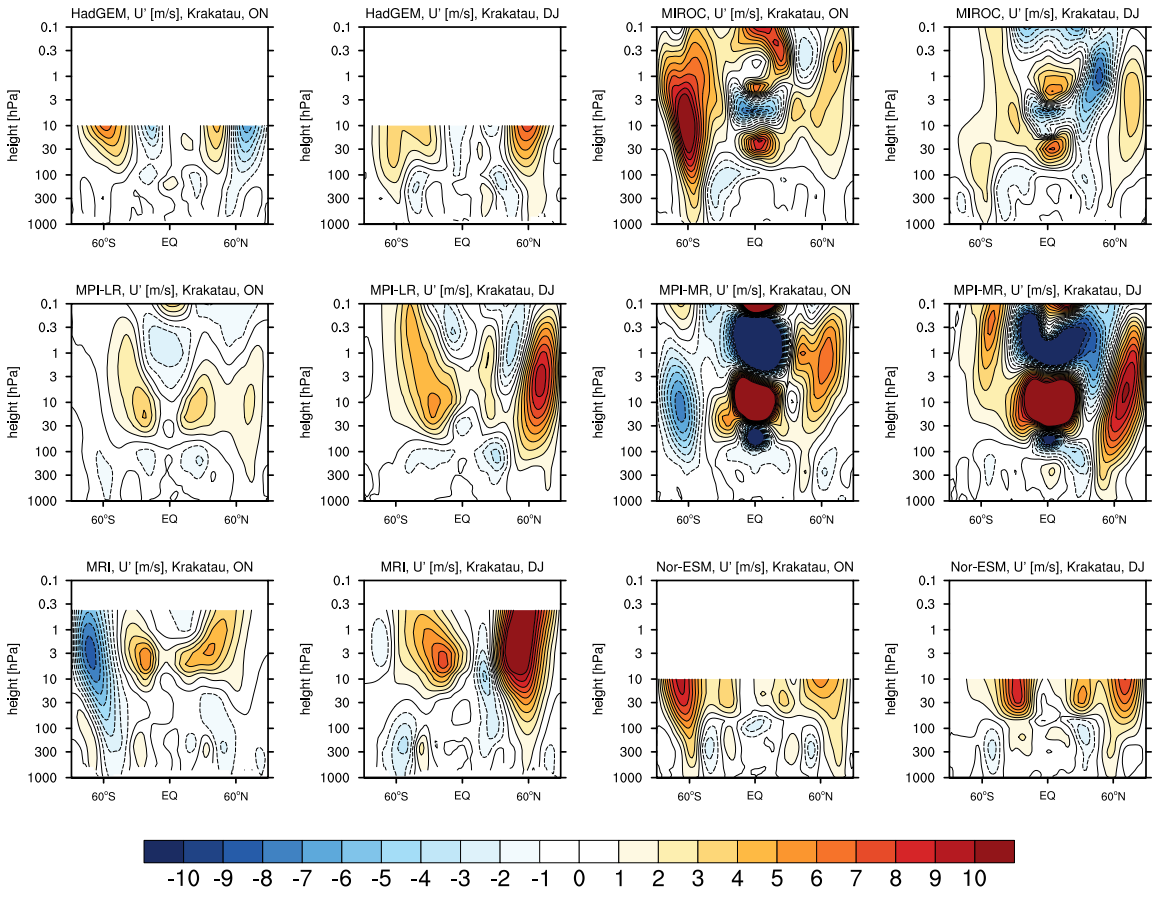

Figure B.1 (Cont.): Ensemble mean of the zonal mean zonal wind anomalies averaged over October-November (ON) and December-January (DJ) for the CMIP5 models given in Table 5.1 after the eruption of Krakatau. Positive anomalies are defined as eastward.

El Chichón

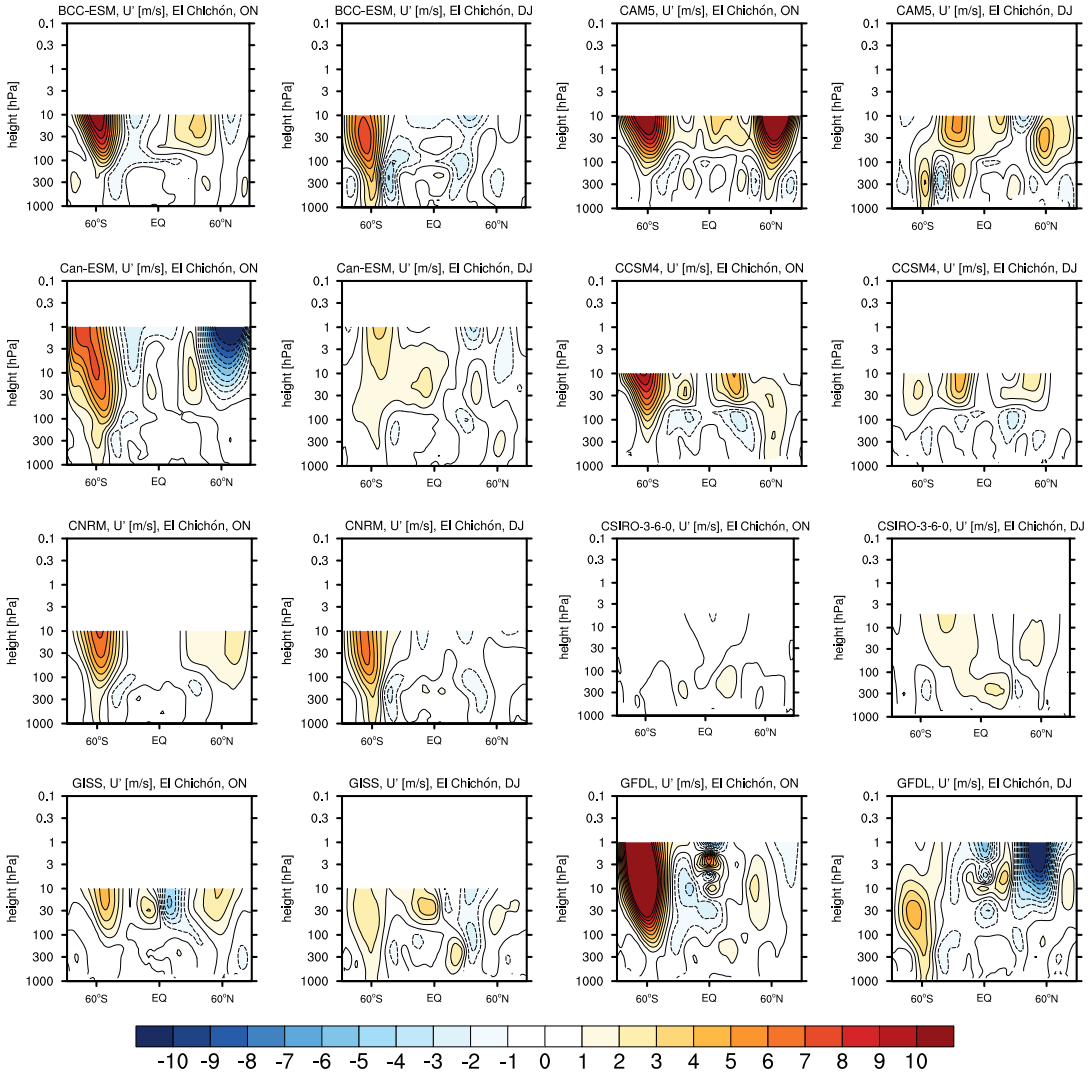

Figure B.2: Ensemble mean of the zonal mean zonal wind anomalies averaged over October-November (ON) and December-January (DJ) for CMIP5 models given in Table 5.1 after the eruption of El Chichón. Positive anomalies are defined as eastward.

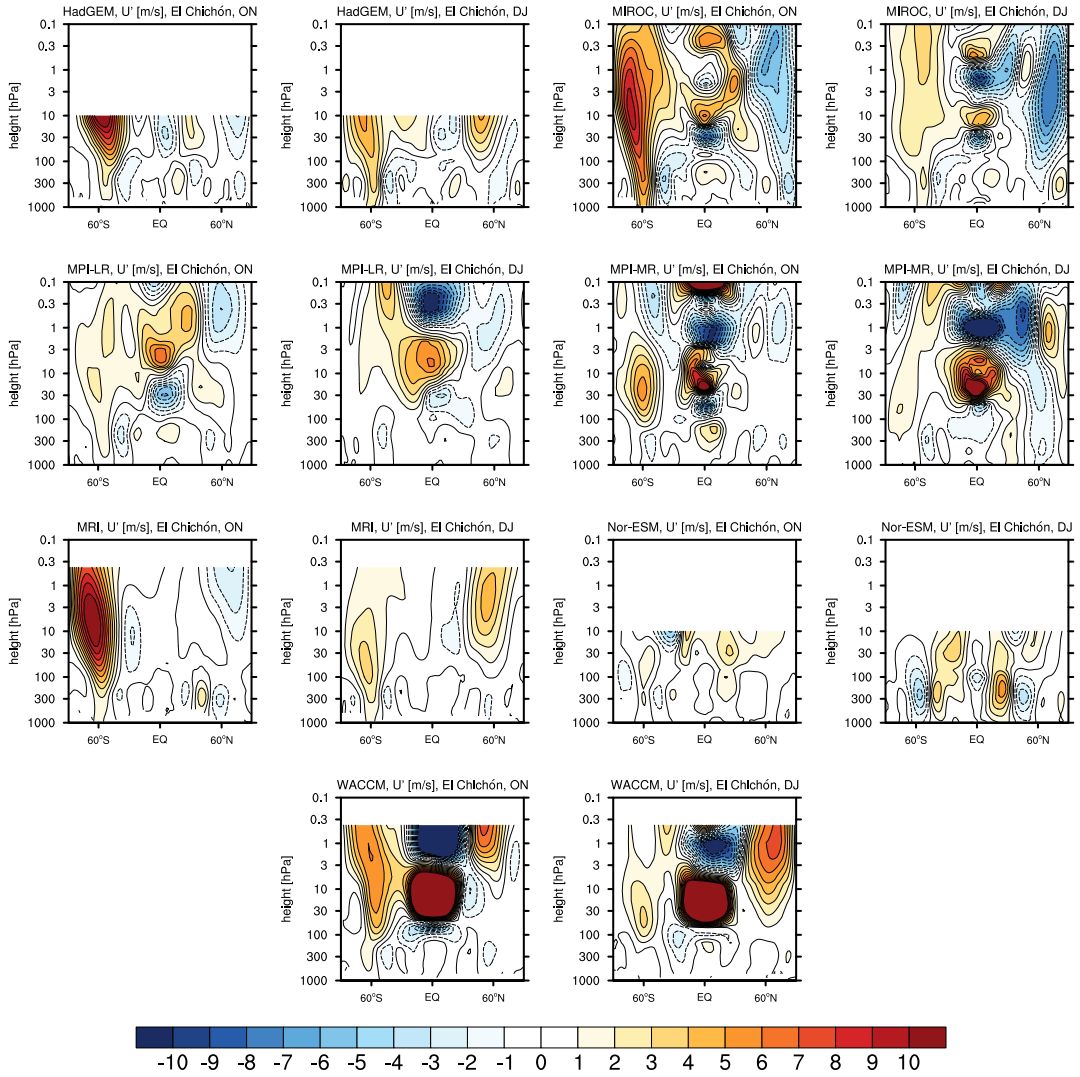

Figure B.2 (Cont.): Ensemble mean of the zonal mean zonal wind anomalies averaged over October-November (ON) and December-January (DJ) for CMIP5 models given in Table 5.1 after the eruption of El Chichón. Positive anomalies are defined as eastward.

Pinatubo

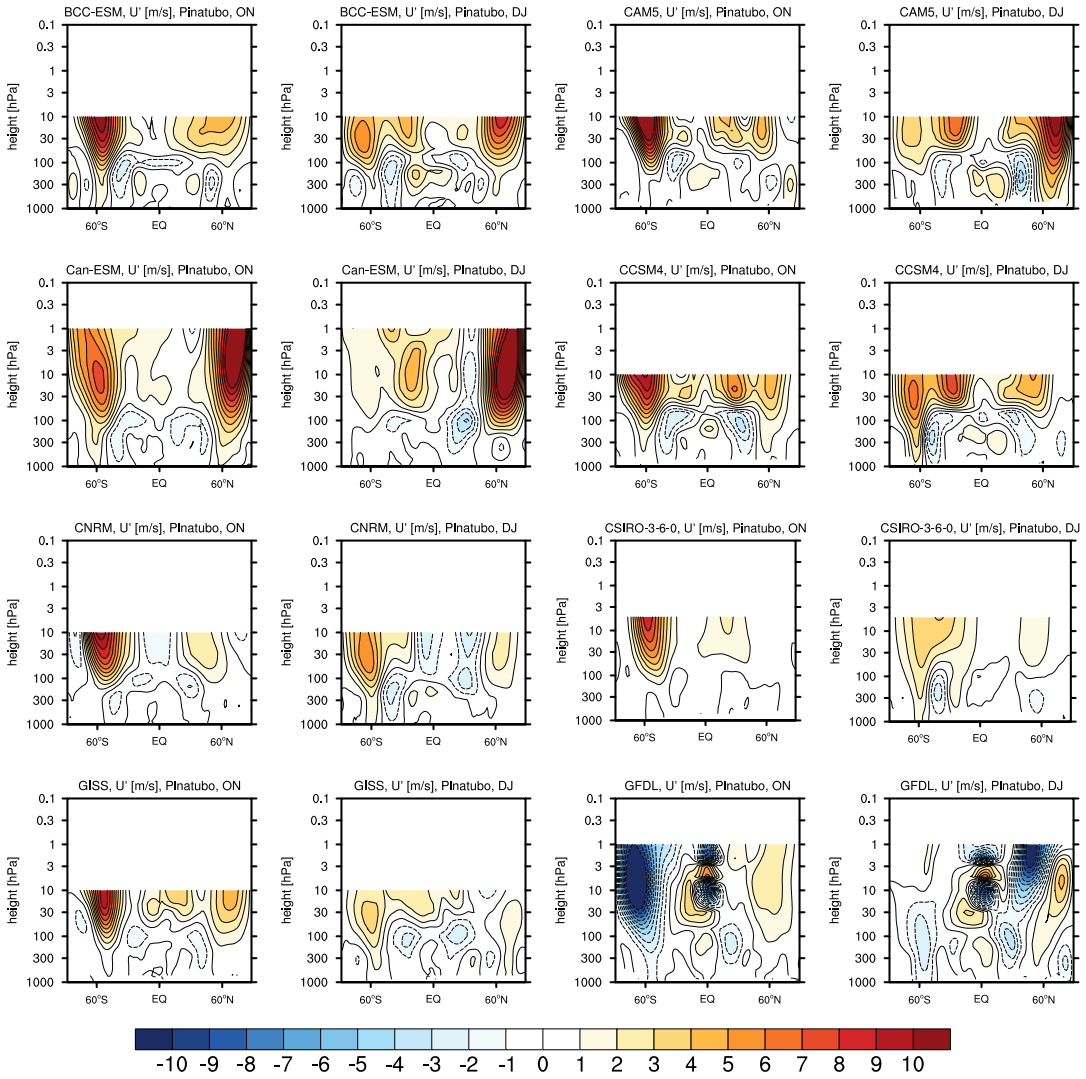

Figure B.3: Ensemble mean of the zonal mean zonal wind anomalies averaged over October-November (ON) and December-January (DJ) for CMIP5 models given in Table 5.1 after the eruption of Pinatubo. Positive anomalies are defined as eastward.

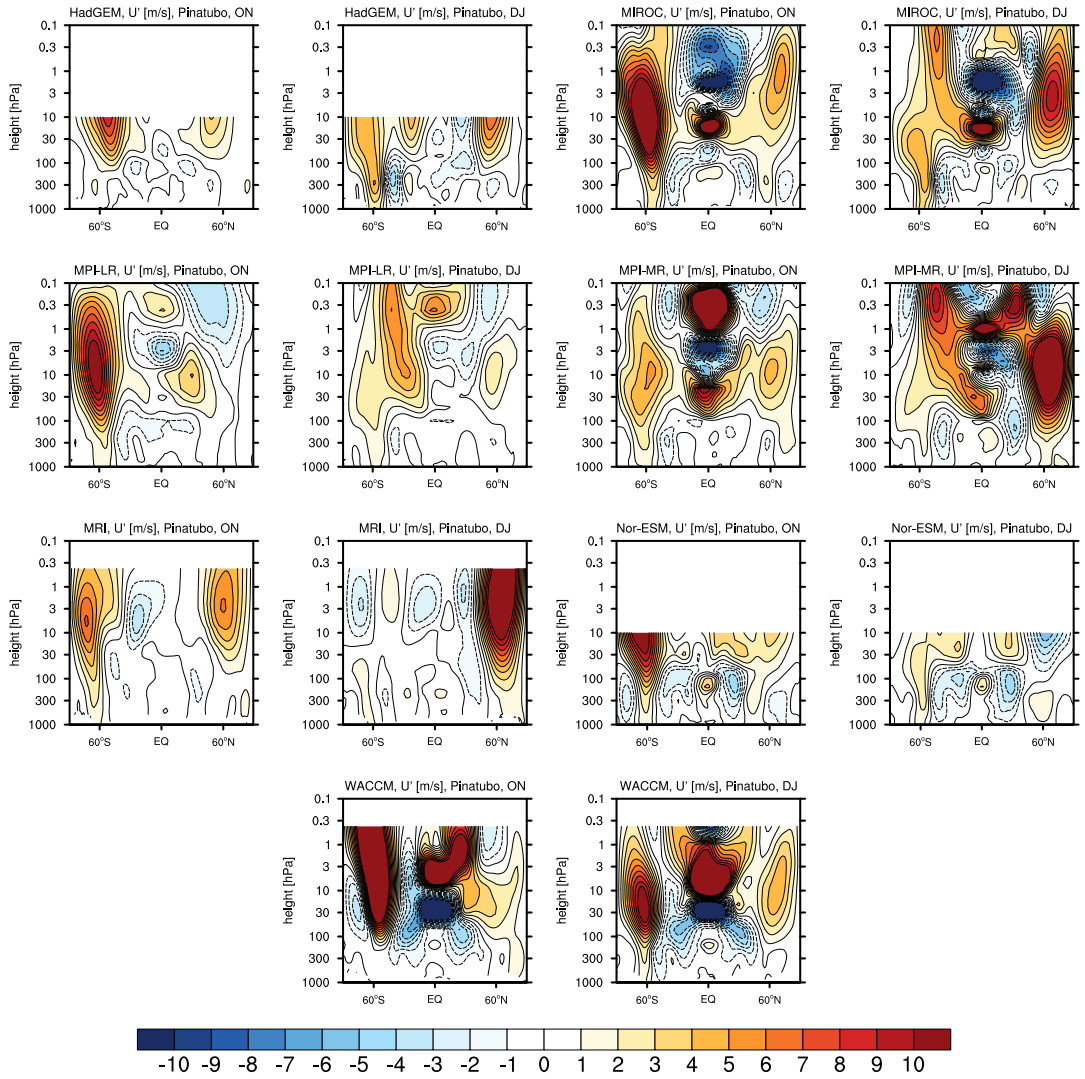

Figure B.3 (Cont.): Ensemble mean of the zonal mean zonal wind anomalies averaged over October-November (ON) and December-January (DJ) for CMIP5 models given in Table 5.1 after the eruption of Pinatubo. Positive anomalies are defined as eastward.

C Correlation of early and mid-winter polar vortex strength in volcanic reference periods

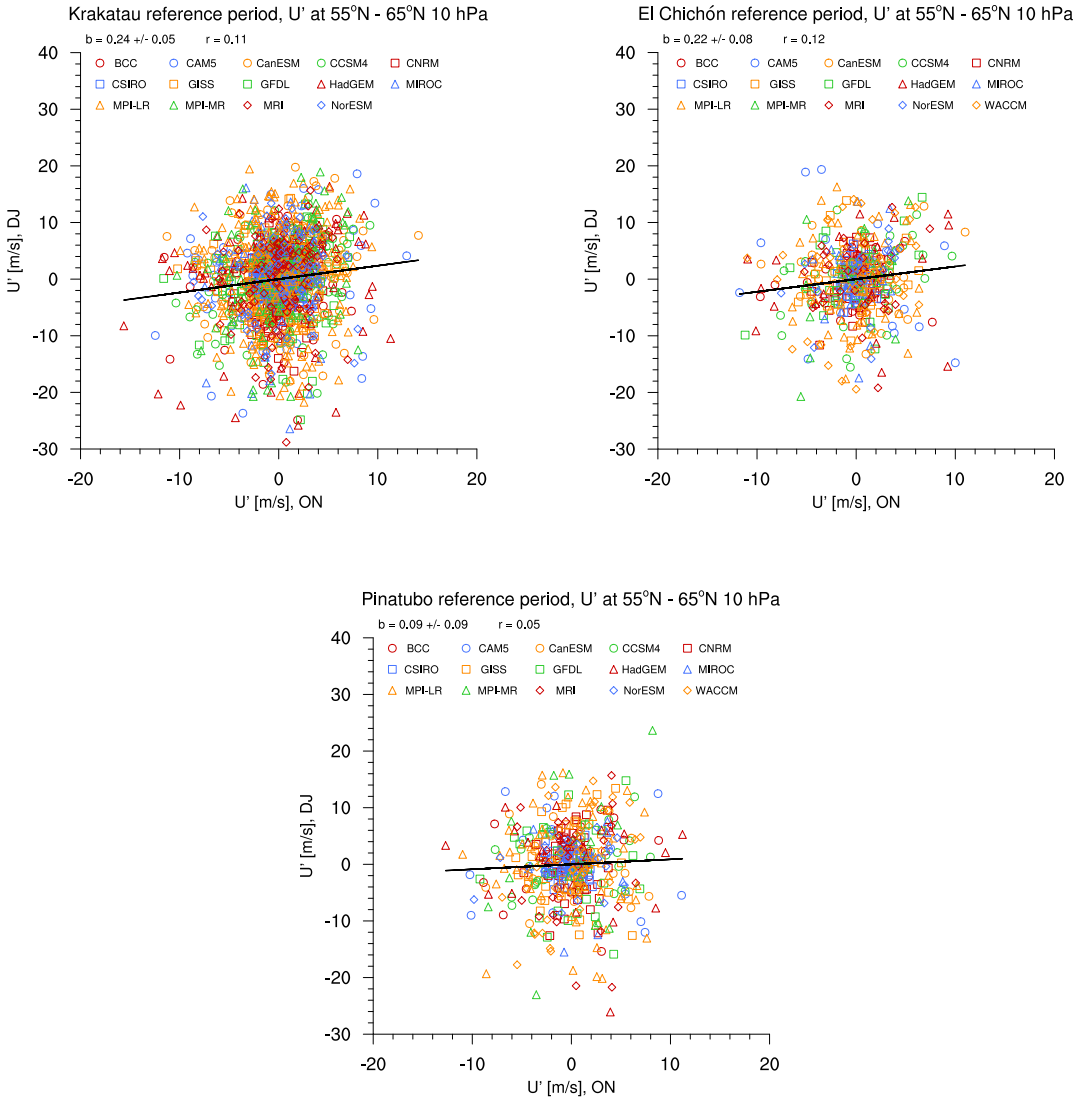

Figure C.1: Correlation of the zonal mean zonal wind anomalies averaged from 55°N to 65°N at 10 *hPa* for the reference periods of the Krakatau eruption (top left), El Chichón eruption (top right) and Pinatubo eruption (bottom) as defined in Table 3.1 in ON (x-axis) with the same quantity in DJ (y-axis). Anomalies are calculated with respect to the climatological mean of each individual reference period and for each individual model, respectively. **b** is the linear regression coefficient including the standard deviation and **r** is the Pearson's correlation coefficient.

D MPI-ESM-LR version 1.1 comparison with ERA-Interim

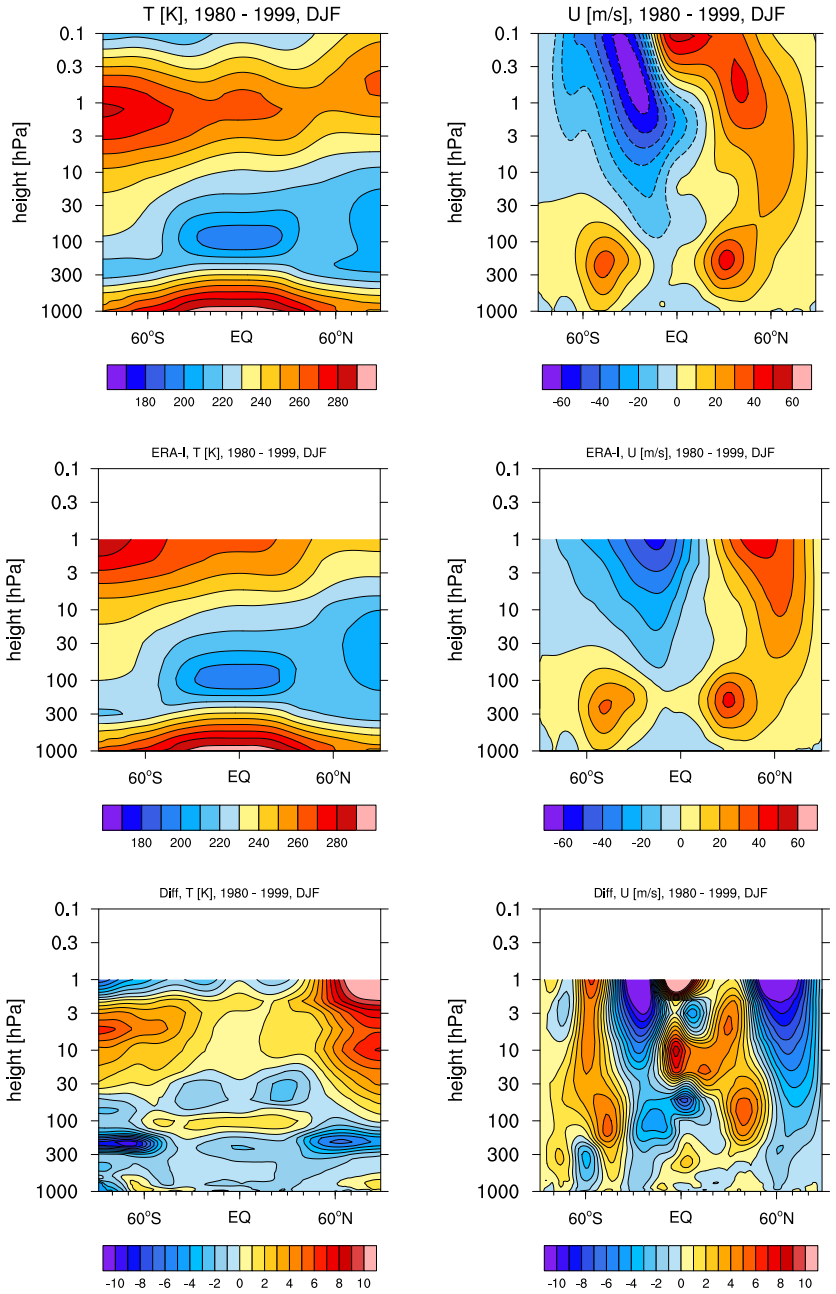

Figure D.1: Zonal mean temperature (left) and zonal wind (right) for the MPI-ESM-LR version 1.1 (top row) and the ERA-Interim reanalysis dataset (middle row) as well as their difference (bottom row) averaged over December-January-February (DJF) in the period from 1980-1999.

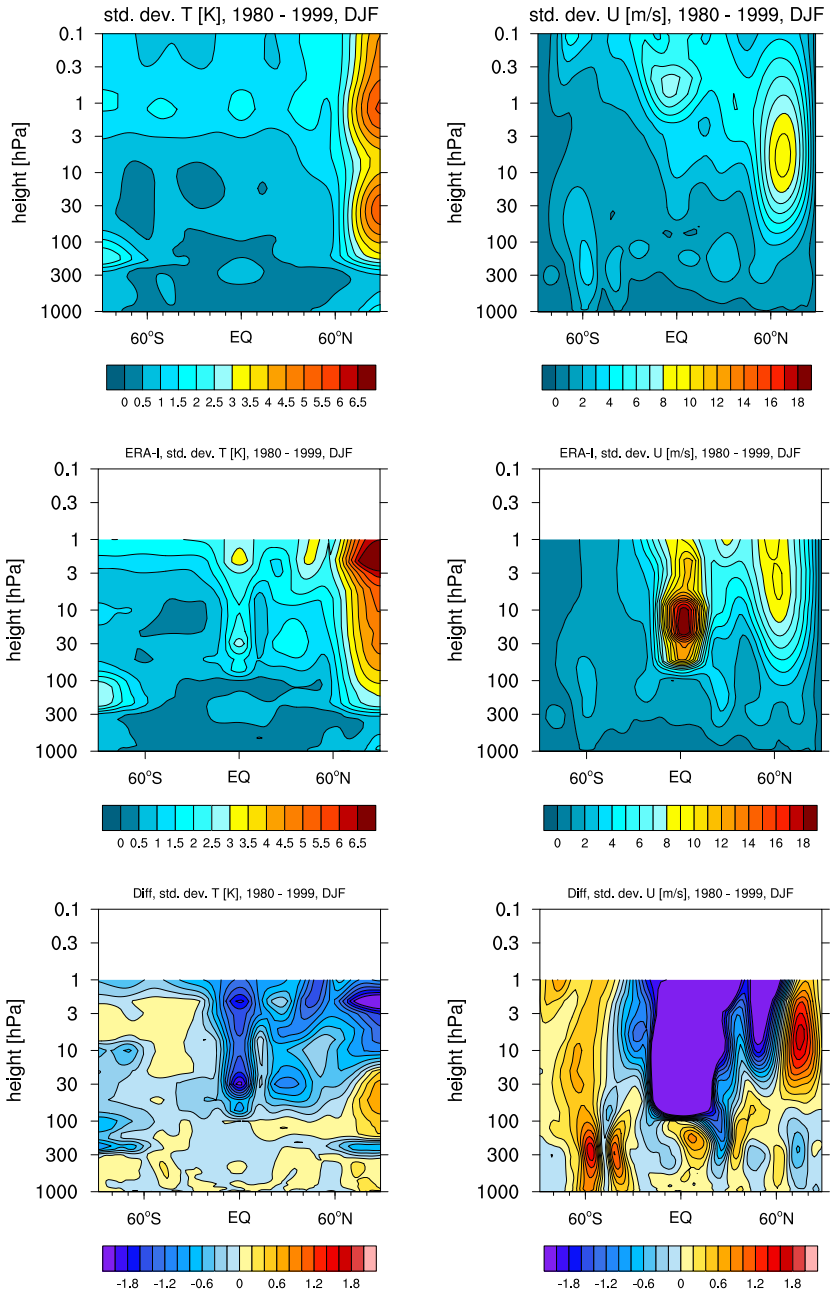

Figure D.2: Standard deviation of the zonal mean temperature (left) and zonal wind (right) for the MPI-ESM-LR version 1.1 (top row) and the ERA-Interim reanalysis dataset (middle row) as well as their difference (bottom row) averaged over December-January-February (DJF) in the period from 1980-1999.

List of Acronyms

AO	Arctic Oscillation
AOD	Aerosol optical depth
BDC	Brewer-Dobson circulation
CFC	Chlorofluorocarbons
Cl	Chlorine
CMIP5	Coupled Model Intercomparison Project, Phase 5
CO_2	Carbon dioxide
CP	Averaged over El Chichón and Pinatubo eruption
DJ	December-January
DJF	December-January-February
ECMWF	European centre for medium-range weather forecasts
ENSO	El Niño Southern Oscillation
EOF	Empirical orthogonal function
EP	Eliassen-Palm
ERA	ECMWF re-analysis
FM	February-March
GCM	Global climate model
HCl	Hydrogen chloride
HF	Hydrogen flouride
H_2O	Water
KP	Averaged over Krakatau and Pinatubo eruption
LIDAR	Light detection and ranging
LR	MPI-ESM-LR, the low resolution version of the MPI-ESM
LW	Longwave
MPI-M	Max Planck Institute for Meteorology
MPI-ESM	Max Planck Institute Earth System Model
MR	MPI-ESM-MR, the mixed resolution version of the MPI-ESM
N_2	Nitrogen
NAM	Northern Annular Mode
NAO	North Atlantic Oscillation
NH	Northern Hemisphere
NIR	Near infra-red
O_3	Ozone
OH	Hydroxide
ON	October-November
PDF	Probability density function
Q^{aer}	Diabatic heating rates due to aerosols
QBO	Quasi-Biennial Oscillation
SAGE	Stratospheric aerosol and gas experiment
SAM	Southern Annular Mode
SH	Southern Hemisphere
SLP	Sea level pressure
SO_2	Sulfur dioxide

SST	Sea surface temperature
SSW	Sudden Stratospheric Warming
SW	Shortwave
TOA	Top of the atmosphere
US	United States of America
UV	Ultraviolet

List of Figures

List of Tables

References

Ammann, C. M. (2003). A monthly and latitudinally varying volcanic forcing dataset in simulations of 20th century climate. *Geophysical Research Letters*, 30.

Ammann, C. M., Joos, F., Schimel, D. S., Otto-Bliesner, B. L., and Tomas, R. A. (2007). Solar influence on climate during the past millennium: results from transient simulations with the NCAR Climate System Model. *Proceedings of the National Academy of Sciences of the United States of America*, 104:3713–3718.

Anchukaitis, K. J., Buckley, B. M., Cook, E. R., Cook, B. I., D'Arrigo, R. D., and Ammann, C. M. (2010). Influence of volcanic eruptions on the climate of the Asian monsoon region. *Geophysical Research Letters*, 37(22).

Andres, R. J. and Kasgnoc, A. D. (1998). A time-averaged inventory of subaerial volcanic sulfur emissions. *Journal of Geophysical Research*, 103:25251.

Angell, J. K. (1997). Stratospheric warming due to Agung, El Chichón, and Pinatubo taking into account the quasi biennial oscillation. *Journal of Geophysical Research: Atmospheres*, 102(D8):9479–9485.

Anstey, J. A. and Shepherd, T. G. (2013). High-latitude influence of the quasi-biennial oscillation. *Quarterly Journal of the Royal Meteorological Society*, 140(678):1–21.

Arfeuille, F., Luo, B. P., Heckendorn, P., Weisenstein, D., Sheng, J. X., Rozanov, E., Schraner, M., Brönnimann, S., Thomason, L. W., and Peter, T. (2013). Modeling the stratospheric warming following the Mt. Pinatubo eruption: uncertainties in aerosol extinctions. *Atmospheric Chemistry and Physics*, 13(22):11221–11234.

Arfeuille, F., Weisenstein, D., MacK, H., Rozanov, E., Peter, T., and Brönnimann, S. (2014). Volcanic forcing for climate modeling: A new microphysics-based data set covering years 1600-present. *Climate of the Past*, 10:359–375.

Auchmann, R., Arfeuille, F., Wegmann, M., Franke, J., Barriendos, M., Prohom, M., Sanchez-Lorenzo, A., Bhend, J., Wild, M., Folini, D., Štěpánek, P., and Brönnimann, S. (2013). Impact of volcanic stratospheric aerosols on diurnal temperature range in Europe over the past 200 years: Observations versus model simulations. *J. Geophys. Res. Atmos.*, 118(16):9064–9077.

Auchmann, R., Brönnimann, S., Breda, L., Bühler, M., Spadin, R., and Stickler, A. (2012). Extreme climate, not extreme weather: The summer of 1816 in Geneva, Switzerland. *Climate of the Past*, 8:325–335.

Ayarzagüena, B., Langematz, U., and Serrano, E. (2011). Tropospheric forcing of the stratosphere: A comparative study of the two different major stratospheric warmings in 2009 and 2010. *J. Geophys. Res.*, 116(D18).

Baldwin, M. P. and Dunkerton, T. J. (1999). Propagation of the Arctic Oscillation from the stratosphere to the troposphere. *Journal of Geophysical Research*, 104(D24):30937.

Baldwin, M. P. and Dunkerton, T. J. (2001). Stratospheric Harbingers of Anomalous Weather Regimes. *Science*, 294(5542):581–584.

Baldwin, M. P., Gray, L. J., Dunkerton, T. J., Hamilton, K., Haynes, P. H., Randel, W. J., Holton, J. R., Alexander, M. J., Hirota, I., Horinouchi, T., Jones, D. B. A., Kinnersley, J. S., Marquardt, C., Sato, M., and Takahashi, M. (2001). The quasi-biennial oscillation. *Rev. Geophys.*, 39(2):179–229.

Baldwin, M. P., Stephenson, D. B., Thompson, D. W. J., Dunkerton, T. J., Charlton, A. J., and O'Neill, A. (2003). Stratospheric memory and skill of extended-range weather forecasts. *Science (New York, N.Y.)*, 301(5633):636–40.

Barnes, J. E. and Hofmann, D. J. (1997). Lidar measurements of stratospheric aerosol over Mauna Loa Observatory. *Geophysical Research Letters*, 24(15):1923–1926.

Bluth, G., Rose, W., Sprod, I., and Krueger, A. (1997). Stratospheric Loading of Sulfur From Explosive Volcanic Eruptions. *The Journal of Geology*, 105:671–684.

Bluth, G. J. S., Doiron, S. D., Schnetzler, C. C., Krueger, A. J., and Walter, L. S. (1992). Global tracking of the SO2 clouds from the June, 1991 Mount Pinatubo eruptions. *Geophys. Res. Lett.*, 19(2):151–154.

Brewer, A. W. (1949). Evidence for a world circulation provided by the measurements of helium and water vapour distribution in the stratosphere. *Quarterly Journal of the Royal Meteorological Society*, 75(326):351–363.

Brönnimann, S. (2007). Impact of El Niño-Southern Oscillation on European climate. *Rev. Geophys.*, 45(3).

Bunzel, F. and Schmidt, H. (2012). The Brewer-Dobson Circulation in a Changing Climate: Impact of the Model Configuration. *J. Atmos. Sci.*, 70(5):1437–1455.

Bunzel, F., Stevens, B., and Schmidt, H. (2013). Numerical studies of stratosphere-troposphere dynamical coupling in a changing climate. *Berichte zur Erdystemforschung*, 137.

Butler, A. H. and Polvani, L. M. (2011). El Niño, La Niña, and stratospheric sudden warmings: A reevaluation in light of the observational record. *Geophys. Res. Lett.*, 38(13).

Cagnazzo, C. and Manzini, E. (2009). Impact of the Stratosphere on the Winter Tropospheric Teleconnections between ENSO and the North Atlantic and European Region. *J. Climate*, 22(5):1223–1238.

Calvo, N., Giorgetta, M. A., Garcia-Herrera, R., and Manzini, E. (2009). Nonlinearity of the combined warm ENSO and QBO effects on the Northern Hemisphere polar vortex in MAECHAM5 simulations. *J. Geophys. Res.*, 114(D13):D13109.

Camp, C. D. and Tung, K.-K. (2007). The Influence of the Solar Cycle and QBO on the Late-Winter Stratospheric Polar Vortex. *J. Atmos. Sci.*, 64(4):1267–1283.

Cattiaux, J. and Cassou, C. (2013). Opposite CMIP3/CMIP5 trends in the wintertime Northern Annular Mode explained by combined local sea ice and remote tropical influences. *Geophysical Research Letters*, 40(14):3682–3687.

Charlton, A. J. and Polvani, L. M. (2007). A New Look at Stratospheric Sudden Warmings. Part I: Climatology and Modeling Benchmarks. *Journal of Climate*, 20(3):449–469.

Charlton-Perez, A. J., Baldwin, M. P., Birner, T., Black, R. X., Butler, A. H., Calvo, N., Davis, N. A., Gerber, E. P., Gillett, N., Hardiman, S., Kim, J., Krüger, K., Lee, Y.-Y., Manzini, E., McDaniel, B. A., Polvani, L., Reichler, T., Shaw, T. A., Sigmond, M., Son, S.-W., Toohey, M., Wilcox, L., Yoden, S., Christiansen, B., Lott, F., Shindell, D., Yukimoto, S., and Watanabe, S. (2013). On the lack of stratospheric dynamical variability in low-top versions of the CMIP5 models. *Journal of Geophysical Research: Atmospheres*, 118:2494–2505.

Charney, J. G. and Drazin, P. G. (1961). Propagation of planetary-scale disturbances from the lower into the upper atmosphere. *Journal of Geophysical Research*, 66(1):83.

Christiansen, B. (2008). Volcanic Eruptions, Large-Scale Modes in the Northern Hemisphere, and the El Niño-Southern Oscillation. *J. Climate*, 21(5):910–922.

Church, J. A., White, N. J., and Arblaster, J. M. (2005). Significant decadal-scale impact of volcanic eruptions on sea level and ocean heat content. *Nature*, 438(7064):74–77.

Cionni, I., Eyring, V., Lamarque, J. F., Randel, W. J., Stevenson, D. S., Wu, F., Bodeker, G. E., Shepherd, T. G., Shindell, D. T., and Waugh, D. W. (2011). Ozone database in support of CMIP5 simulations: results and corresponding radiative forcing. *Atmospheric Chemistry and Physics*, 11(21):11267–11292.

Cole-Dai, J. (2010). Volcanoes and climate. *Wiley Interdisciplinary Reviews: Climate Change*, 1(6):824–839.

Collins, M. (2004). Predictions of Climate Following Volcanic Eruptions. In *Volcanism and the Earth's Atmosphere*, pages 283–300. American Geophysical Union.

Crooks, S. A. and Gray, L. J. (2005). Characterization of the 11-Year Solar Signal Using a Multiple Regression Analysis of the ERA-40 Dataset. *J. Climate*, 18(7):996–1015.

Crowley, T. J. and Unterman, M. B. (2012). Technical details concerning development of a 1200-yr proxy index for global volcanism. *Earth System Science Data Discussions*, 5:1–28.

Crowley, T. J., Zielinski, G., Vinther, B., Udisti, R., Kreutz, K., Cole-Dai, J., and Castellano, E. (2008). Volcanism and the little ice age. *PAGES news*, 16(2):22–23.

Dee, D. P., Uppala, S. M., Simmons, A. J., Berrisford, P., Poli, P., Kobayashi, S., Andrae, U., Balmaseda, M. A., Balsamo, G., Bauer, P., Bechtold, P., Beljaars, A. C. M., van de Berg, L., Bidlot, J., Bormann, N., Delsol, C., Dragani, R., Fuentes, M., Geer, A. J., Haimberger, L., Healy, S. B., Hersbach, H., Hólm, E. V., Isaksen, L., Kallberg, P., Köhler, M., Matricardi, M., Mcnally, A. P., Monge-Sanz, B. M., Morcrette, J. J., Park, B. K., Peubey, C., de Rosnay, P., Tavolato, C., Thépaut, J. N., and Vitart, F. (2011). The ERA-Interim reanalysis: Configuration and performance of the data assimilation system. *Quarterly Journal of the Royal Meteorological Society*, 137(656):553–597.

Deser, C., Phillips, A., Bourdette, V., and Teng, H. (2010). Uncertainty in climate change projections: the role of internal variability. *Climate Dynamics*, 38(3-4):527–546.

Ding, Y., Carton, J. A., Chepurin, G. A., Stenchikov, G., Robock, A., Sentman, L. T., and Krasting, J. P. (2014). Ocean response to volcanic eruptions in Coupled Model Intercomparison Project 5 simulations. *Journal of Geophysical Research: Oceans*, 119(9):5622–5637.

Dobson, G. M. B. (1956). Origin and distribution of the polyatomic molecules in the atmosphere. *Proceedings of the Royal Society of London. Series A, Mathematical and Physical Sciences*, pages 187–193.

Driscoll, S., Bozzo, A., Gray, L. J., Robock, A., and Stenchikov, G. (2012). Coupled model intercomparison project 5 (cmip5) simulations of climate following volcanic eruptions. *J. Geophys. Res.*, 117(D17105).

Farman, J. C., Gardiner, B. G., and Shanklin, J. D. (1985). Large losses of total ozone in Antarctica reveal seasonal ClOx/NOx interaction. *Nature*, 315(6016):207–210.

Feldstein, S. B. (2000). The Timescale, Power Spectra, and Climate Noise Properties of Teleconnection Patterns. *Journal of Climate*, 13(24):4430–4440.

Fischer, E. M., Luterbacher, J., Zorita, E., Tett, S. F. B., Casty, C., and Wanner, H. (2007). European climate response to tropical volcanic eruptions over the last half millennium. *Geophys. Res. Lett.*, 34(5):L05707.

Forsyth, P. Y. (1988). In the wake of Etna, 44 BC. *Classical Antiquity*, pages 49–57.

Franklin, B. (1784). Meteorological imaginations and conjectures. *Manchester Literary and Philosophical Society Memoirs and Proceedings*, 2(122).

Gao, C., Robock, A., and Ammann, C. (2008). Volcanic forcing of climate over the past 1500 years: An improved ice core-based index for climate models. *Journal of Geophysical Research D: Atmospheres*, 113.

García-Herrera, R., Calvo, N., Garcia, R. R., and Giorgetta, M. A. (2006). Propagation of ENSO temperature signals into the middle atmosphere: A comparison of two general circulation models and ERA-40 reanalysis data. *J. Geophys. Res.*, 111(D6):D06101—-.

Garfinkel, C. I., Butler, A. H., Waugh, D. W., Hurwitz, M. M., and Polvani, L. M. (2012). Why might stratospheric sudden warmings occur with similar frequency in El Niño and La Niña winters? *J. Geophys. Res.*, 117(D19).

Gerber, E. P., Butler, A., Calvo, N., Charlton-Perez, A., Giorgetta, M., Manzini, E., Perlwitz, J., Polvani, L. M., Sassi, F., Scaife, A. A., Shaw, T. A., Son, S.-W., and Watanabe, S. (2012). Assessing and Understanding the Impact of Stratospheric Dynamics and Variability on the Earth System. *Bull. Amer. Meteor. Soc.*, 93(6):845–859.

Gerber, E. P. and Polvani, L. M. (2009). Stratosphere-Troposphere Coupling in a Relatively Simple AGCM: The Importance of Stratospheric Variability. *J. Climate*, 22(8):1920–1933.

Gerlach, T. (2011). Volcanic versus anthropogenic carbon dioxide. *Eos*, 92:201–202.

Gillett, N. P. (2004). Detection of volcanic influence on global precipitation. *Geophysical Research Letters*, 31(12):L12217.

Giorgetta, M. A., Jungclaus, J., Reick, C. H., Legutke, S., Bader, J., Böttinger, M., Brovkin, V., Crueger, T., Esch, M., Fieg, K., Glushak, K., Gayler, V., Haak, H., Hollweg, H.-D., Ilyina, T., Kinne, S., Kornblueh, L., Matei, D., Mauritsen, T., Mikolajewicz, U., Mueller, W., Notz, D., Pithan, F., Raddatz, T., Rast, S., Redler, R., Roeckner, E., Schmidt, H., Schnur, R., Segschneider, J., Six, K. D., Stockhause, M., Timmreck, C., Wegner, J., Widmann, H., Wieners, K.-H., Claussen, M., Marotzke, J., and Stevens, B. (2013). Climate and carbon cycle changes from 1850 to 2100 in MPI-ESM simulations for the coupled model intercomparison project phase 5. *J. Adv. Model. Earth Syst.*, 5:572–597.

Gleckler, P. J., AchutaRao, K., Gregory, J. M., Santer, B. D., Taylor, K. E., and Wigley, T. M. L. (2006). Krakatoa lives: The effect of volcanic eruptions on ocean heat content and thermal expansion. *Geophysical Research Letters*, 33.

Graf, H.-F., Kirchner, I., Robock, A., and Schult, I. (1993). Pinatubo eruption winter climate effects: model versus observations. *Climate Dynamics*, 9(2):81–93.

Graf, H.-F., Li, Q., and Giorgetta, M. A. (2007). Volcanic effects on climate: revisiting the mechanisms. *Atmospheric Chemistry and Physics*, 7(17):4503–4511.

Graf, H.-F., Zanchettin, D., Timmreck, C., and Bittner, M. (2014). Observational constraints on the tropospheric and near-surface winter signature of the Northern Hemisphere stratospheric polar vortex. *Climate Dynamics*, 43(12):3245–3266.

Gray, L. J., Beer, J., Geller, M., Haigh, J. D., Lockwood, M., Matthes, K., Cubasch, U., Fleitmann, D., Harrison, G., Hood, L., Luterbacher, J., Meehl, G. A., Shindell, D., van Geel, B., and White, W. (2010). Solar Influence on Climate. *Reviews of Geophysics*, 48(4):RG4001.

Gregory, J. M. (2010). Long-term effect of volcanic forcing on ocean heat content. *Geophysical Research Letters*, 37.

Guo, S., Bluth, G. J. S., Rose, W. I., Watson, I. M., and Prata, A. J. (2004). Re-evaluation of SO2 release of the 15 June 1991 Pinatubo eruption using ultraviolet and infrared satellite sensors. *Geochemistry, Geophysics, Geosystems*, 5.

Haigh, J. D. (1996). The Impact of Solar Variability on Climate. *Science*, 272(5264):981–984.

Hawkins, E. and Sutton, R. (2009). The Potential to Narrow Uncertainty in Regional Climate Predictions. *Bulletin of the American Meteorological Society*, 90(8):1095–1107.

Hofmann, D. J., Oltmans, S. J., Komhyr, W. D., Harris, J. M., Lathrop, J. A., Langford, A. O., Deshler, T., Johnson, B. J., Torres, A., and Matthews, W. A. (1994). Ozone loss in the lower stratosphere over the United States in 1992–1993: Evidence for heterogeneous chemistry on the Pinatubo aerosol. *Geophysical Research Letters*, 21(1):65–68.

Holton, J. R. and Lindzen, R. S. (1972). An Updated Theory for the Quasi-Biennial Cycle of the Tropical Stratosphere. *Journal of the Atmospheric Sciences*, 29(6):1076–1080.

Holton, J. R. and Mass, C. (1976). Stratospheric Vacillation Cycles. *Journal of the Atmospheric Sciences*, 33(11):2218–2225.

Holton, J. R. and Tan, H.-C. (1980). The Influence of the Equatorial Quasi-Biennial Oscillation on the Global Circulation at 50 mb. *J. Atmos. Sci.*, 37(10):2200–2208.

Hurrell, J. W. (1995). Decadal trends in the north atlantic oscillation: regional temperatures and precipitation. *Science (New York, N.Y.)*, 269(5224):676–9.

Ilyina, T., Six, K. D., Segschneider, J., Maier-Reimer, E., Li, H., and Núñez Riboni, I. (2013). Global ocean biogeochemistry model HAMOCC: Model architecture and performance as component of the MPI-Earth system model in different CMIP5 experimental realizations. *J. Adv. Model. Earth Syst.*, 5(2):287–315.

Joseph, R. and Zeng, N. (2011). Seasonally Modulated Tropical Drought Induced by Volcanic Aerosol. *Journal of Climate*, 24(8):2045–2060.

Jungclaus, J. H., Fischer, N., Haak, H., Lohmann, K., Marotzke, J., Matei, D., Mikolajewicz, U., Notz, D., and von Storch, J. S. (2013). Characteristics of the ocean simulations in the Max Planck Institute Ocean Model (MPIOM) the ocean component of the MPI-Earth system model. *J. Adv. Model. Earth Syst.*, 5(2):422–446.

Karpechko, A. Y., Gillett, N. P., Dall'Amico, M., and Gray, L. J. (2010). Southern Hemisphere atmospheric circulation response to the El Chichón and Pinatubo eruptions in coupled climate models. *Quarterly Journal of the Royal Meteorological Society*, 136(652):1813–1822.

Karpechko, A. Y. and Manzini, E. (2012). Stratospheric influence on tropospheric climate change in the Northern Hemisphere. *Journal of Geophysical Research: Atmospheres*, 117.

Kirchner, I., Stenchikov, G. L., Graf, H.-F., Robock, A., and Antuña, J. C. (1999). Climate model simulation of winter warming and summer cooling following the 1991 Mount Pinatubo volcanic eruption. *J. Geophys. Res.*, 104(D16):19039–19055.

Kodera, K. (1994). Influence of volcanic eruptions on the troposphere through stratospheric dynamical processes in the northern hemisphere winter. *J. Geophys. Res.*, 99(D1):1273–1282.

Kodera, K. (1995). On the origin and nature of the interannual variability of the winter stratospheric circulation in the northern hemisphere. *J. Geophys. Res.*, 100(D7):14077–14087.

Kodera, K. and Kuroda, Y. (2000). Tropospheric and stratospheric aspects of the Arctic Oscillation. *Geophysical Research Letters*, 27:3349–3352.

Kodera, K. and Kuroda, Y. (2002). Dynamical response to the solar cycle. *J. Geophys. Res.*, 107(D24):4749.

Krismer, T. R., Giorgetta, M. A., and Esch, M. (2013). Seasonal aspects of the quasi-biennial oscillation in the Max Planck Institute Earth System Model and ERA-40. *J. Adv. Model. Earth Syst.*, 5(2):406–421.

Labitzke, K. (1972). Temperature Changes in the Mesosphere and Stratosphere Connected with Circulation Changes in Winter. *Journal of the Atmospheric Sciences*, 29(4):756–766.

Labitzke, K. and Loon, H. V. (1988). Associations between the 11-year solar cycle, the QBO and the atmosphere. Part I: the troposphere and stratosphere in the northern hemisphere in winter. *Journal of Atmospheric and Terrestrial Physics*, 50(3):197–206.

Labitzke, K. and McCormick, M. P. (1992). Stratospheric temperature increases due to Pinatubo aerosols. *Geophys. Res. Lett.*, 19(2):207–210.

Labitzke, K. G. and Loon, H. (1999). *The Stratosphere*. Springer Science & Business Media.

Lindzen, R. S. and Holton, J. R. (1968). A Theory of the Quasi-Biennial Oscillation. *Journal of the Atmospheric Sciences*, 25(6):1095–1107.

Madden, R. A. (1976). Estimates of the Natural Variability of Time-Averaged Sea-Level Pressure. *Monthly Weather Review*, 104(7):942–952.

Manney, G. L., Krüger, K., Sabutis, J. L., Sena, S. A., and Pawson, S. (2005). The remarkable 2003-2004 winter and other recent warm winters in the Arctic stratosphere since the late 1990s. *Journal of Geophysical Research: Atmospheres*, 110(D4):D04107.

Manzini, E., Giorgetta, M. A., Esch, M., Kornblueh, L., and Roeckner, E. (2006). The Influence of Sea Surface Temperatures on the Northern Winter Stratosphere: Ensemble Simulations with the MAECHAM5 Model. *J. Climate*, 19(16):3863–3881.

Manzini, E., Karpechko, A. Y., Anstey, J., Baldwin, M. P., Black, R. X., Cagnazzo, C., Calvo, N., Charlton-Perez, A., Christiansen, B., Davini, P., Gerber, E., Giorgetta, M., Gray, L., Hardiman, S. C., Lee, Y.-Y., Marsh, D. R., McDaniel, B. A., Purich, A., Scaife, A. A., Shindell, D., Son, S.-W., Watanabe, S., and Zappa, G. (2014). Northern winter climate change: Assessment of uncertainty in CMIP5 projections related to stratosphere-troposphere coupling. *Journal of Geophysical Research: Atmospheres*, 119(13):2013JD021403.

Marsh, D. R., Mills, M. J., Kinnison, D. E., Lamarque, J.-F., Calvo, N., and Polvani, L. M. (2013). Climate Change from 1850 to 2005 Simulated in CESM1(WACCM). *Journal of Climate*, 26(19):7372–7391.

Marshall, A. G. and Scaife, A. A. (2009). Impact of the QBO on surface winter climate. *Journal of Geophysical Research: Atmospheres*, 114.

Marshall, A. G., Scaife, A. A., and Ineson, S. (2009). Enhanced Seasonal Prediction of European Winter Warming following Volcanic Eruptions. *Journal of Climate*, 22(23):6168–6180.

Matsuno, T. (1971). A Dynamical Model of the Stratospheric Sudden Warming. *Journal of the Atmospheric Sciences*, 28(8):1479–1494.

Matthes, K., Kuroda, Y., Kodera, K., and Langematz, U. (2006). Transfer of the solar signal from the stratosphere to the troposphere: Northern winter. *J. Geophys. Res.*, 111(D6):D06108.

McCormick, M. P. and Veiga, R. E. (1992). SAGE II measurements of early Pinatubo aerosols. *Geophysical Research Letters*, 19(2):155–158.

Metzner, D., Kutterolf, S., Toohey, M., Timmreck, C., Niemeier, U., Freundt, A., and Krüger, K. (2012). Radiative forcing and climate impact resulting from SO2 injections based on a 200,000-year record of Plinian eruptions along the Central American Volcanic Arc.

Miller, G. H., Geirsdóttir, A., Zhong, Y., Larsen, D. J., Otto-Bliesner, B. L., Holland, M. M., Bailey, D. A., Refsnider, K. A., Lehman, S. J., Southon, J. R., and Others (2012). Abrupt onset of the Little Ice Age triggered by volcanism and sustained by sea-ice/ocean feedbacks. *Geophysical Research Letters*, 39(2).

Mizuta, R., Yoshimura, H., Murakami, H., Matsueda, M., Endo, H., Ose, T., Kamiguchi, K., Hosaka, M., Sugi, M., Yukimoto, S., Kosonoki, S., and Kitoh, A. (2012). Climate Simulations Using MRI-AGCM3.2 with 20-km Grid. *Journal of the Meteorological Society of Japan*, 90A:233–258.

Mlynczak, M. G., Mertens, C. J., Garcia, R. R., and Portmann, R. W. (1999). A detailed evaluation of the stratospheric heat budget: 2. Global radiation balance and diabatic circulations. *Journal of Geophysical Research*, 104(D6):6039.

Muthers, S., Anet, J. G., Raible, C. C., Brönnimann, S., Rozanov, E., Arfeuille, F., Peter, T., Shapiro, A. I., Beer, J., Steinhilber, F., Brugnara, Y., and Schmutz, W. (2014). Northern hemispheric winter warming pattern after tropical volcanic eruptions: Sensitivity to the ozone climatology. *J. Geophys. Res. Atmos.*, page 2013JD020138.

Newman, P. A., Nash, E. R., Kawa, S. R., Montzka, S. A., and Schauffler, S. M. (2006). When will the Antarctic ozone hole recover? *Geophysical Research Letters*, 33(12):L12814.

Newman, P. A., Nash, E. R., and Rosenfield, J. E. (2001). What controls the temperature of the Arctic stratosphere during the spring? *J. Geophys. Res.*, 106(D17):19999–20010.

Niemeier, U., Timmreck, C., Graf, H.-F., Kinne, S., Rast, S., and Self, S. (2009). Initial fate of fine ash and sulfur from large volcanic eruptions. *Atmospheric Chemistry and Physics*, 9(22):9043–9057.

Oman, L., Robock, A., Stenchikov, G. L., and Thordarson, T. (2006). High-latitude eruptions cast shadow over the African monsoon and the flow of the Nile. *Geophysical Research Letters*, 33(18):L18711.

Oppenheimer, C. (2003). Climatic, environmental and human consequences of the largest known historic eruption: Tambora volcano (Indonesia) 1815. *Progress in Physical Geography*, 27:230–259.

Otterå, O. H. (2008). Simulating the effects of the 1991 Mount Pinatubo volcanic eruption using the ARPEGE atmosphere general circulation model. *Advances in Atmospheric Sciences*, 25(2):213–226.

Perlwitz, J. and Graf, H.-F. (1995). The Statistical Connection between Tropospheric and Stratospheric Circulation of the Northern Hemisphere in Winter. *Journal of Climate*, 8(10):2281–2295.

Polvani, L. M. and Kushner, P. J. (2002). Tropospheric response to stratospheric perturbations in a relatively simple general circulation model. *Geophys. Res. Lett.*, 29(7):14–18.

Polvani, L. M. and Waugh, D. W. (2004). Upward Wave Activity Flux as a Precursor to Extreme Stratospheric Events and Subsequent Anomalous Surface Weather Regimes. *J. Climate*, 17(18):3548–3554.

Quiroz, R. S. (1983). The isolation of stratospheric temperature change due to the El Chichón volcanic eruption from nonvolcanic signals. *Journal of Geophysical Research*, 88(C11):6773.

Ramachandran, S., Ramaswamy, V., Stenchikov, G. L., and Robock, A. (2000). Radiative impact of the Mount Pinatubo volcanic eruption: Lower stratospheric response. *J. Geophys. Res.*, 105(D19):24409–24429.

Rampino, M. R. and Self, S. (1982). Historic eruptions of Tambora (1815), Krakatau (1883), and Agung (1963), their stratospheric aerosols, and climatic impact. *Quaternary Research*, 18:127–143.

Reichler, T., Kim, J., Manzini, E., and Kröger, J. (2012). A stratospheric connection to Atlantic climate variability. *Nature Geoscience*, 5(11):783–787.

Reichler, T., Kushner, P. J., and Polvani, L. M. (2005). The Coupled StratosphereTroposphere Response to Impulsive Forcing from the Troposphere. *Journal of the Atmospheric Sciences*, 62(9):3337–3352.

Reick, C. H., Raddatz, T., Brovkin, V., and Gayler, V. (2013). Representation of natural and anthropogenic land cover change in MPI-ESM. *J. Adv. Model. Earth Syst.*, 5(3):459–482.

Rind, D., Balachandran, N. K., and Suozzo, R. (1992). Climate Change and the Middle Atmosphere. Part II: The Impact of Volcanic Aerosols. *Journal of Climate*, 5:189–208.

Robock, A. (2000). Volcanic eruptions and climate. *Rev. Geophys.*, 38(2):191–219.

Robock, A. (2005). Cooling following large volcanic eruptions corrected for the effect of diffuse radiation on tree rings. *Geophys. Res. Lett.*, 32(6):L06702.

Robock, A., Adams, T., Moore, M., Oman, L., and Stenchikov, G. (2007). Southern Hemisphere atmospheric circulation effects of the 1991 Mount Pinatubo eruption. *Geophysical Research Letters*, 34(23):n/a–n/a.

Robock, A. and Mao, J. (1992). Winter warming from large volcanic eruptions. *Geophys. Res. Lett.*, 19(24):2405–2408.

Robock, A. and Mao, J. (1995). The Volcanic Signal in Surface Temperature Observations. *J. Climate*, 8(5):1086–1103.

Robock, A. and Mass, C. (1982). The mount st. Helens volcanic eruption of 18 may 1980: large short-term surface temperature effects. *Science (New York, N.Y.)*, 216:628–630.

Russell, P. B., Livingston, J. M., Pueschel, R. F., Bauman, J. J., Pollack, J. B., Brooks, S. L., Hamill, P., Thomason, L. W., Stowe, L. L., Deshler, T., Dutton, E. G., and Bergstrom, R. W. (1996). Global to microscale evolution of the Pinatubo volcanic aerosol derived from diverse measurements and analyses. *Journal of Geophysical Research: Atmospheres*, 101(D13):18745–18763.

Sassi, F., Kinnison, D., Boville, B. A., Garcia, R. R., and Roble, R. (2004). Effect of El Niño-Southern Oscillation on the dynamical, thermal, and chemical structure of the middle atmosphere. *J. Geophys. Res.*, 109(D17):D17108.

Sato, M., Hansen, J. E., McCormick, M. P., and Pollack, J. B. (1993). Stratospheric aerosol optical depths, 18501990. *Journal of Geophysical Research: Atmospheres*, 98(D12):22987–22994.

Scaife, A., Spangehl, T., Fereday, D., Cubasch, U., Langematz, U., Akiyoshi, H., Bekki, S., Braesicke, P., Butchart, N., Chipperfield, M., Gettelman, A., Hardiman, S., Michou, M., Rozanov, E., and Shepherd, T. G. (2012). Climate change projections and stratosphere-troposphere interaction. *Climate Dynamics*, 38(9-10):2089–2097.

Scherhag, R. (1952). Die explosionsartigen Stratosphärenerwärmungen des Spätwinters 1951/52. *Berichte des deutschen Wetterdienstes in der US-Zone*, 6(38):51–63.

Schmidt, G. A., Jungclaus, J. H., Ammann, C. M., Bard, E., Braconnot, P., Crowley, T. J., Delaygue, G., Joos, F., Krivova, N. A., Muscheler, R., and Others (2012). Climate forcing reconstructions for use in PMIP simulations of the Last Millennium (v1. 1). *Geoscientific Model Development*, 5:185–191.

Schmidt, H., Brasseur, G. P., and Giorgetta, M. A. (2010). Solar cycle signal in a general circulation and chemistry model with internally generated quasi-biennial oscillation. *J. Geophys. Res.*, 115(D1):D00I14.

Schmidt, H., Rast, S., Bunzel, F., Esch, M., Giorgetta, M., Kinne, S., Krismer, T., Stenchikov, G., Timmreck, C., Tomassini, L., and Walz, M. (2013). Response of the middle atmosphere to anthropogenic and natural forcings in the CMIP5 simulations with the Max Planck Institute Earth system model. *J. Adv. Model. Earth Syst.*, 5(1):98–116.

Schneider, D. P., Ammann, C. M., Otto-Bliesner, B. L., and Kaufman, D. S. (2009). Climate response to large, high-latitude and low-latitude volcanic eruptions in the Community Climate System Model. *Journal of Geophysical Research*, 114(D15):D15101.

Scott, R. K. and Polvani, L. M. (2006). Internal Variability of the Winter Stratosphere. Part I: Time-Independent Forcing. *Journal of the Atmospheric Sciences*, 63(11):2758–2776.

Segschneider, J., Beitsch, A., Timmreck, C., Brovkin, V., Ilyina, T., Jungclaus, J., Lorenz, S. J., Six, K. D., and Zanchettin, D. (2013). Impact of an extremely large magnitude volcanic eruption on the global climate and carbon cycle estimated from ensemble Earth System Model simulations. *Biogeosciences*, 10(2):669–687.

Self, S. (2006). The effects and consequences of very large explosive volcanic eruptions. *Philosophical transactions. Series A, Mathematical, physical, and engineering sciences*, 364:2073–2097.

Self, S., Gertisser, R., Thordarson, T., Rampino, M. R., and Wolff, J. A. (2004). Magma volume, volatile emissions, and stratospheric aerosols from the 1815 eruption of Tambora. *Geophysical Research Letters*, 31.

Shepherd, T. G. and McLandress, C. (2011). A Robust Mechanism for Strengthening of the Brewer-Dobson Circulation in Response to Climate Change: Critical-Layer Control of Subtropical Wave Breaking. *Journal of the Atmospheric Sciences*, 68:784–797.

Shindell, D. T., Schmidt, G. A., Mann, M. E., and Faluvegi, G. (2004). Dynamic winter climate response to large tropical volcanic eruptions since 1600. *J. Geophys. Res.*, 109(D5):D05104.

Sigl, M., McConnell, J. R., Toohey, M., Curran, M., Das, S. B., Edwards, R., Isaksson, E., Kawamura, K., Kipfstuhl, S., Kruger, K., Layman, L., Maselli, O. J., Motizuki, Y., Motoyama, H., Pasteris, D. R., and Severi, M. (2014). Insights from Antarctica on volcanic forcing during the Common Era. *Nature Clim. Change*, 4(8):693–697.

Solomon, S. (1999). Stratospheric ozone depletion: A review of concepts and history. *Reviews of Geophysics*, 37(3):275.

Stenchikov, G., Delworth, T. L., Ramaswamy, V., Stouffer, R. J., Wittenberg, A., and Zeng, F. (2009). Volcanic signals in oceans. *Journal of Geophysical Research: Atmospheres (1984–2012)*, 114(D16).

Stenchikov, G., Hamilton, K., Robock, A., Ramaswamy, V., and Schwarzkopf, M. D. (2004). Arctic oscillation response to the 1991 Pinatubo eruption in the SKYHI general circulation model with a realistic quasi-biennial oscillation. *J. Geophys. Res.*, 109(D3):D03112.

Stenchikov, G., Hamilton, K., Stouffer, R. J., Robock, A., Ramaswamy, V., Santer, B., and Graf, H.-F. (2006). Arctic Oscillation response to volcanic eruptions in the IPCC AR4 climate models. *J. Geophys. Res.*, 111(D7):D07107.

Stenchikov, G., Robock, A., Ramaswamy, V., Schwarzkopf, M. D., Hamilton, K., and Ramachandran, S. (2002). Arctic Oscillation response to the 1991 Mount Pinatubo eruption: Effects of volcanic aerosols and ozone depletion. *J.-Geophys.-Res.*, 107(D24):4803.

Stenchikov, G. L., Kirchner, I., Robock, A., Graf, H.-F., Antuña, J. C., Grainger, R. G., Lambert, A., and Thomason, L. (1998). Radiative forcing from the 1991 Mount Pinatubo volcanic eruption. *J. Geophys. Res.*, 103(D12):13837–13857.

Stevens, B. (2013). The Max Planck Institute for Meteorology Earth System Model [Special Issue]. *Journal of Advances in Modeling Earth Systems*, 5(1).

Stevens, B., Giorgetta, M., Esch, M., Mauritsen, T., Crueger, T., Rast, S., Salzmann, M., Schmidt, H., Bader, J., Block, K., Brokopf, R., Fast, I., Kinne, S., Kornblueh, L., Lohmann, U., Pincus, R., Reichler, T., and Roeckner, E. (2013). Atmospheric component of the MPI-M Earth System Model: ECHAM6. *J. Adv. Model. Earth Syst.*, 5(2):146–172.

Stothers, R. B. (1984). The Great Tambora Eruption in 1815 and Its Aftermath. *Science*, 224(4654):1191–1198.

Stothers, R. B. (1996). Major optical depth perturbations to the stratosphere from volcanic eruptions: Pyrheliometric period, 18811960. *Journal of Geophysical Research*, 101:3901.

Stothers, R. B. (2001). Major optical depth perturbations to the stratosphere from volcanic eruptions: Stellar extinction period, 19611978. *Journal of Geophysical Research*, 106:2993.

Tanaka, T. Y., Orito, K., Sekiyama, T. T., Shibata, K., Chiba, M., and Tanaka, H. (2003). MASINGAR, a global tropospheric aerosol chemical transport model coupled with MRI/JMA98 GCM. *Papers in Meteorology and Geophysics*, 53(4):119–138.

Taylor, K. E., Stouffer, R. J., and Meehl, G. A. (2011). An Overview of CMIP5 and the Experiment Design. *Bull. Amer. Meteor. Soc.*, 93(4):485–498.

Tebaldi, C. and Knutti, R. (2007). The Use of the Multi-Model Ensemble in Probabilistic Climate Projections. *Philosophical Transactions: Mathematical, Physical and Engineering Sciences*, 365(1857):pp. 2053–2075.

Textor, C., Graf, H.-F., Timmreck, C., and Robock, A. (2004). Emissions from volcanoes. In Granier, C., Artaxo, P., and Reeves, C., editors, *Emissions of Atmospheric Trace Compounds*, volume 18, pages 269–303. Springer Netherlands.

Thomas, M. A., Giorgetta, M. A., Timmreck, C., Graf, H.-F., and Stenchikov, G. (2009a). Simulation of the climate impact of Mt. Pinatubo eruption using ECHAM5 - Part 2: Sensitivity to the phase of the QBO and ENSO. *Atmospheric Chemistry and Physics*, 9(9):3001–3009.

Thomas, M. A., Timmreck, C., Giorgetta, M. A., Graf, H.-F., and Stenchikov, G. (2009b). Simulation of the climate impact of Mt. Pinatubo eruption using ECHAM5 - Part 1: Sensitivity to the modes of atmospheric circulation and boundary conditions. *Atmospheric Chemistry and Physics*, 9(2):757–769.

Thompson, D. W. J. and Wallace, J. M. (1998). The Arctic oscillation signature in the wintertime geopotential height and temperature fields. *Geophysical Research Letters*, 25(9):1297–1300.

Thompson, D. W. J. and Wallace, J. M. (2000). Annular Modes in the Extratropical Circulation. Part I: Month-to-Month Variability. *Journal of Climate*, 13(5):1000–1016.

Thompson, D. W. J. and Wallace, J. M. (2001). Regional Climate Impacts of the Northern Hemisphere Annular Mode. *Science*, 293(5527):85–89.

Timmreck, C. (2012). Modeling the climatic effects of large explosive volcanic eruptions. *WIREs Clim Change*, 3(6):545–564.

Timmreck, C., Graf, H.-F., Lorenz, S. J., Niemeier, U., Zanchettin, D., Matei, D., Jungclaus, J. H., and Crowley, T. J. (2010). Aerosol size confines climate response to volcanic supereruptions. *Geophys. Res. Lett.*, 37(24):L24705.

Timmreck, C., Graf, H.-F., Zanchettin, D., Hagemann, S., Kleinen, T., and Krüger, K. (2012). Climate response to the Toba super-eruption: Regional changes. *Quaternary International*, 258(0):30–44.

Timmreck, C., Lorenz, S. J., Crowley, T. J., Kinne, S., Raddatz, T. J., Thomas, M. A., and Jungclaus, J. H. (2009). Limited temperature response to the very large AD 1258 volcanic eruption. *Geophys. Res. Lett.*, 36(21):L21708.

Tomassini, L., Gerber, E. P., Baldwin, M. P., Bunzel, F., and Giorgetta, M. (2012). The role of stratosphere-troposphere coupling in the occurrence of extreme winter cold spells over northern Europe. *J. Adv. Model. Earth Syst.*, 4(4):M00A03.

Toohey, M., Krüger, K., Bittner, M., Timmreck, C., and Schmidt, H. (2014). The impact of volcanic aerosol on the Northern Hemisphere stratospheric polar vortex: mechanisms and sensitivity to forcing structure. *Atmospheric Chemistry and Physics*, 14(11):13063–13079.

Toohey, M., Krüger, K., Niemeier, U., and Timmreck, C. (2011). The influence of eruption season on the global aerosol evolution and radiative impact of tropical volcanic eruptions.

Toohey, M., Krüger, K., and Timmreck, C. (2013). Volcanic sulfate deposition to Greenland and Antarctica: A modeling sensitivity study. *J. Geophys. Res. Atmos.*, 118(10):4788–4800.

Trenberth, K. E. and Dai, A. (2007). Effects of Mount Pinatubo volcanic eruption on the hydrological cycle as an analog of geoengineering. *Geophysical Research Letters*, 34(15):L15702.

Trepte, C. R. and Hitchman, M. H. (1992). Tropical stratospheric circulation deduced from satellite aerosol data. *Nature*, 355:626–628.

Trepte, C. R., Veiga, R. E., and McCormick, M. P. (1993). The poleward dispersal of Mount Pinatubo volcanic aerosol. *Journal of Geophysical Research*, 98:18563.

Uppala, S. M., Kallberg, P. W., Simmons, A. J., Andrae, U., Bechtold, V. D. C., Fiorino, M., Gibson, J. K., Haseler, J., Hernandez, A., Kelly, G. A., Li, X., Onogi, K., Saarinen, S., Sokka, N., Allan, R. P., Andersson, E., Arpe, K., Balmaseda, M. A., Beljaars, A. C. M., Berg, L. V. D., Bidlot, J., Bormann, N., Caires, S., Chevallier, F., Dethof, A., Dragosavac, M., Fisher, M., Fuentes, M., Hagemann, S., Hólm, E., Hoskins, B. J., Isaksen, L., Janssen, P. A. E. M., Jenne, R., Mcnally, A. P., Mahfouf, J.-F., Morcrette, J.-J., Rayner, N. A., Saunders, R. W., Simon, P., Sterl, A., Trenberth, K. E., Untch, A., Vasiljevic, D., Viterbo, P., and Woollen, J. (2005). The ERA-40 re-analysis. *Q.J.R. Meteorol. Soc.*, 131(612):2961–3012.

Valcke, S. (2013). The OASIS3 coupler: a European climate modelling community software. *Geoscientific Model Development*, 6(2):373–388.

van Loon, H. and Labitzke, K. (1987). The Southern Oscillation. Part V: The Anomalies in the Lower Stratosphere of the Northern Hemisphere in Winter and a Comparison with the Quasi-Biennial Oscillation. *Mon. Wea. Rev.*, 115(2):357–369.

Veryard, R. G. and Ebdon, R. A. (1961). Fluctuations in tropical stratospheric winds. *Meteorol. Mag*, 90:125–143.

Waugh, D. W. and Polvani, L. M. (2010). *The Stratosphere: Dynamics, Transport, and Chemistry*, volume 190 of *Geophysical Monograph Series*. American Geophysical Union, Washington, D. C.

Wegmann, M., Brönnimann, S., Bhend, J., Franke, J., Folini, D., Wild, M., and Luterbacher, J. (2014). Volcanic influence on European summer precipitation through monsoons: Possible cause for Years Without a Summer. *Journal of Climate*, 27(10):3683–3691.

Yukimoto, S., Adachi, Y., Hosaka, M., Sakami, T., Yoshimoro, H., Hirabara, M., Tanaka, T. Y., Shindo, E., Tsujino, H., Deushi, M., Mizuta, R., Yabu, S., Obata, A., Nakano, H., Koshiro, T., Ose, T., and Kitoh, A. (2012). A New Global Climate Model of the Meteorological Research Institute: MRI-CGCM3-Model Description and Basic Performance. *Journal of the Meteorological Society of Japan*, 90A:23–64.

Zanchettin, D., Bothe, O., Graf, H. F., Lorenz, S. J., Luterbacher, J., Timmreck, C., and Jungclaus, J. H. (2013a). Background conditions influence the decadal climate response to strong volcanic eruptions. *Journal of Geophysical Research D: Atmospheres*, 118:4090–4106.

Zanchettin, D., Bothe, O., Timmreck, C., Bader, J., Beitsch, A., Graf, H.-F., Notz, D., and Jungclaus, J. H. (2014). Inter-hemispheric asymmetry in the sea-ice response to volcanic forcing simulated by MPI-ESM (COSMOS-Mill). *Earth System Dynamics*, 5(1):121–168.

Zanchettin, D., Rubino, A., Matei, D., Bothe, O., and Jungclaus, J. H. (2013b). Multidecadal-to-centennial SST variability in the MPI-ESM simulation ensemble for the last millennium. *Climate Dynamics*, 40(5-6):1301–1318.

Zanchettin, D., Timmreck, C., Bothe, O., Lorenz, S. J., Hegerl, G., Graf, H.-F., Luterbacher, J., and Jungclaus, J. H. (2013c). Delayed winter warming: A robust decadal response to strong tropical volcanic eruptions? *Geophys. Res. Lett.*, 40(1):204–209.

Zanchettin, D., Timmreck, C., Graf, H.-F., Rubino, A., Lorenz, S., Lohmann, K., Krüger, K., and Jungclaus, J. H. (2012). Bi-decadal variability excited in the coupled ocean-atmosphere system by strong tropical volcanic eruptions. *Climate Dynamics*, 39(1-2):419–444.

Zanchettin, D., Timmreck, C., Khodri, M., Robock, A., Hegerl, G., Schmidt, A., Toohey, M., Pausata, F. S. R., Black, B., Bothe, O., and Others (2015). Application for a Model Intercomparison Project on the climatic response to Volcanic forcing (VolMIP) as CMIP6-Endorsed MIP.

Zhong, Y., Miller, G. H., Otto-Bliesner, B. L., Holland, M. M., Bailey, D. A., Schneider, D. P., and Geirsdottir, A. (2011). Centennial-scale climate change from decadally-paced explosive volcanism: a coupled sea ice-ocean mechanism. *Climate Dynamics*, 37(11-12):2373–2387.

Zielinski, G. A. (2000). Use of paleo-records in determining variability within the volcanism-climate system. *Quaternary Science Reviews*, 19(1):417–438.

Acknowledgements

First and foremost I would like to express my gratitude to my supervisors Dr. Claudia Timmreck and Dr. Hauke Schmidt for their guidance and advice. Especially in times when things did not worked out as initially hoped, their constant support and positive attitude helped enormously. Both of them had always time for discussing my issues and problems. Thank you very much!

I thank my advisory panel chair, Dr. Johann Jungclaus, for his interest in my research and for reviewing my work during all stages of my PhD term. His suggestions during the panel meetings help a lot in keeping my work on track.

I would also like to thank Prof. Martin Claußen as the principal evaluator of my thesis for his support and interest. Thanks as well to Prof. Bjorn Stevens and the whole Atmosphere in the Earth Department for a really nice and inspiring working environment.

I greatly appreciate the fruitful discussions with Prof. Kirstin Krüger and Dr. Matthew Toohey of the MiKliP ALARM project. Their willingness to share their extensive knowledge of volcanic eruptions and atmospheric dynamics helped exceptionally during all stages of my PhD project.

I would like to thank my colleagues in the Middle and Upper Atmosphere Group and Stratosphere and Climate Group, Ulrike Niemeier, Elisa Manzini, Sebastian Rast, Katharina Meraner, Sebastian Müller, Tobias Haufschild, and my former colleagues working on stratosphere related topics Thomas Krismer, Sebastian Schirber for their excellent internal peer-reviews of my work and nice working atmosphere during my PhD. Special thanks to Felix Bunzel and Rabea Athmer for their help with the TEM framework and the Tambora experiments.

I am very glad for the support from the International Max Planck Research School on Earth System Modelling. Without the tremendous work of Antje Weitz, Cornelia Kampmann and Wiebke Böhm, who kept all the administrative tasks as little as possible, this thesis would not have been possible.

Also many thanks to my colleagues, friends, tennis partners and room-mates at the Max Planck Institute: Eileen Hertwig, Laura Niederdrenk, Freja Vamborg, Sebastian Sonntag, Jan Ackmann, Florian Rauser, Marlene Klockmann, Ann-Kristin Naumann, Dirk Olonscheck, Mathias Heinze, Frank Sienz, Andreas Veira, Josiane Salameh, Jessica Engels, Philipp de Vrese, Thomas Schöngaßner, Thomas Keitzl, Anurag Dipankar, Rohit Gosh, Miriam Ferrer-Gonzales, Dagmar Fläschner, Chris Hedemann, Jörg Budanowitz, Vladimir Lapin, Chiel van Heerwaarden, Antonija Rimac, Vera Schemann, Davide Zanchettin, Max Popp, Suvarchal Kumar, Jade Garcia, Pierre Mohr-Durdez, Guido Cionni, Leif Denby, Christina Klasa, Rosi Grimm, Christine Radermacher and Malte Rieck. Through lunch and coffee breaks, tennis games, evening drinks and nice chats all of you made it fun to work at the MPI-M. Cheers!

Last but not least, I would like to thank my family, especially my parents Christina and Lothar as well as Ewa and Tomasz for their support all these years. The biggest thanks goes to Magda for believing in me and always being there. Kocham cie.

I dedicate this work to Marcus Bittner.